METEOROLOGY HYDROLOGY
AND WATER MANAGEMENT
IMGW-PIB Science Journal since 2013

VOL. 12 | ISSUE 2 | 2024

ISNN 2299-3835

# Circulation types and their relationships with extreme wind energy generation events in Poland

Bogdan Bochenek[1], Paweł Dąbek[1], Mikołaj Ostraszewski[1], Zbigniew Ustrnul[2,3], Jakub Jurasz[1]

[1] Wrocław University of Science and Technology, Poland

[2] Jagiellonian University Department of Climatology, Poland

[3] Institute of Meteorology and Water Management – National Research Institute, Poland

Abstract

This study investigates the influence of different atmospheric circulation types on wind energy production in Poland from 1948 to 2019. By utilizing the ERA5 reanalysis dataset, which provides detailed atmospheric and surface parameters, and the Litynski calendar of circulation types, this research is directed toward understanding how various circulation patterns affect wind energy generation. The study specifically focuses on periods of energy droughts (days with very low wind energy production) and energy floods (days with very high wind energy production). The analysis reveals trends, along with annual and seasonal variations in the frequency of energy droughts and floods. Over the period of study, the number of drought days varied from 51 to 108 per year, while the number of flood days varied from 44 to 97 per year. Cyclonic circulation types with NW winds are found to be the most favorable for wind energy production, leading to higher daily energy generation. Conversely, anticyclonic circulation types with winds from the north, northeast, and east are more likely to result in energy droughts. Certain seasons exhibit higher variability in the number of drought and flood days, influenced by the prevailing circulation types. The standard deviation of the number of drought days in summer is 7.3 compared to 4.8 in spring; for flood days the standard deviation for winter is 8.4 and for summer only 3.4.

Keywords

Renewable energy, wind farms, circulation types, OSM, drought, flood.

Submitted 23 August 2024, revised 8 October 2024, accepted 10 October 2024

DOI: 10.26491/mhwm/194453

## 1. Introduction

Renewable energy sources are becoming increasingly important in the global effort to mitigate climate change (Moomaw et al. 2012). The shift toward renewables, such as solar and wind energy, is driven by the need to reduce greenhouse gas emissions and dependency on fossil fuels. However, the variability of these energy sources poses challenges for energy systems, particularly in ensuring consistent energy supply (Pryor et al. 2005; Harrison, Wallace 2006; Jerez et al. 2015). The impact of climate change on weather patterns further complicates the matter, potentially exacerbating periods of energy surplus and deficit.

In Poland, the adoption of photovoltaic (PV) systems has seen significant growth in recent years, supported by favorable policies and technological advances (Igliński et al. 2023). Conversely, onshore wind turbines experienced a decline in new investments as the result of regulatory and market challenges. However, the situation is likely to improve in response to new regulations concerning the siting of wind parks relative to human settlements.

The reliability and safety of the energy system are critical concerns, particularly in the face of energy droughts (periods of very low energy production) and energy floods (periods of very high energy production). These extremes are often influenced by weather conditions, which can lead to significant fluctuations in renewable energy output. Understanding these patterns is essential for developing strategies to stabilize the energy grid and ensure a reliable energy supply.

Circulation-type calendars, such as the Litynski classification developed for the territory of Poland, as well as the Grosswetterlagen classification focused on Central Europe (particularly Germany), classify atmospheric circulation patterns and their impacts on weather. These classifications are critical for understanding weather variability and its implications for various environmental and climatic studies (Ustrnul et al. 2010, 2013; Wypych et al. 2014; Ustrnul et al. 2015; Wypych et al. 2017). The Litynski calendar, developed by Jan Litynski in 1969, categorizes 27 types of atmospheric circulation based on sea level pressure over Central Europe (Lityński 1969). Similarly, the Grosswetterlagen classification (initially named the Hess-Brezowsky classification), first published in 1952, provides a framework for analyzing synoptic weather patterns over Central Europe and their long-term climatic impacts (Hess, Brezowsky 1952). The COST733 project further harmonized these classifications across Europe, facilitating the comparison of various methods and their applications in climate research (e.g., Huth et al. 2008; Niedzwiedź, Lupikasza 2019; Niedźwiedź, Ustrnul 2021).

Circulation types play a pivotal role in determining the availability of renewable energy resources (Correira et al. 2017; Grams et al. 2017). Different atmospheric circulation patterns can lead to variations in wind speed and solar irradiance, directly affecting the performance of wind turbines and PV systems. By analyzing these weather types, it is possible to predict periods of low and high energy production, enabling better planning and management of energy resources. Van der Wiel et al. (2019) investigated the impact of large-scale weather regimes on renewable energy production and energy demand in Europe. Their findings indicate that certain weather regimes, such as 'Scandinavian blocking' and 'North Atlantic oscillation negative', lead to lower renewable energy production and higher energy demand, increasing the risk of energy shortfalls. Similarly, Dumas et al. (2019) assessed the vulnerability of electrical grid components to extreme weather events, emphasizing the need for resilient energy systems capable of adapting to these challenges (Dumas et al. 2019; Van der Wiel et al. 2019). Moreover, Gonçalves et al. (2024) and Muyuan et al. (2023) examined the variability in wind and solar energy production under different weather regimes. They highlighted the complexity of predicting energy shortfalls based solely on large-scale weather patterns and underscored the importance of accurate weather prediction models for effective energy planning and management.

Understanding the relationship between weather patterns and renewable energy production has significant implications for energy policy and management (del Rio et al. 2018). It can inform the development of policies that support the integration of renewable energy into the grid, enhance predictive maintenance of energy infrastructure, and improve the design of energy storage systems to buffer against production variability (Brown, Reichenberg 2021).

With these considerations, the main goal of this study is to evaluate the relationship between different weather circulation types in Poland and the occurrence of periods with very low (droughts) and very high (floods) production of wind energy. By establishing this relationship, the study is directed toward providing insights into the impacts of weather patterns on renewable energy production, thereby contributing to more resilient and adaptive energy systems.

## 2. Material and methods

The primary data source for this study is the ERA5 reanalysis dataset, which provides a comprehensive set of atmospheric and surface parameters at high spatial and temporal resolution (Hersbach et al. 2020). Specifically, we utilized the *u* and *v* wind components, temperature, and specific humidity data from the 133rd model level, which is the closest to 100 m above ground level (agl) in the ERA5 model. Additionally, surface-level air pressure data were extracted to facilitate further calculations.

Wind speed at the height of 100 m agl was adjusted for variations in air density, which can significantly affect the actual wind speed experienced by wind turbines (Hoxha et al. 2023). The steps and formulas are specified in the supplementary materials. For computations of power generation with specific wind speed, a 3.5 MW wind turbine was used (https://en.wind-turbine-models.com/turbines/1247-vestas-v112-3.45, data access 2024.07.01).

To accurately assess wind energy production across Poland, the locations of wind turbines were extracted from OpenStreetMap (OSM, https://www.openstreetmap.org, data access 2024.07.01). The final database consisted of 4949 wind turbines (Fig. 1a) with simulated yearly wind energy production (Fig. 1b). Using these coordinates, the potential power generated at each turbine site was calculated by applying wind speed data from the ERA5 reanalysis dataset nearest point. The wind speed values, adjusted for air density, were used to estimate the power output based on the specific power curve of the wind turbines (Jurasz et al. 2024).

The Litynski calendar of circulation types was used to categorize atmospheric circulation patterns affecting Poland (Lityński 1969; Pianko-Kluczyńska 2007; Nowosad 2008; Kulesza 2017). This calendar classifies circulation types based on synoptic situations. By linking these circulation types to wind speed and energy production data, we analyzed how different atmospheric patterns impact wind energy generation. This classification helps in understanding the variability of wind energy production in relation to prevalent weather conditions.

The frequency of energy droughts and floods using specific thresholds was calculated to analyze the impact of circulation types on renewable energy production. Droughts were defined as days when energy production fell below the 20th percentile, and floods as days when production exceeded the 80th percentile. Using R, occurrences of droughts and floods were classified and their frequencies for each circulation type were computed. This was achieved using the dplyr (Wickham, Francois 2014) and ggplot2 (Wickham 2016) libraries, which facilitated the analysis and visualization of trends and seasonal variations.

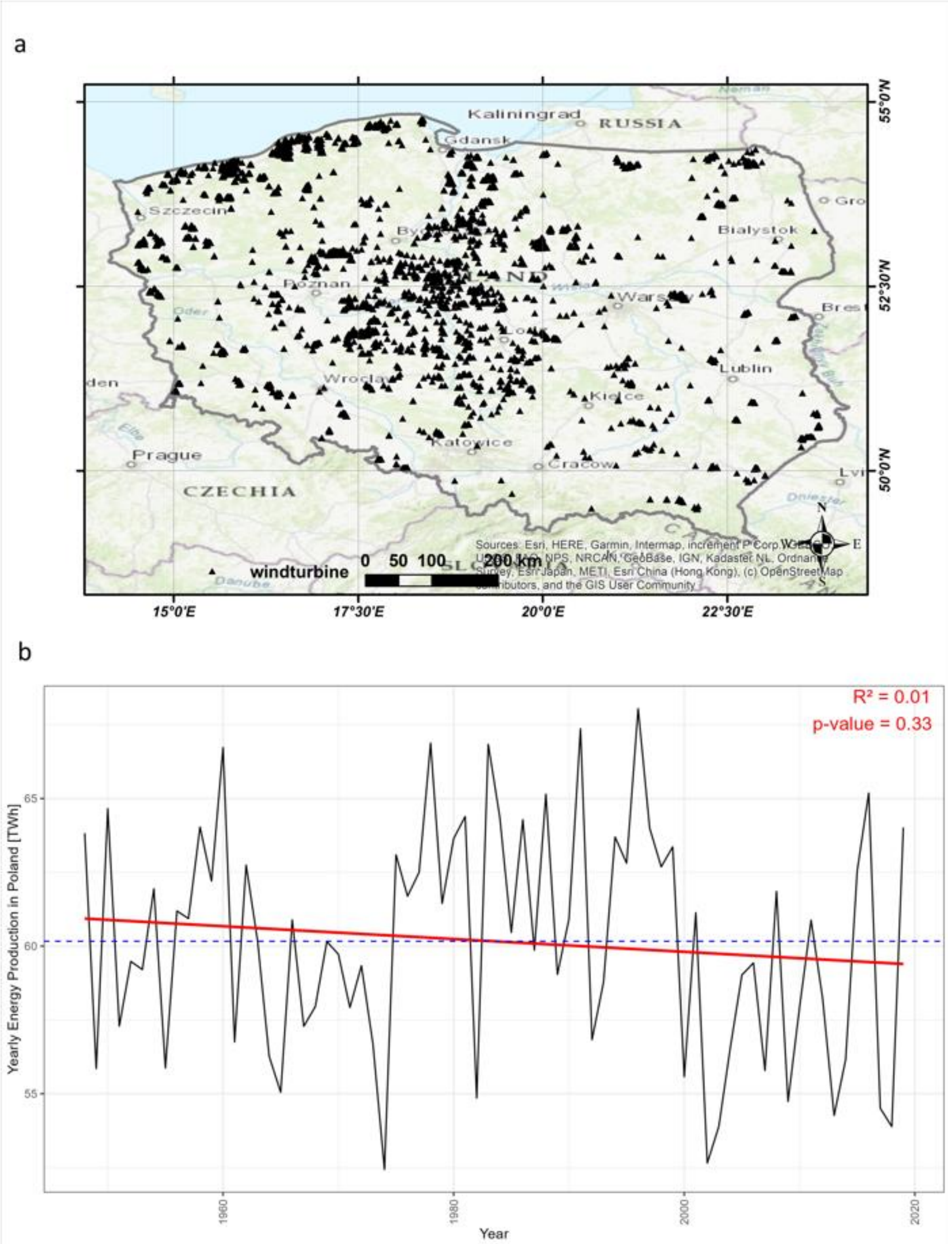


Fig. 1. Locations of OSM turbines (a) and simulated yearly wind energy production from OSM turbines in Poland (b).

## 3. Results

### 3.1. Trends in energy droughts and floods

Figure 2 shows the annual trend in drought days from 1948 to 2019, indicating variability with some noticeable peaks and dips. Notably, there are several years with a high number of drought days, such as from the early 1960s to the early 1970s and from the 2000s until the end of the period, with peak counts reaching 108 days in 1974. Conversely, there are periods with fewer drought days, particularly in the 1950s, 1970, and 1990s, with counts dropping to 51 days in 1958. Despite this variability, the overall trend shows a slight increase, but this trend is not statistically significant (p-value 0.54).

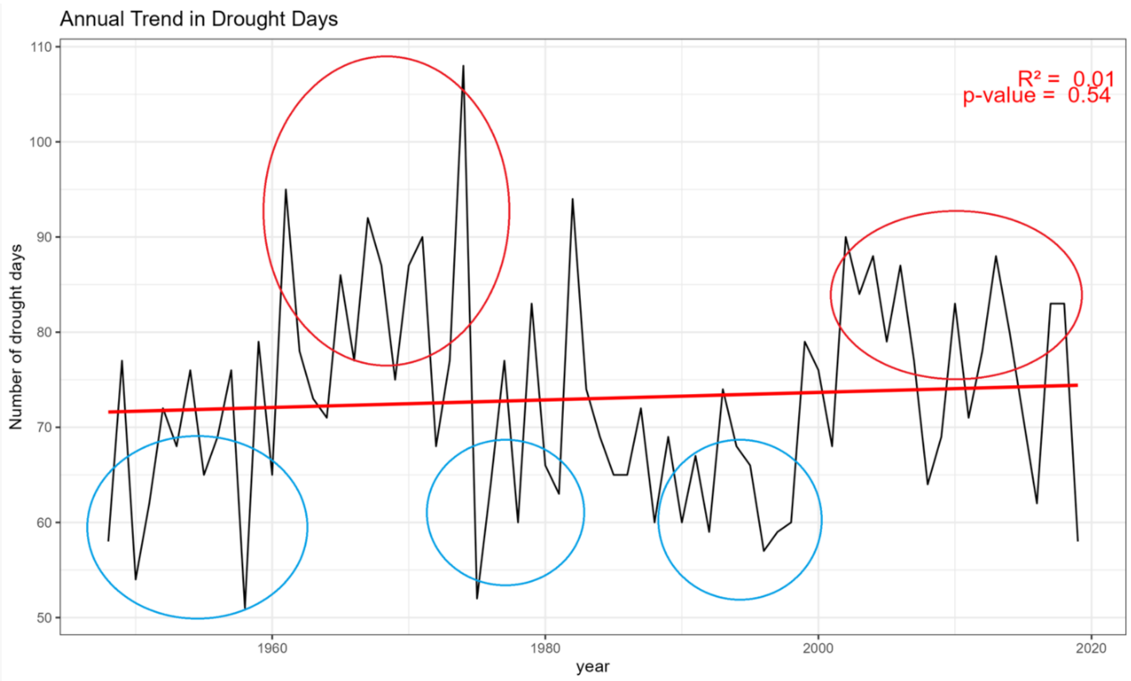


Fig. 2. Trends in annual number of days with energy droughts. Periods with high or low numbers of drought days are highlighted with red or blue shapes, respectively.

Similarly, the annual trend in flood days over the same period shows significant fluctuations (Fig. 3). High flood day counts are observed from the 1980s to the 1990s, with peaks reaching 97 days in 1983 and 1991. On the other hand, the number of flood days decreased in the early 1970s and early 2000s, with counts dropping to 44 days in 2002. The overall trend indicates a slight decrease in flood days, yet this trend is also not statistically significant (p-value 0.48).

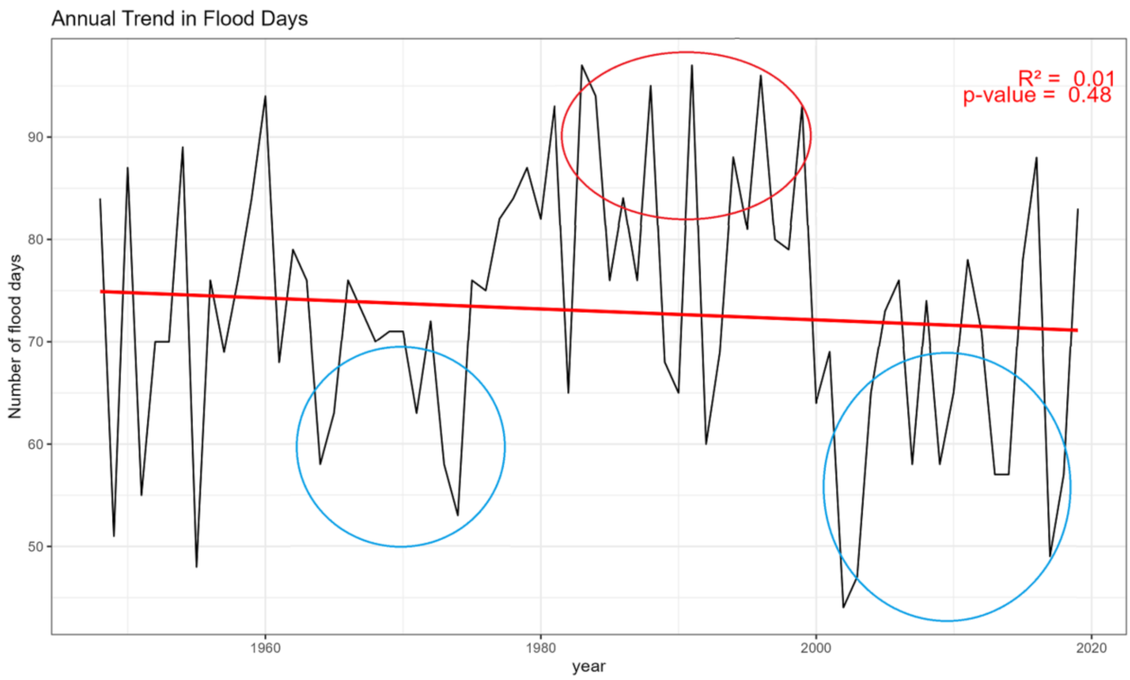


Fig. 3. Trends in annual number of days with energy floods.

The seasonal trends in drought days reveal distinct patterns across different seasons (Fig. 4). The number of drought days in autumn fluctuates between 10 and 35, with occasional peaks above 30, particularly in the 1960s. The overall trend is relatively stable, with a slight increase that is not statistically significant. Drought days in spring range from 5 to 25, showing a general decrease over time. Peaks are observed in the late 1950s, 1960s, and mid-1970s, but the trend is not statistically significant. Summer exhibits the highest variability, with drought days ranging from 20 to 50. Notable peaks occur in the early 1960s and mid-2000s. The overall trend shows a slight decrease, but this is not statistically significant. Winter drought days vary from 5 to 25, with peaks in the 1950s, early 1970s, 1980s, and 2000s. The overall trend remains stable with no significant changes.

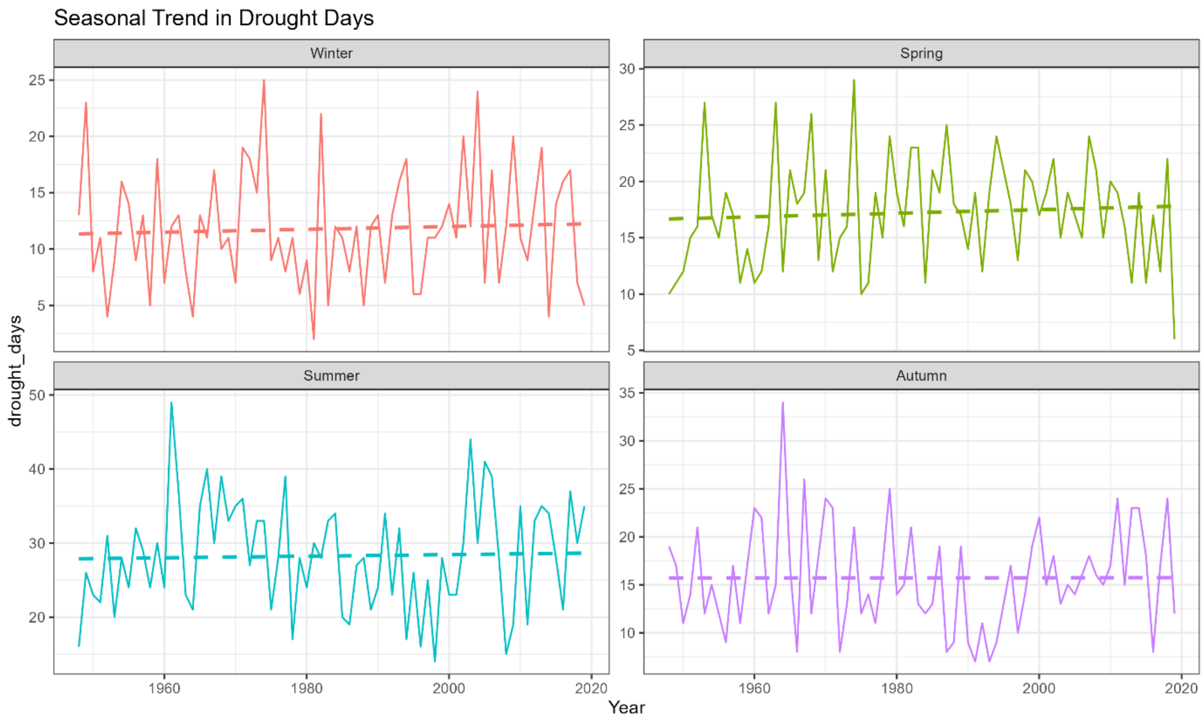


Fig. 4. Trends in annual number of days with energy droughts in seasons with different ranges on the y-axis to highlight seasonal variability.

Flood days in autumn (Fig. 5) fluctuate between 10 and 35, with noticeable peaks in the 1950s, 1970s, and 1990s. The overall trend is stable with a slight decrease, not statistically significant. In spring, flood days vary from 5 to 25, showing a general decrease over time, with peaks in the 1960s, early 1980s, and 1990s. The trend is not statistically significant. In summer, flood days range from 0 to 15, with high variability and peaks in the early 1970s and late 1990s. The overall trend shows a slight decrease, which is not statistically significant. In 2003, there were no flood days. Winter was the most variable season, with flood days ranging from 10 to 50 and noticeable peaks in the late 1980s and mid-1990s. The overall trend remains stable, without significant changes.

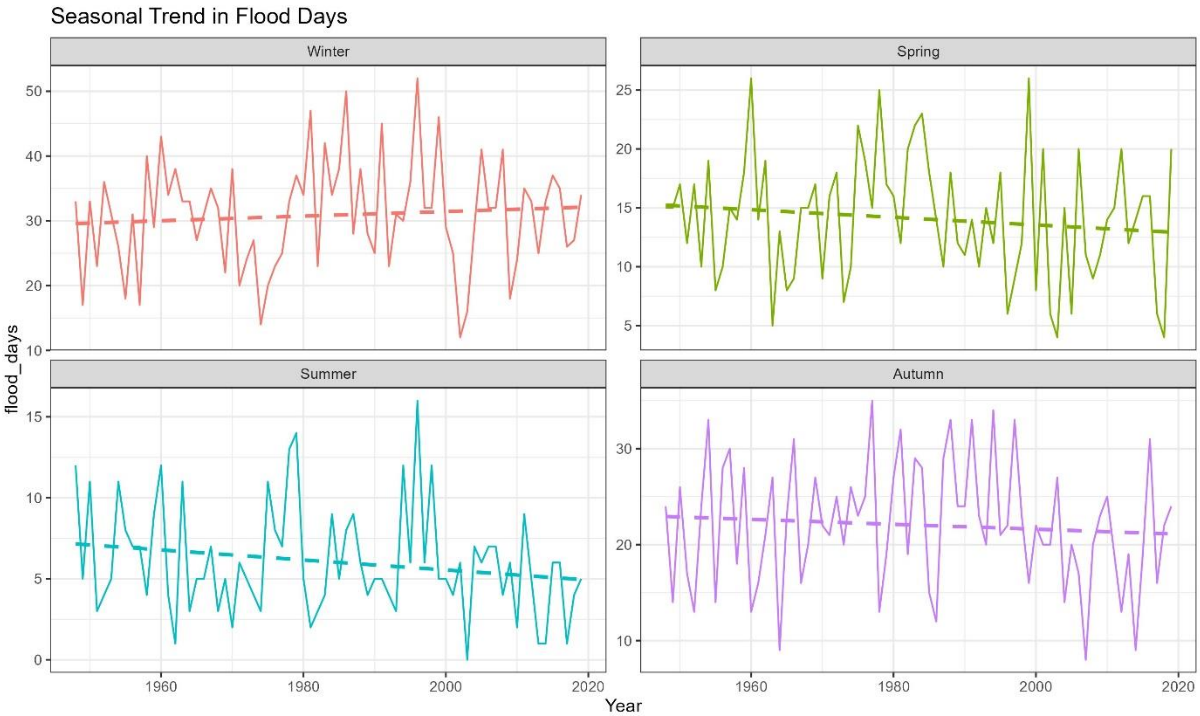


Fig. 5. Trends in annual number of days with energy floods in seasons with different ranges on the y-axis to highlight seasonal variability.

### 3.2. Circulation types

The frequency of different atmospheric circulation types varies significantly in Poland, influencing the country's weather patterns over time. Figure 6 shows the frequency of these circulation types from 1948 to 2019, highlighting the distribution and dominance of specific types throughout this period. Circulation types are categorized along the x-axis, with their corresponding frequencies on the y-axis. The bar chart is color-coded to differentiate between the various circulation types. The grey bars represent circulation types without significant cyclonic or anticyclonic dominance (neutral pressure pattern), blue anticyclonic, and red cyclonic types, showing distinct variations in their occurrences. Notably, certain types, particularly those represented by the blue (E, N and NE winds) and red bars (SW and NW winds), appear more frequently than others.

Figure 7 presents the frequencies of circulation types in different seasons of the year. In autumn, the most dominant are cyclonic types with SW and NW winds; in spring, anticyclonic types with NE and N winds; in summer, anticyclonic types with NE and N winds; and in winter, cyclonic types with SW winds.

Having assigned circulation types for all days in this database, for days with a given circulation type, the mean daily sum of wind energy that could be produced by all wind turbines in Poland was calculated. Figure 8 shows that the highest values of daily wind energy are expected on days with anticyclonic circulation types and NW winds, while the lowest values are for anticyclonic types with no advection.

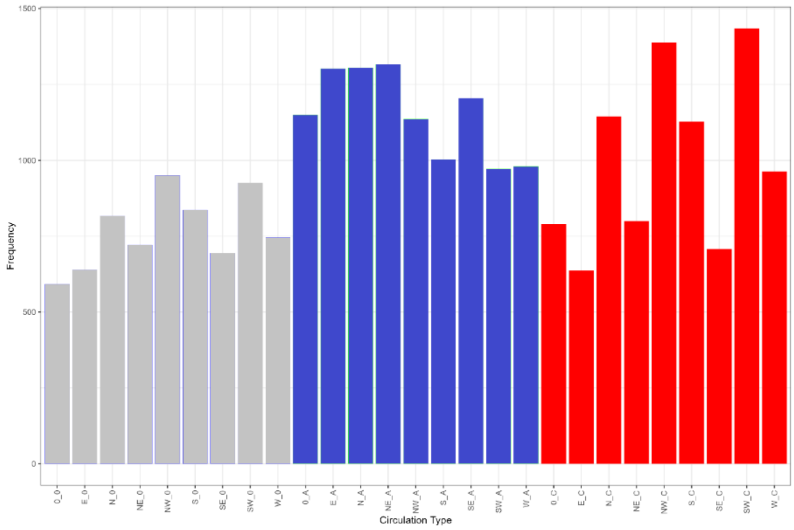


Fig. 6. Frequency of circulation types 1948-2019.

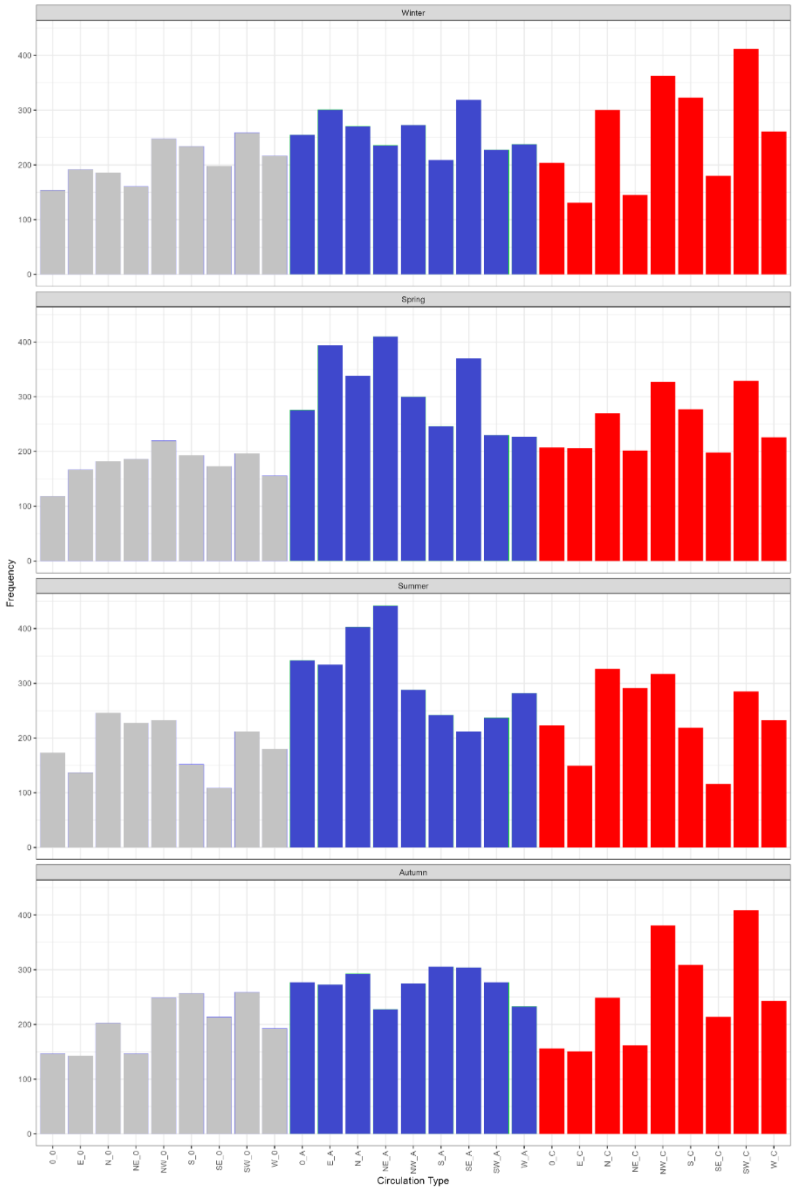


Fig. 7. Frequency of circulation types by season.

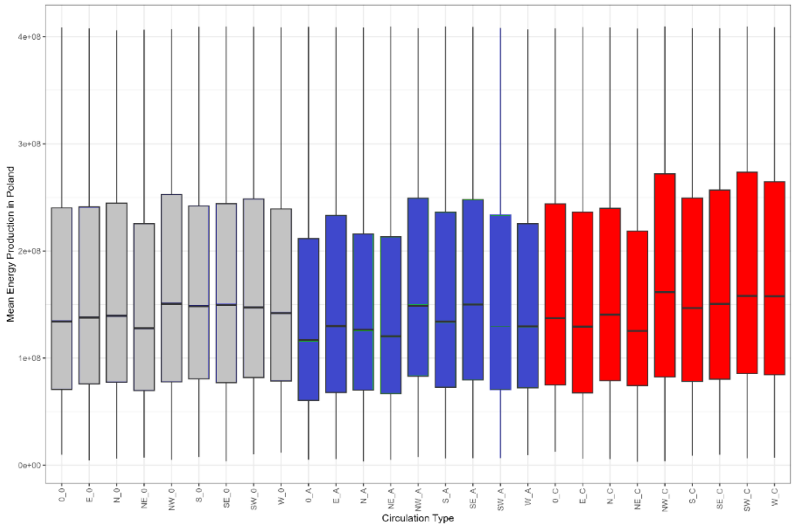


Fig. 8. Mean daily sum of wind energy production for days with different circulation types.

As defined in Section 2, the frequency of energy droughts (Fig. 9) and floods (Fig. 10) were calculated for circulation types in Poland. While cyclonic types with N, NE, and E winds and without advection are the most likely associated with energy droughts, anticyclonic types with NW and SW winds are strongly connected to the energy of floods. Days with cyclonic types with SE winds are responsible for the least number of droughts and the greatest number of floods.

Figures 11 and 12 present the frequencies of drought and flood days by season. Droughts are least common in winter and autumn. Usually, anticyclonic circulation types are responsible for the largest number of droughts, which are mostly visible in summer and spring. On the other hand, floods are seldom seen in summer, mostly associated with cyclonic circulation types.

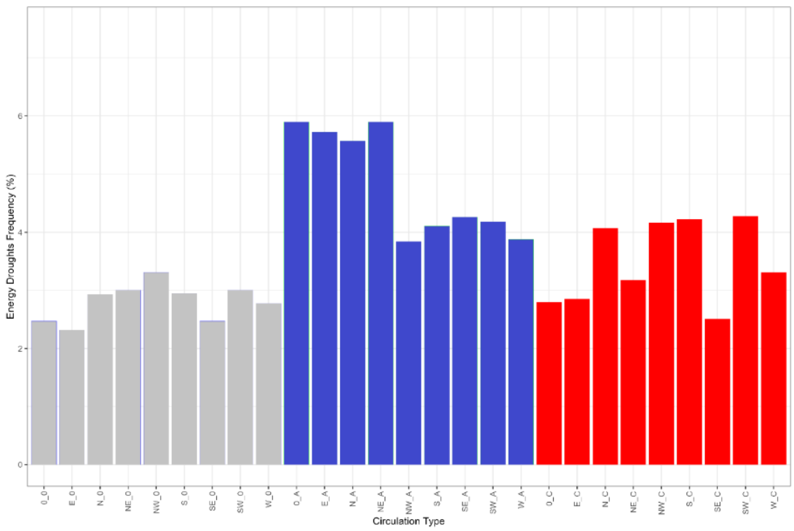


Fig. 9. Frequency of days with energy droughts for circulation types.

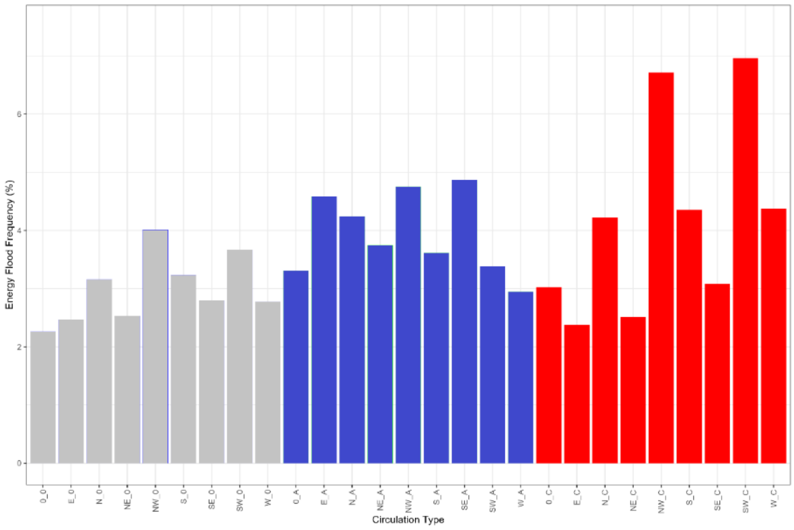


Fig. 10. Frequency of days with energy floods for circulation types.

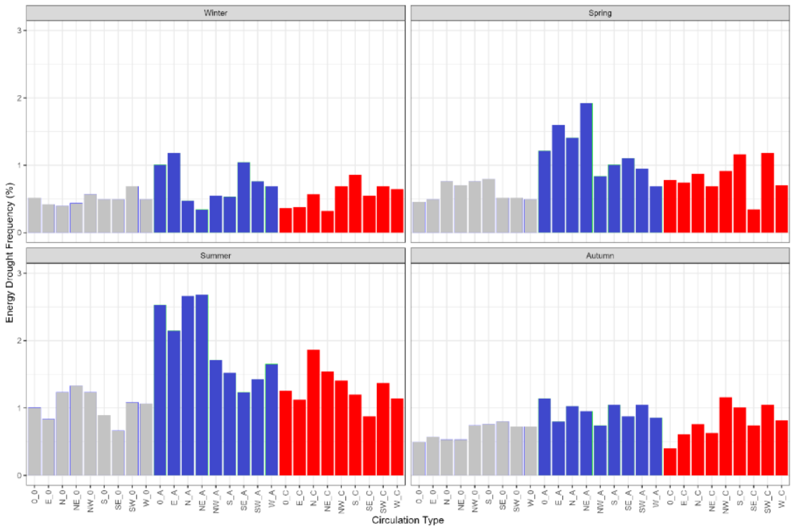


Fig. 11. Frequency of days with energy droughts for circulation types by season.

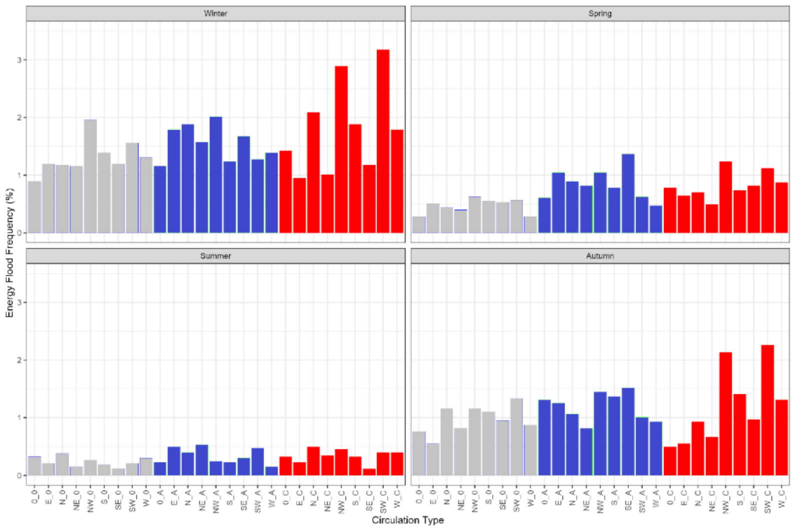


Fig. 12. Frequency of days with energy floods for circulation types by season.

## 4. Discussion

The findings of this study underscore the significant impacts of atmospheric circulation types on wind energy production in Poland. Analysis of data from 1948 to 2019 reveals that specific circulation types are related to very low (energy droughts) and very high (energy floods) wind energy production. These insights are critical for improving the reliability and resilience of renewable energy systems.

The results indicate that cyclonic circulation types, particularly those with NW winds, are most conducive to high wind energy production. These patterns tend to create stable, strong wind conditions that are ideal for wind turbines. Conversely, anticyclonic circulation types, especially with N, NE, and E winds, are more likely to result in less favorable wind conditions conducive to energy droughts. This understanding can help in forecasting and managing wind energy production more effectively.

The study highlights distinct seasonal variations in wind energy production. For instance, summer and spring exhibit higher variability in energy production, with anticyclonic types leading to more stable conditions in summer, whereas winter and autumn show more consistent patterns with cyclonic types. This seasonal insight is crucial for planning energy storage and distribution, ensuring that energy supply can meet demand throughout the year.

The ability to predict periods of energy surplus and deficit based on atmospheric circulation types has profound implications for energy policy and management. Policymakers can use these findings to develop strategies that enhance the integration of renewable energy into the national grid. For example, during anticipated periods of energy drought, alternative energy sources or stored energy can be used to maintain a stable supply. Similarly, during energy floods, excess energy can be stored or redistributed to avoid curtailment.

Understanding the relationship between weather patterns and wind energy production can help in designing more robust energy systems. By anticipating periods of low and high production, energy providers can better manage grid stability, e.g., by optimizing the use of energy storage systems, improving the maintenance schedules of wind turbines, and ensuring that the energy grid can handle fluctuations in energy production without compromising reliability.

This study, while comprehensive, has several limitations. The use of the ERA5 reanalysis dataset provides a high level of detail, but real-world factors such as turbine maintenance, operational efficiency, and local topography were not fully accounted for. Additionally, while the Litynski calendar of circulation types offers a robust framework for categorizing weather patterns, future research could benefit from incorporating more localized meteorological data and advanced predictive models. This research also has employed a simplified approach, assuming that all wind turbines have the same power and height, which is not the case in reality, although there are not sufficient data to examine the question in greater detail.

Further research is needed to explore the long-term impacts of climate change on these atmospheric circulation patterns and their subsequent effects on wind energy production. Understanding how these patterns might shift in the future will be crucial for developing adaptive strategies that ensure the continued growth and stability of renewable energy systems in Poland.

## 5. Conclusion

This study provides insights into the relationship between atmospheric circulation types and wind energy production in Poland. By identifying the weather patterns that lead to energy droughts and floods, this research contributes to the development of more resilient and adaptive energy systems. These findings are essential for policymakers and energy planners aiming to enhance the reliability and efficiency of renewable energy sources, ultimately supporting the transition to a sustainable energy future.

The authors also see the rationale for using other classifications of circulation types, including those based on automated methods (e.g., using machine learning techniques), to assess their impact on electricity production. It is necessary to examine to what extent the application of mesoscale classifications will allow for an even better determination of the influence of circulation conditions on anemological conditions.

## Acknowledgments

We gratefully acknowledge Polish high-performance computing infrastructure PLGrid (HPC Center: ACK Cyfronet AGH) for providing computer facilities and support within computational grant no. PLG/2023/016587.

This work documents the results of research project no. 2022/47/B/ST8/01113 funded by the National Science Centre (Narodowe Centrum Nauki) titled: Method to quantify the energy droughts of renewable sources based on historical and climate change projections data.

## References

Brown T., Reichenberg L., 2021, Decreasing market value of variable renewables can be avoided by policy action, Energy Economics, 100, DOI: 10.1016/j.eneco.2021.105354.

Correia J.M., Bastos A., Brito M.C., Trigo R.M., 2017, The influence of the main large-scale circulation patterns on wind power production in Portugal, Renewable Energy, 102, 214-223, DOI: 10.1016/j.renene.2016.10.002.

Dumas M., Kc B., Cunliff C.I., 2019, Extreme weather and climate vulnerabilities of the electric grid: a summary of environmental sensitivity quantification methods, Technical Report No. ORNL/TM-2019/1252, Oak Ridge National Lab., Oak Ridge, TN (United States), DOI: 10.2172/1558514.

Gonçalves A.C.R., Costoya X., Nieto R., Liberato M.L.R., 2024, Extreme weather events on energy systems: a comprehensive review on impacts, mitigation, and adaptation measures, Sustainable Energy Research, 11, DOI: 10.1186/s40807-023-00097-6.

Grams C., Beerli R., Pfenninger S., Staffell I., Wernli H., 2017, Balancing Europe's wind-power output through spatial deployment informed by weather regimes, Nature Climate Change, 7, 557-562, DOI: 10.1038/nclimate3338.

Harrison G., Wallace A.R., 2006, Sensitivity of wave energy to climate change, IEEE Transactions on Energy Conversion, 20 (4), 870-877, DOI: 10.1109/TEC.2005.853753.

Hersbach H., Bell B., Berrisford P., Hirahara S., Horányi A., Muñoz Sabater J., Nicolas J., Peubey C., Radu R., Schepers D., Simmons A., Soci C., Abdalla S., Abellan X., Balsamo G., Bechtold P., Biavati G., Bidlot J., Bonavita M., Thépaut J.-N., 2020, The ERA5 global reanalysis, Quarterly Journal of the Royal Meteorological Society, 146 (730), 1999-20249, DOI: 10.1002/qj.3803.

Hess P., Brezowsky H., 1952, Berichte des Deutschen Wetterdienstes in der US-Zone, No. 33: Katalog der Grosswetterlagen Europas, Deutscher Wetterdienst Zentralamt Bad Kissingen, 39 pp.

Hoxha B., Kuriqi A., Filkoski R.V., 2023, Influence of seasonal air density fluctuations on wind speed distribution in complex terrains in the context of energy yield, Energy, Ecology and Environment, 8, 175-187, DOI: 10.1007/s40974-023-00301-9.

Huth R., Beck C., Philipp A., Demuzere M., Ustrnul Z., Cahynová M., Kyselý J., Tveito O.E., 2008, Classifications of Atmospheric Circulation Patterns, Annals of the New York Academy of Sciences, 1146 (1), 105-152, DOI: 10.1196/annals.1446.019.

Igliński B., Piechota G., Kielkowska U., Kujawski W., Pietrzak M.B., Skrzatek M., 2023, The assessment of solar photovoltaic in Poland: the photovoltaics potential, perspectives and development, Clean Technologies and Environmental Policy, 25, 281-298, DOI: 10.1007/s10098-022-02403-0.

Jerez S., Tobin I., Vautard R., Montávez J.P., López-Romero J.M., Thais F., Bartok B., Christensen O.B., Colette A., Déqué M., Nikulin G., Kotlarski S., van Meijgaard E., Teichmann C., Wild M., 2015, The impact of climate change on photovoltaic power generation in Europe, Nat Communications, 6, DOI: 10.1038/ncomms10014.

Jurasz J., Guezgouz M., Campana P.E., Kaźmierczak B., Kuriqi A., Bloomfield H., Hingray B., Canales F.A., Hunt J.D., Sterl S., Elkadeem M.R., 2024, Complementarity of wind and solar power in North Africa: potential for alleviating energy droughts and impacts of the North Atlantic Oscillation, Renewable and Sustainable Energy Reviews, 191, DOI: 10.1016/j.rser.2023.114181.

Kulesza K., 2017, Nowe spojrzenie na klasyfikację typów cyrkulacji atmosfery J. Lityńskiego, Prace Geograficzne, 150, 79-94, DOI: 10.4467/20833113PG.17.018.7322.

*Lityński* J., *1969*, Liczbowa klasyfikacja typów cyrkulacji i typów pogody dla Polski, Prace PIHM, 97, 3-14.

Moomaw W., Yamba F., Kamimoto M., Maurice L., Nyboer J., Urama K., Weir T., Jäger-Waldau A., Krey V., Sims R., Steckel J., Sterner M., Stratton R., Verbruggen A., Wiser R., 2012, Renewable energy and climate change, [in:] Renewable Energy Sources and Climate Change Mitigation, Special Report of the IPCC, 161-207, DOI: 10.1017/CBO9781139151153.005.

Muyuan L., Yao J., Shen Y., Yuan B., Simmonds I., Liu Y., 2023, Impact of synoptic circulation patterns on renewable energy-related variables over China, Renewable Energy, 215, DOI: 10.1016/j.renene.2023.05.133.

Niedźwiedź T., Łupikasza E., 2019, Atmospheric circulation in the investigation of Polish climatologists, Przegląd Geofizyczny, 64 (1-2), DOI: 10.32045/PG-2019-004.

Niedźwiedź T., Ustrnul Z., 2021, Change of Atmospheric Circulation, [in:] Climate Change in Poland: Past, Present, Future, M. Falarz (ed.), Springer, 123-150.

Nowosad M., 2008, Remarks about the Lityński classification calendar of the types of the atmospheric circulation, [in:] Advaces in Weather and Circulation Type Classification & Applications, COST 733 Mid-term Conference, Book of abstracts, Jagiellonian University Kraków, Institute of Meteorology and Water Management, Branch in Krakow, p. 66.

Pianko-Kluczyńska K., 2007, Nowy kalendarz typów cyrkulacji atmosfery według J. Lityńskiego, Wiadomości Meteorologii, Hydrologii, Gospodarki Wodnej, 51 (4), 65-85.

Pryor S., Barthelmie R., Kjellström E., 2005, Analyses of the potential climate change impact on wind energy resources in northern Europe using output from a Regional Climate Model, Climate Dynamics, 25, 815-835, DOI: 10.1007/s00382-005-0072-x.

del Río P., Peñasco C., Mir-Artigues P., 2018, An overview of drivers and barriers to concentrated solar power in the European Union, Renewable and Sustainable Energy Reviews, 81, 1019-1029, DOI: 10.1016/j.rser.2017.06.038.

Ustrnul Z., Czekierda D., Wypych A., 2010, Extreme values of air temperature in Poland according to different atmospheric circulation classifications, Physics and Chemistry of the Earth, 35 (9-12), 429-436, DOI: 10.1016/j.pce.2009.12.012.

Ustrnul Z., Wypych A., Czekierda D., 2013, Composite circulation index of weather extremes (the example for Poland), Meteorologische Zeitschrift, 22 (5), 551-559, DOI: 10.1127/0941-2948/2013/0464.

Ustrnul Z., Wypych A., Henek E., Maciejewski M., Bochenek B., 2015, Climatologically based warning system against meteorological hazards and weather extremes: the example for Poland, Natural Hazards, 77 (3), 1711-1729, DOI: 10.1007/s11069-015-1673-2.

Wypych A., Ustrnul Z., Henek E., 2014, Meteorological hazards – visualization system for National Protection Against Extreme Hazards for Poland, Meteorology Hydrology and Water Management, 2 (1), 37-42, DOI: 10.26491/mhwm/28306.

Wypych A., Ustrnul Z., Sulikowska A., Chmielewski F.-M., Bochenek B., 2017, Spatial and temporal variability of the frost-free season in Central Europe and its circulation background, International Journal of Climatology, 37 (8), 3340-3352, DOI: 10.1002/joc.4920.

Wickham H., 2016, ggplot2: Elegant Graphics for Data Analysis, Springer International Publishing, 213 pp., DOI: 10.1007/978-0-387-98141-3.

Wickham H., François R., 2014, dplyr: A Grammar of Data Manipulation, https://dplyr.tidyverse.org/.

van der Wiel K., Bloomfield H.C., Lee R.W., Stoop L.P., Blackport R., Screen J.A., Selten F.M., 2019, The influence of weather regimes on European renewable energy production and demand, Environmental Research. Letters, 14, DOI: 10.1088/1748-9326/ab38d3.

## Appendix

```
#!/usr/bin/env python
import cdsapi
import time
import eccodes
import numpy as np
import os

def generate_days(last_day):
    return [f"{day:02}" for day in range(1, last_day + 1)]

def compute_saturation_vapor_pressure(T):
    """Compute saturation vapor pressure given temperature in Celsius."""
    return 6.112 * np.exp(17.67 * T / (T + 243.5))

def compute_actual_vapor_pressure(q, p):
    """Compute actual vapor pressure given specific humidity and pressure."""
    return q * p / (0.622 + (0.378 * q))

def compute_relative_humidity(T, q, p):
    """Compute relative humidity given temperature in Celsius, specific humidity, and pressure."""
    e_s = compute_saturation_vapor_pressure(T)
    e = compute_actual_vapor_pressure(q, p)
    return (e / e_s) * 100

def compute_q_air(t, rh, p):
```

```
    return (p*100-
rh/100*611*np.exp((17.27*t)/(237.3+t)))/(287.058*(t+273.15))+(rh/100*611*np.exp((17.27*t)/(237.3+t)))/(46
1.495*(t+273.15))

def compute_ws(u, v, q_air):
    return np.sqrt(u**2+v**2)*(q_air/1.225)**(1/3)

c = cdsapi.Client()

def process_grib_file(input_filename1, input_filename2, output_filename):
    # Open the input grib file
    with open(input_filename1, 'rb') as fin1, open(input_filename2, 'rb') as fin2, open(output_filename, 'wb') as
out_file:
        # Create a new GRIB file for writing
        with open(output_filename, 'wb') as fout:
            while True:
                t, u, v, q = None, None, None, None
                # Extract parameters from the first file
                for _ in range(4): # Since there are 4 parameters in the first file
                    gid1 = eccodes.codes_grib_new_from_file(fin1)
                    if gid1 is None:
                        break
                    paramId1 = eccodes.codes_get(gid1, 'paramId')
                    if paramId1 == 130:
                        t = eccodes.codes_get_array(gid1, 'values') - 273.15
                    elif paramId1 == 131:
                        u = eccodes.codes_get_array(gid1, 'values')
                    elif paramId1 == 132:
                        v = eccodes.codes_get_array(gid1, 'values')
                    elif paramId1 == 133:
                        q = eccodes.codes_get_array(gid1, 'values')
                # Extract pressure from the second file
                gid2 = eccodes.codes_grib_new_from_file(fin2)
                if gid2 is None:
                    break
                p = eccodes.codes_get_array(gid2, 'values')/100
                # Check if we have all parameters
                if all([x is not None for x in [t, u, v, q, p]]):
```

```
            rh = compute_relative_humidity(t, q, p)
            q_air = compute_q_air(t, rh, p)
            ws = compute_ws(u, v, q_air)
        #quantiles = [0, 25, 50, 75, 100]  # Percentiles: min, Q1, median, Q3, max
        #for q1 in quantiles:
        #value = np.percentile(ws, q1)
        #    print(f"{q1}th percentile: {value}")
        # Check if ws is scalar, and if so, convert it to an array
        if np.isscalar(ws):
            ws_array = np.full_like(u, ws)
        else:
            ws_array = ws
        # Clone the gid1 (temperature) to create a new grib message for ws
        new_gid = eccodes.codes_clone(gid1)
        eccodes.codes_set(new_gid, 'paramId', 10)  # Some unused parameter ID for ws
        eccodes.codes_set_array(new_gid, 'values', ws_array)
        # Write the new message to the output grib file
        eccodes.codes_write(new_gid, out_file)
        # Release the grib IDs
        eccodes.codes_release(gid1)
        eccodes.codes_release(gid2)
        eccodes.codes_release(new_gid)


# Loop over years from 1940 to 2022
for year in range(1943, 1979):
    # Loop over all months in a year
    for month in range(1, 13):
        # Generate start and end date for the month
        if month in [4, 6, 9, 11]:
            last_day = 30
        elif month == 2:
            if (year % 4 == 0 and year % 100 != 0) or (year % 400 == 0):
                last_day = 29
            else:
                last_day = 28
        else:
            last_day = 31
```

```
start_date = f"{year}-{month:02}-01"
end_date = f"{year}-{month:02}-{last_day}"
output_filename = f"ERA5-133ml_uvtq_{year}{month:02}.grib"
output_filename2 = f"ERA5-133ml_p_{year}{month:02}.grib"
print(f"Retrieving data for {start_date} to {end_date}...")
c.retrieve('reanalysis-era5-complete', {
    'date': f'{start_date}/to/{end_date}',
    'levelist': '133',
    'levtype': 'ml',
    'param': '130/131/132/133',
    'stream': 'oper',
    'time': '00/to/23/by/1',
    'type': 'an',
    'area': '90/-180/-90/180',
    'grid': '0.25/0.25',
    'format': 'grib',
}, output_filename)

c.retrieve('reanalysis-era5-single-levels',
{
    'product_type': 'reanalysis',
    'variable': 'surface pressure',
    'year': year,
    'month': f"{month:02}",
    'day': generate_days(last_day),
    'time': [
        '00:00', '01:00', '02:00',
        '03:00', '04:00', '05:00',
        '06:00', '07:00', '08:00',
        '09:00', '10:00', '11:00',
        '12:00', '13:00', '14:00',
        '15:00', '16:00', '17:00',
        '18:00', '19:00', '20:00',
        '21:00', '22:00', '23:00',
    ],
    'grid': '0.25/0.25',
    'format': 'grib',
},output_filename2)
```

```
output_ws_filename = f"ERA5-133ml_ws_{year}{month:02}.grib"
# Process the downloaded grib file
process_grib_file(output_filename,output_filename2,output_ws_filename)
# Wait for 1 second before sending the next request
time.sleep(1)
os.remove(output_filename)
os.remove(output_filename2)
```

# Temperature trend analysis: a case study of Kabul, Afghanistan

Homayoon Raoufi, Shirullah Taqwa

Kunduz University, Afghanistan

Sayeed Nabi Attayee

University of Tehran, Iran

Abstract

Climate change is one of the most important problems significantly affecting the exosphere, both directly and indirectly. The impacts of climate change can be disastrous not only for the environment but also for the lives, safety, and property of major populations, particularly in Afghanistan. This study assesses the variability of temperature trends in Kabul, Afghanistan. The predictands, i.e., the daily observed temperature data, were collected from local organizations, and the predictors were gleaned from the outputs of global climate models (GCM) based on the Fifth Assessment Report (AR5) of the Intergovernmental Panel on Climate Change (IPCC). Two statistical downscaling models were used to simulate future climate conditions under three scenarios. Trend analysis was conducted by linear regression, and the performance of the two downscaling methods was checked by using measured indicators. The results revealed that temperature will increase from 2025 to 2100 relative to 1990-2020 under three model regional climate predictions (RCP). By 2100, the maximum temperature would increase by 1.8°C (7.7%), 2.5°C (10.3%), and 3.7°C (14.3%) according to RCP 2.6, RCP 4.5 and RCP 8.5, respectively. Moreover, the annual average temperature for the period of 2025-2100 was predicted to rise by 2.3°C (12.9%) under RCP 2.6, 2.6°C (14.3%) under RCP 4.5, and 3.6°C (18.8%) under RCP 8.5 relative to the reference period (1990-2020). Minimum temperatures also increase in the range of 2.2°C (19.9%) under RCP 2.6, 2.9°C (24.9%) under RCP 4.5 and 4.3°C (32.7%) under RCP 8.5. These temperature increases would affect ecosystems, crop production, human health, and many other sectors.

Keywords

Climate change, temperature trends, downscaling models, reference and projection periods, Kabul, Afghanistan.

Submitted 9 May 2024, revised 24 September 2024, accepted 10 October 2024

DOI: 10.26491/mhwm/194452

## 1. Introduction

Climate change is currently the most important topic globally. Many studies have determined the occurrence and effects of climate change worldwide (Saddique et al. 2019), but their impacts are not uniform across the globe: some regions are more susceptible to climate change (Munawar et al. 2022). It is widely accepted that human activities are major drivers of recent global climate change and global warming recorded since the pre-industrial era (Solomon et al. 2009). Changes in atmospheric properties impose a wide range of direct and indirect impacts on the environment, agriculture, food security, human health, and the hydrological cycle (Javadinejad et al. 2021). Meteorological properties change frequently, through significant changes in local distributional properties of temperature and precipitation, among other atmospheric variables (IPCC 2007a, 2007b, 2013). Changes in temperature variability can occur from diurnal to multi-decadal time scales and from the local to the global scale, potentially even displaying opposing signals in different seasons and at different spatial scales (IPCC 2022). According to the Intergovernmental Panel on Climate Change (IPCC) 6th assessment report, the projected average warming in Afghanistan will be about 1.4-6.0°C by the end of 2100.

In particular, the impacts of climate change are very serious for Afghanistan. Extreme events, including heat waves, floods, and droughts, are increasing, and they threaten the lives, safety, and property of major human populations (WBG 2021). The majority of Afghanistan's population relies on available natural resources directly or indirectly for their livelihoods (UNDP 2017). The increased frequency of extreme climatic events in Afghanistan has caused great economic losses (UNDP 2017) and threatens the foundations of the country's economy, stability, and food security. For example, the impacts of climate change have negative consequences for crop production; a reduction in crop yields reduces food security and damages the livelihoods of people. The country needs to promote and strengthen adaptation strategies to reduce the risks of climate change. It is important to know how trends, such as temperature trends, are changing.

Temperature trends were assessed by statistical downscaling models in this study. The observational data were acquired from local organizations such as the Ministry of Agriculture, Irrigation and Livestock (MAIL), the Ministry of Energy and Water (MEW), and the Meteorological Department of Afghanistan (MDA). The modeling study employed General Circulation Models (GCM) based on the Fifth Assessment Report (AR5) of the IPCC that is available in the Coupled Model Intercomparison Project Phase 5 (CMIP5). The GCMs support the assessment of potential climate change impacts on a global scale (Disasa, Haofang 2022). Predictors, in the statistical downscaling model (SDSM) for the relationship between the National Centers for Environmental Prediction (NCEP) predictors and local predictands (precipitation), were applied for screening purposes (Saddique et al. 2019; Munawar et al. 2022). The NCEP and National Center for Atmospheric Research (NCAR) data were acquired from the GCM (CanESM2) model.

The SDSM and the Long-Ashton research station weather generator (LARS-WG) are two well-known statistical downscaling models to downscale GCM outputs such as temperature, rainfall, and solar radiation (Saddique et al. 2019). Hence, many recent studies have focused on the evaluation and comparison of the two models in terms of their ability to simulate mean temperature and extreme temperature frequencies using a parametric distribution at a local scale (Hassan et al. 2014). The minimum temperature ($T_{min}$), maximum temperature ($T_{max}$), and average temperature ($T_{ave}$) were evaluated by using observed and generated climatic data under three representative concentration pathways (RCP) scenarios: RCP 2.6, RCP 4.5, and RCP 8.5. Future projections from the two models did not agree; the results of LARS-WG were close to the reference period, whereas SDSM projections differed significantly. Hassan et al. (2014) claimed that the different results arose from differences in downscaling strategies and basic concepts. Both models, however, can be adopted as downscaling tools for future periods (Hashmi et al. 2011; Hassan et al. 2014).

For Afghanistan, there are not many published papers on atmospheric trend analyses in recent years based on either of the two models. The main objective of this study is to assess atmospheric temperature change in the reference and future periods (1990-2100). The results will help to define the scale of change in temperature trends, thus supporting policies for adaptation and mitigation strategies to reduce climate change impacts.

## 2. Materials and methods

### 2.1. Study area

Afghanistan, located in the heart of south-central Asia between 33°56'2.54" N and 67°42'12.35" E (Sarwary et al. 2023), has a semi-arid climate (UNDP 2017; WBG 2021; Rasouli 2022). There is great variation in the climate, soil, topography, vegetation, and natural ecosystems of the country (Aich et al. 2017). Temperature varies greatly by season and altitude, with mountain regions ranging from <0 to >35°C. The average surface air temperature is 13.37°C with a range of 1.92°C, 13.74°C, 24.26°C and 13.41°C in December-February, March-May, June-August, and September-November, respectively. The average annual precipitation is 337.97 mm with a range of 134.35, 146.04, 22.03, and 35.05 mm in December-February, March-May, June-August, and September-November, respectively (WBG 2021).

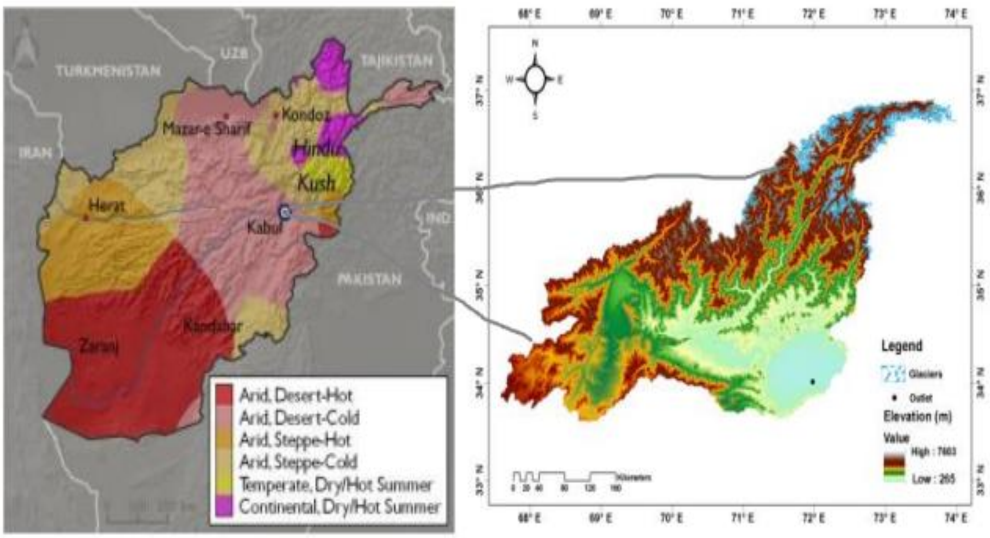


Fig. 1. The study area (USAID 2016; Bokhari et al. 2018).

This study was conducted in Kabul, the capital of Afghanistan, south of the Hindu-Kush mountain range. The climate of Kabul is affected by the climate of the Hindu-Kush mountains. This region has a continental, cold, semi-arid climate with rainfall concentrated in the winter and spring months. Winter (January-March) is a very cold season with snowfall, while spring is more humid with higher precipitation frequency. Summer has very low precipitation; it is the warmest season, with a longer sunshine period of about 356.8 hours per month in July and very low humidity (36% in June). Autumn has low rainfall of 3.7 mm, 18.6 mm, and 21.6 mm for October, November, and December, respectively, with warm afternoons and cool evenings. Kabul is situated at 34.45 N and 69.00 E at an elevation of 1805 m above mean sea level and covers a total area of 4655.25 km$^2$ (Table 1). The local steppe climate influences Kabul, which receives little yearly rainfall. The average annual temperature is 11.4°C, and the annual total precipitation is 362 mm. The driest month is June with about 1 mm of precipitation. Most rainfalls in March average

88 mm. July, with an average temperature of 23.2°C, is the warmest month. The lowest average temperature for the year is –2.9°C in January.

Table 1. Details of the meteorological stations in Kabul.

| Station name | Lat (N) | Long (E) | Elevation (m) | Annual rainfall (mm) | Mean temperature (C) |
|---|---|---|---|---|---|
| Kabul – airport | 34.55 | 69.21 | 1791 | 197 | 14.10 |

## 2.2. Data description

### 2.2.1. Site data

The daily observed maximum ($T_{max}$) and minimum temperature ($T_{min}$) were acquired from the meteorological stations collected by local organizations, including MDA, MAIL, and MEW, from 2003 to 2020 and online data sets. The thirty years of data (1990-2020) were used as the observed data period.

### 2.2.2. NCEP/NCAR reanalysis data

The daily reanalysis data for the baseline period were acquired from the NCEP/NCAR. NCEP predictors, in the SDSM model, for the relationship among the NCEP predictors and local predictands were applied for screening purposes (Saddique et al. 2019; Munawar et al. 2022). The NCEP/NCAR data were acquired from the GCM (CanESM2) model.

## 2.3. RCP Scenario Data

The Coupled Model Intercomparison Project Phase 5 (CMIP5) IPCC report that provides a wider picture of future climate change scenarios was used. Three future climate change scenarios, including a mitigation scenario (RCP 2.6), a medium stabilization scenario (RCP 4.5), and an extreme scenario (RCP 8.5) (Saddique et al. 2019) were selected for the periods of 1990-2100. RCPs describe different levels of greenhouse gases and other radiative forcing that might occur in the future. RCP 2.6 leads to a very low forcing level, RCP 4.5 leads to a medium forcing level, and RCP 8.5 leads to very high emission scenarios (Wayne 2013). Trend analysis was conducted by parametric methods such as regression.

## 2.4. Projection and downscaling

Downscaling of $T_{min}$ and $T_{max}$ was performed using two models, SDSM and LARS-WG. The available observed data were obtained from MAIL, AMD, and MEW and the missing data were derived from the open-source datasets for the period of 1990-2020.

LARS-WG is a stochastic weather generator that was applied for the simulation of weather data for reference and future climatic variable conditions. The observed climatic data ($T_{max}$ and $T_{min}$) were used in LARS-WG to generate time series for future periods. The future climate scenarios were generated for the periods of 2025 -2100 for selected RCPs (RCP 2.6, RCP 4.5, and RCP 8.5) based on the baseline parameters.

SDSM was used to develop the relationship between the predictands ($T_{max}$ and $T_{min}$) and NCEP/NCAR predictors. NCEP predictors were used to simulate the time series data for the periods. The performance of the models to generate synthetic time series was calibrated and validated (Saddique et al. 2019; Javadinejad et al. 2021).

### 2.5. Model performance

Trend analysis was conducted by parametric methods such as linear regression as given by equation 1:

$$Y = a + bX \tag{1}$$

where: $X$ is the explanatory variable; $Y$ is the dependent variable; $a$ is the intercept, $b$ is the slope of the line.

The performances of the models were estimated by comparing the observed and generated $T_{min}$ and $T_{max}$ data by using statistical indicators. These indicators were computed by the equation 2-6 as follows:

$$R = \frac{\sum(X-\bar{x})(y-\overline{y})}{\sqrt{(x-\overline{x})^2 - \sum(y-\overline{y})^2}} \tag{2}$$

$$R^2 = \text{Var-Exp by mod/ Total variance} \tag{3}$$

$$MAE = \frac{\sum_{i=1}^{n}[x_i - y_i]}{n} \tag{4}$$

$$RMSE = \sqrt{\frac{\sum_{i=1}^{n}((Xi - Yi)2}{n}} \tag{5}$$

$$NRMSE = RMSE/Xi \tag{6}$$

Here: $R$ is the correlation coefficient; $R^2$ is the determination coefficient; $MAE$ is mean absolute error; $RMSE$ is root mean square error; $NRMSR$ is normalized root mean square error; $X$ and $Y$ are the values of variables; and $\bar{x}$ and $\bar{y}$ are the means of variables. $Xi$ is the observed value of variables; $Yi$ is the simulated value by the models; and n is the measured number (Ababaei et al. 2010; Delavar et al. 2016; Kounani et al. 2021; Munawar et al. 2022).

## 3. Results

### 3.1. Evaluation criteria

The results of the statistical measures proved both models were efficient over the validation period for the variables $T_{min}$ and $T_{max}$. Table 2 illustrates measured indices of the statistical downscaling models. The models (SDSM and LARS-WG) were assessed (validated) by using statistical measures: $R$, $R^2$, $MAE$, $RMSE$, and NRMSE (%) between observed and simulated data. The results of statistical measurements proved that both models are efficient for the estimation of $T_{min}$ and $T_{max}$, as shown in Table 2.

Table 2. Performance indicators of maximum and minimum temperature

| Variables | Models | *R* | $R^2$ | *MAE* | *RMSE* | *NRMSE* (%) |
|---|---|---|---|---|---|---|
| $T_{min}$ | LARS-WG | 0.9996 | 0.9992 | 4.49 | 0.158 | 0.94 |
| | SDSM | 0.99 | 0.99 | 0.1121 | 0.159 | 0.85 |
| $T_{max}$ | LARS-WG | 0.9989 | 0.9979 | 0.161 | 0.17 | 0.82 |
| | SDSM | 0.99 | 0.99 | 0.02 | 0.006 | 0.03 |

## 3.2. Temperature trend analysis for observation data

To analyze the variation of temperature variables for Kabul meteorological stations, daily observed data from local data sets (MAIL 2022; MDA 2022; MEW 2022) were used. The monthly and yearly averages of temperature are shown in Figure 2.

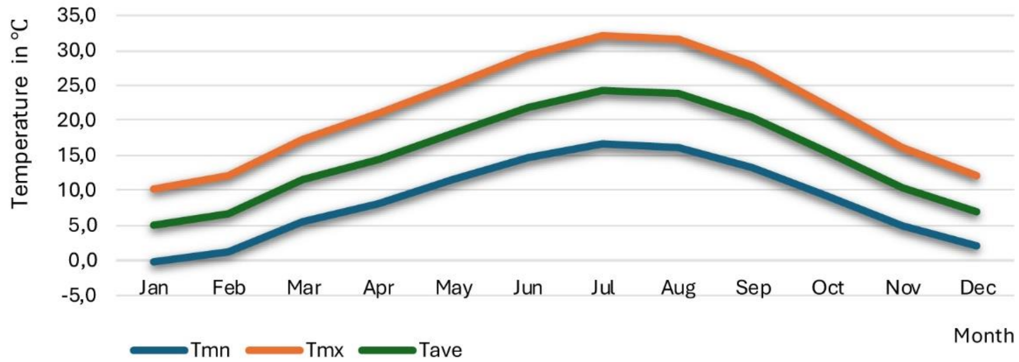


Fig. 2. The average monthly maximum ($T_{max}$), mean ($T_{ave}$), and minimum ($T_{min}$) temperatures during the reference period (1990-2020).

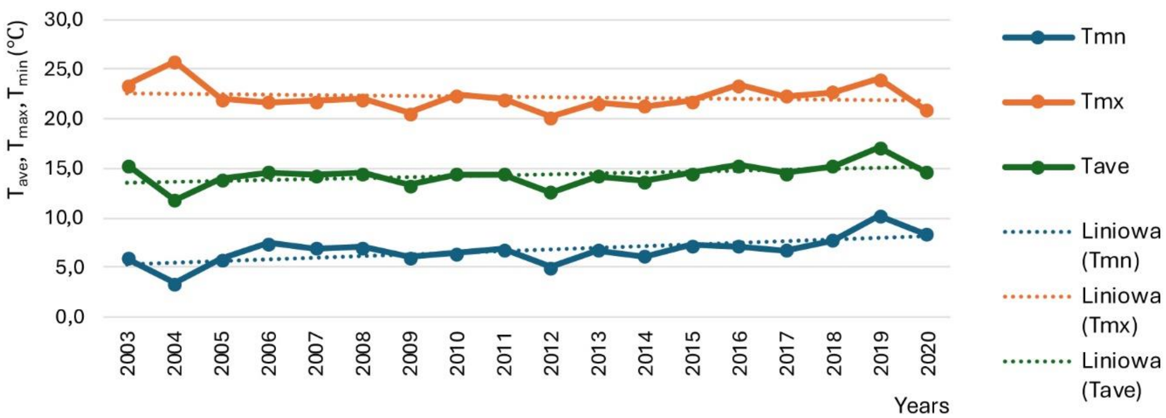


Fig. 3. Multi-year sequence (2003-2020) of the average annual maximum ($T_{max}$), annual mean ($T_{ave}$), and annual minimum ($T_{min}$) temperature.

Analysis of average monthly temperature trends indicates that January is the coldest month and July is the warmest month, with a range of –2 to 16.7°C in $T_{min}$, 5.0-24.3°C in average temperature, and 10.2-32.1°C in $T_{max}$.

## 3.3. Temperature trend analysis for the future

Annual changes were projected for maximum, average, and minimum temperatures under three RCPs for the future (2025-2100). Table 3 shows the projected average temperature during 2025-2100 based on the reference period (1990-2020) under RCP 2.6, RCP 4.5, and RCP 8.5. Moreover, Figure 3 shows the average temperature change compared to the future and baseline periods.

Table 3. Average annual average temperature during reference (1990-2020) and future (2025-2100) periods.

| Annual average temperature (°C) | | | | |
|---|---|---|---|---|
| | Ref. | RCP 2.6 | RCP 4.5 | RCP 8.5 |
| 1990 | 15.1 | | | |
| 1995 | 15.7 | | | |
| 2000 | 15.7 | | | |
| 2005 | 15.3 | | | |
| 2010 | 15.4 | | | |
| 2015 | 15.9 | | | |
| 2020 | 15.7 | | | |
| 2025 | | 16.8 | 16.7 | 17.0 |
| 2030 | | 16.8 | 17.0 | 17.3 |
| 2040 | | 17.1 | 17.1 | 17.6 |
| 2050 | | 17.7 | 18.0 | 18.8 |
| 2060 | | 17.7 | 18.1 | 18.9 |
| 2070 | | 17.7 | 19.0 | 20.7 |
| 2080 | | 20.6 | 19.1 | 17.8 |
| 2090 | | 17.8 | 19.2 | 21.9 |
| 2100 | | 18.5 | 19.5 | 22.6 |
| Average | 15.6 | 17.8 | 18.2 | 19.2 |
| Difference | | 2.3 | 2.6 | 3.6 |
| Change (%) | | 12.9 | 14.3 | 18.8 |

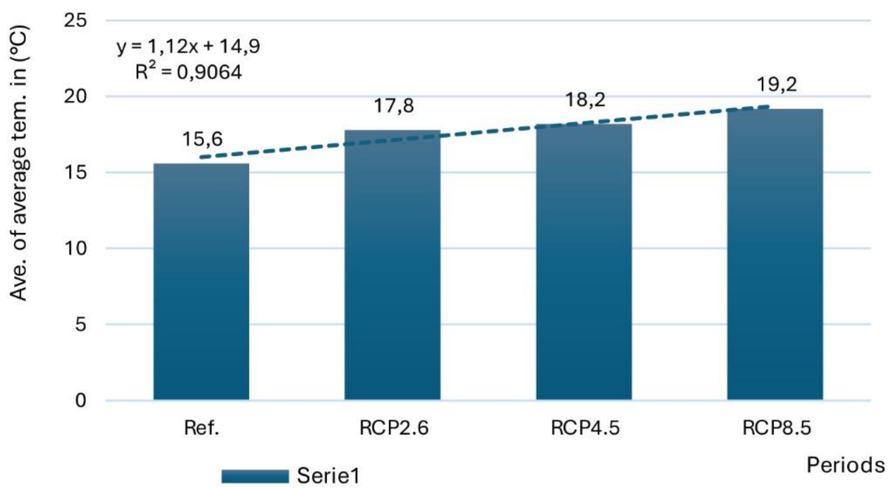


Fig. 4. The comparison of annual average temperature for the reference and future periods under different RCPs.

Average annual maximum temperature was shown in Table 4 and Figure 5 during reference and future periods.

Table 4. Average annual maximum temperature during reference (1990-2020) and future (2025-2100) periods.

| Annual maximum temperature (°C) | | | | |
|---|---|---|---|---|
| | Ref. | RCP2.6 | RCP4.5 | RCP8.5 |
| 1990 | 21.9 | | | |
| 1995 | 22.4 | | | |
| 2000 | 22.1 | | | |
| 2005 | 22.1 | | | |
| 2010 | 22.3 | | | |
| 2015 | 22.6 | | | |
| 2020 | 22.1 | | | |
| 2025 | | 23.5 | 23.8 | 24.1 |
| 2030 | | 23.6 | 23.5 | 23.7 |
| 2040 | | 23.3 | 23.4 | 23.6 |
| 2050 | | 24.2 | 24.6 | 25.3 |
| 2060 | | 24.0 | 24.4 | 25.1 |
| 2070 | | 24.4 | 25.7 | 27.1 |
| 2080 | | 24.2 | 25.6 | 27.0 |
| 2090 | | 24.5 | 25.8 | 28.5 |
| 2100 | | 25.0 | 26.3 | 29.0 |
| Average | 22.2 | 24.1 | 24.8 | 25.9 |
| Difference | | 1.8 | 2.5 | 3.7 |
| Change (%) | | 7.7 | 10.3 | 14.3 |

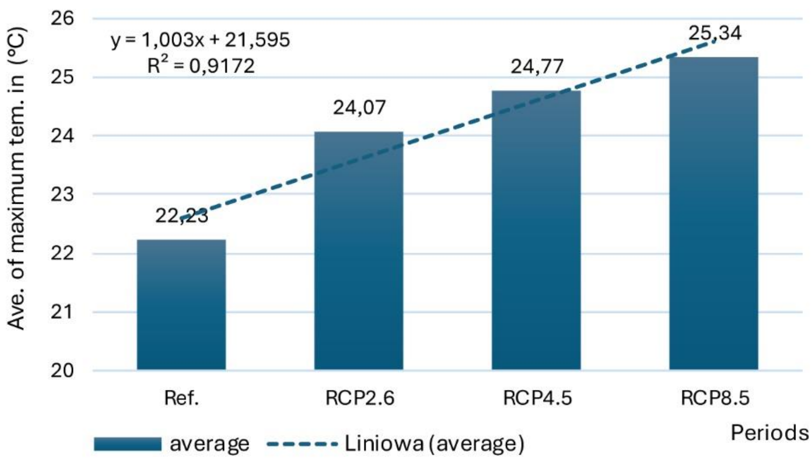


Fig. 5. The comparison of average maximum temperature for the reference (1990-2020) and future (2025-2100) periods under RCP 2.6, 4.5, and 8.5.

Table 5 and Figure 6 illustrated the average minimum temperature based on reference periods.

Table 5. Average annual minimum temperature during reference (1990-2020) and future (2025-2100) periods.

| Annual minimum temperature (°C) | | | | |
|---|---|---|---|---|
| | Ref. | RCP2.6 | RCP4.5 | RCP8.5 |
| 1990 | 8.3 | | | |
| 1995 | 9.0 | | | |
| 2000 | 9.2 | | | |
| 2005 | 8.5 | | | |

| | | | | |
|---|---|---|---|---|
| 2010 | 8.5 | | | |
| 2015 | 9.2 | | | |
| 2020 | 9.3 | | | |
| 2025 | | 10.1 | 10.6 | 11.0 |
| 2030 | | 10.1 | 10.6 | 11.0 |
| 2040 | | 10.9 | 10.9 | 11.4 |
| 2050 | | 11.2 | 11.6 | 12.4 |
| 2060 | | 11.5 | 11.9 | 12.8 |
| 2070 | | 11.1 | 12.4 | 13.9 |
| 2080 | | 11.5 | 12.7 | 14.3 |
| 2090 | | 11.2 | 12.4 | 15.6 |
| 2100 | | 12.1 | 13.3 | 16.3 |
| Average | 8.9 | 11.1 | 11.8 | 13.2 |
| Difference | | 2.2 | 2.9 | 4.3 |
| Change (%) | | 19.9 | 24.9 | 32.7 |

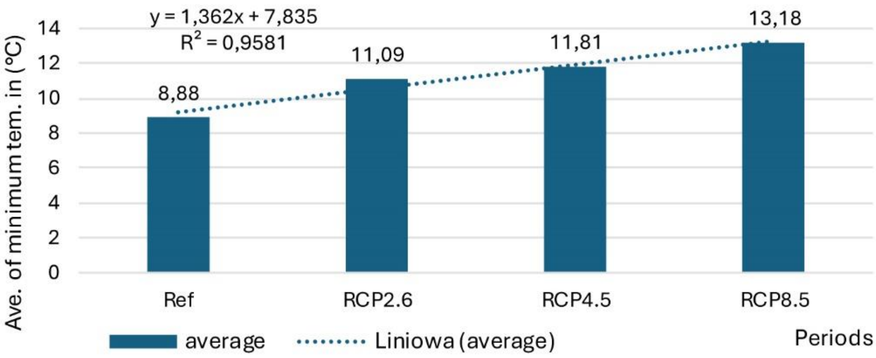


Fig. 6. The comparison of average minimum temperature for the reference (1990-2020) and future (2025-2100) periods under RCP 2.6, 4.5 and 8.5.

The annual change in temperature trends (average, maximum, and minimum temperature) is shown in Tables 6-8. Table 9 shows the monthly change in temperature trends. Table 9 shows the change in temperature trends by month (maximum, average, and minimum temperature) over the projection period (2025-2100)

The monthly projected $T_{min}$ showed an increase ranging between 2.38°C, 3.20°C, and 4.61°C under RCP 2.6, RCP 4.5, and RCP 8.5, respectively. The monthly projected maximum temperature showed an increase ranging between 1.88°C, 2. ° C, and 3.92°C under RCP 2.6, RCP 4.5, and RCP 8.5, respectively. Also, the monthly projected average temperature showed an increase ranging between 2.13, 2.92, and 4.26°C under RCP 2.6, RCP 4.5, and RCP 8.5, respectively. The results showed a continuously increasing trend of projected temperature in future scenarios.

Table 6. Annual changes of maximum temperature during the projection period (2025-2100) under RCP 2.6, RCP 4.5, and RCP 8.5.

| Annual change in maximum temperature (°C) | | | |
|---|---|---|---|
| | RCP2.6 | RCP4.5 | RCP8.5 |
| 2025 | 1.3 | 1.6 | 1.8 |
| 2030 | 1.4 | 1.2 | 1.5 |
| 2040 | 1.1 | 1.1 | 1.4 |
| 2050 | 2.0 | 2.4 | 3.1 |
| 2060 | 1.8 | 2.2 | 2.9 |
| 2070 | 2.1 | 3.5 | 4.9 |
| 2080 | 1.9 | 3.3 | 4.8 |
| 2090 | 2.2 | 3.6 | 6.3 |
| 2100 | 2.7 | 4.0 | 6.8 |
| Avg. | 1.8 | 2.5 | 3.7 |

Table 7. Annual change in average temperature during the projection period (2025-2100) under RCP2.6, RCP4.5 and RCP8.5.

| Annual change in average temperature (°C) | | | |
|---|---|---|---|
| | RCP 2.6 | RCP 4.5 | RCP 8.5 |
| 2025 | 1.2 | 1.1 | 1.4 |
| 2030 | 1.2 | 1.4 | 1.7 |
| 2040 | 1.5 | 1.5 | 2.0 |
| 2050 | 2.1 | 2.4 | 3.2 |
| 2060 | 2.1 | 2.5 | 3.3 |
| 2070 | 2.1 | 3.4 | 5.1 |
| 2080 | 5.0 | 3.5 | 2.2 |
| 2090 | 2.2 | 3.6 | 6.3 |
| 2100 | 2.9 | 3.9 | 7.0 |
| Ave. | 2.2 | 2.6 | 3.6 |

Table 8. Annual change in minimum temperature during the projection period (2025-2100) under RCP 2.6, RCP 4.5 and RCP 8.5.

| Annual change in minimum temperature (°C) | | | |
|---|---|---|---|
| | RCP 2.6 | RCP 4.5 | RCP 8.5 |
| 2025 | 1.23 | 1.7 | 2.14 |
| 2030 | 1.26 | 1.68 | 2.13 |
| 2040 | 2.03 | 2.06 | 2.5 |
| 2050 | 2.3 | 2.67 | 3.47 |
| 2060 | 2.64 | 3.06 | 3.89 |
| 2070 | 2.22 | 3.49 | 5.04 |
| 2080 | 2.61 | 3.83 | 5.42 |
| 2090 | 2.36 | 3.51 | 6.68 |
| 2100 | 3.21 | 4.38 | 7.44 |
| Avg. | 2.2 | 2.9 | 4.3 |

Table 9. Changes in temperature trends by month ($T_{min}$, $T_{max,}$ and $T_{avg}$) under RCP 2.6, RCP 4.5, and RCP 8.5 over the period 2025-2100.

| | $T_{min}$ | | | $T_{max}$ | | | $T_{avg}$ | | |
|---|---|---|---|---|---|---|---|---|---|
| | RCP 2.6 | RCP 4.5 | RCP 8.5 | RCP 2.6 | RCP 4.5 | RCP 8.5 | RCP 2.6 | RCP 4.5 | RCP 8.5 |
| Jan | 2.56 | 3.57 | 5.11 | 2.06 | 3.14 | 4.08 | 2.31 | 3.35 | 4.60 |
| Feb | 3.64 | 4.88 | 6.28 | 2.85 | 3.96 | 4.92 | 3.24 | 4.42 | 5.60 |
| Mar | 3.86 | 4.76 | 6.27 | 2.66 | 3.42 | 4.76 | 3.26 | 4.09 | 5.52 |
| Apr | 3.96 | 4.65 | 6.07 | 3.70 | 4.58 | 6.06 | 3.83 | 4.62 | 6.07 |
| May | 3.07 | 3.54 | 4.75 | 2.95 | 3.81 | 5.10 | 3.01 | 3.68 | 4.93 |
| Jun | 2.34 | 2.84 | 3.99 | 2.66 | 3.47 | 4.64 | 2.50 | 3.16 | 4.32 |
| Jul | 1.79 | 2.55 | 3.73 | 1.22 | 1.78 | 2.96 | 1.50 | 2.16 | 3.35 |
| Aug | 1.33 | 2.28 | 3.58 | 1.33 | 1.74 | 3.05 | 1.33 | 2.01 | 3.32 |
| Sep | 1.05 | 2.04 | 3.53 | 0.63 | 1.14 | 2.79 | 0.84 | 1.59 | 3.16 |
| Oct | 1.67 | 2.57 | 4.12 | 0.61 | 1.16 | 2.81 | 1.14 | 1.86 | 3.46 |
| Nov | 1.74 | 2.52 | 4.06 | 0.79 | 1.52 | 2.82 | 1.26 | 2.02 | 3.44 |
| Dec | 1.71 | 2.37 | 3.94 | 1.23 | 2.09 | 3.12 | 1.47 | 2.23 | 3.53 |

## 4. Discussion and conclusion

This study was carried out to estimate temperature variables in the reference (1990-2020) and future (2025-2100) periods under RCP 2.6, RCP 4.5, and RCP 8.5 by using two statistical downscaling models (SDSM and LARS-WG). In general, according to the performance indicators, both models (SDSM and LARS-WG) are efficient for downscaling and projecting, but the LARS-WG model was approximately more suitable. The temperature trends (minimum, maximum, and average temperature) are shown to increase by a range of 0.28°C, 0.69°C, and 0.48°C, respectively the reference period (1990-2020).

The future temperature is predicted to increase from 2025 to 2100 at much higher rates compared to the reference period, under three RCPs. Average temperature showed an increase under RCP 2.6, RCP 4.5, and RCP 8.5 of 2.3°C, 2.6°C, and 3.6°C, respectively. Average temperature would increase by 12.9%, 14.3%, and 18.8% (Table 3, Fig. 4) by 2100 under RCP 2.6, RCP 4.5 and RCP 8.5, respectively. Maximum temperature would increase under RCP 2.6, RCP 4.5, and RCP 8.5 by 1.8°C, 2.5°C, and 3. ° C, respectively, for the future periods. Maximum temperature would increase by 7.7%, 10.3%, and 14.3% under RCP 2.6, RCP 4.5, and RCP 8.5, respectively, by 2100 compared to the reference period. Moreover, an increase in annual minimum temperature by 2100 was predicted at 2.2 C, 2.9 C, and 4.3 C under RCP 2.6, RCP 4.5, and RCP 8.5, respectively. The minimum temperature would increase at a rate of 19.9%, 24.9%, and 32.7% (Table 5, Fig. 6) under RCP 2.6, RCP 4.5, and RCP 8.5, respectively, during 2025-2100. Temperature increases with a range of values have been reported in many studies, such as Aich et al. (2017), Hassanyar et al. (2017), UNDP (2017), and WBG (2021). A 1°C increase from 1900-2017 was reported in WBG (2021). Annual temperatures have also been projected to increase by 3.50°C and 7.00°C (NEPA 2018), or 1.70°C and 2.30°C (Sarwary et al. 2023) by 2050; increases of 2.00°C and 6.50°C (FAO 2016) or 2.70°C and 5.50°C (WBG 2021) by 2100 under RCP 4.5 and RCP 8.5, respectively, relative to the baseline period in Afghanistan. The temperature increase was projected to occur most rapidly during spring and summer at higher altitudes (central highlands and Hindu Kush) (NEPA 2018). Moreover, an increase in global mean temperature by 0.30-1.70°C under RCP 2.6, 1.10-2.60°C under RCP 4.5, and

2.60-4.80°C under RCP 8.5 has been projected by the end of the 21st century (2081-2100) relative to 1986-2005 (IPCC 2014). The global mean temperature is expected to increase by 1.40-5.80 C by 2100 (Sarwary et al. 2023).

This study revealed that temperature trends increase during reference and future periods. Climatic variation can affect many aspects of environmental systems. Although this study highlights temperature trends, additional climatic factors such as precipitation, wind speed, and solar radiation need further study. An increase in temperature would affect ecosystems, agricultural production, human health, and more environmental systems.

Afghanistan has faced a higher increasing temperature than the global average over the century, and it shows extreme vulnerability to hazards such as drought and flood. Findings revealed that an increase in temperatures (average temperature and maximum temperature) harms wheat production because of heat and drought stress, while the increase in minimum temperature has a positive effect on wheat production. This vulnerability is amplified by poverty, undernourishment, food insecurity, and inequality. These are the driving forces of negative impacts on agriculture, natural resources, natural ecosystems, forests, water resources, and society.

## References


Ababaei B., Sohrabi T., Mirzaei F., Rezaverdinejad V., Karimi B., 2010, Climate change impact on wheat yield and analysis of the related risks: (case study: Esfahan Ruddasht Region), The Knowledge Water and Soil, 20 (3), 136-150.

Aich V., Noor A.A., Alec K., Ahmad J.K., Fred H., Heiko P., Andrew S., Eva N.P., 2017, Climate change in Afghanistan deduced from reanalysis and Coordinated Regional Climate Downscaling Experiment (CORDEX) – South Asia simulations, Climate, 5 (2), DOI: 10.3390/cli5020038.

Bokhari S.A.A., Burhan A., Jahangir A., Shakeel A., Haris M., Ghulam R., 2018, Future climate change projections of the Kabul River Basin using a multi-model ensemble of high-resolution statistically downscaled data, Earth Systems and Environment, 2, 477-497, DOI: 10.1007/s41748-018-0061-y.

Chen Y.-J., Lin H.-J., Liou J.-J., Cheng C.-T., Cheng Y.-M., 2022, Assessment of flood risk map under climate change RCP8.5 scenarios in Taiwan, Water, 14 (2), DOI: 10.3390/w14020207.

Delavar N., Akhavan S., Mehnathkesh A., 2016, Climate change impact on some factors affecting rainfed wheat growth (case study: Chaharmahal and Bakhtiari Province), Journal of Water and Soil Science, 21 (2), 131-149, DOI: 10.18869/acadpub.jstnar.21.2.131.

Disasa K.N., Haofang Y., 2022, Evaluating climate change impact of rainfed maize production yield in Southern Ethiopia, DOI: 10.21203/rs.3.rs-1212888/v1.

Fanseca A.R., Santos J.A., 2019, Predicting hydrologic flows under climate change: The Tâmega Basin as an analog for the Mediterranean region, Science of the Total Environment, 668, 1013-1024, DOI: 10.1016/j.scitotenv.2019.01.435.

FAO, 2016, Climate Change in Afghanistan. What Does It Mean for Rural Livelihoods and Food Security?, Report, Food and Agriculture Organization of the United Nations, available online at https://www.unep.org/resources/report/climate-change-afghanistan-what-does-it-mean-rural-livelihoods-and-food-security (data access 25.11.2024).

Gancalves C., Honrado J.P., Cerejeira J., Sousa R., Fernandes P.M., Vaz A.S., Alves M., Araújo M., Carvalho-Santos C., Fonsece A., Fraga H., Gonçalves J.F., Lomba A., Pinto E., Vicente J.R., Santos J.A., 2022, On the development of a regional climate change adaptation plan: integrating model-assisted projections and stakeholders perceptions, Science of the Total Environment, 805, DOI: 10.1016/j.scitotenv.2021.150320.

Goudarzi M., Salahi, B., Hussaini S.A, 2015, Performance assessment of LARS-WG and SDSM downscaling models in simulation of climate changes Urmia Lake Basin, (in Persian),Iran-Watershed Management Science and Engineering, 31 (4), 11-22.

Hashmi M.Z., Asaad Y.S., Bruce W.M., 2011, Comparison of SDSM and LARS-WG for simulation and downscaling of extreme precipitation events in a watershed, Stochastic Environment Research and Risk Assessment, 25, 475-484, DOI: 10.1007/s00477-010-0416-x.

Hassan W.H, Forqan S.H., 2020, The effect of climate change on the maximum temperature in Southwest Iraq using HadCM3 and CanESM2 modeling, SN Applied Sciences, 2, DOI: 10.1007/s42452-020-03302-z.

Hassan Z., Shamsudin S., Harun S., 2014, Application of SDSM and LARS-WG for simulating and downscaling of rainfall and temperature, Theoretical and Applied Climatology, 116, 243-257, DOI: 10.1007/s00704-013-0951-8.

Hassanyar M.H., Hassani S., Dozier J., 2017, Ensemble GCMs climate change projections for Kabul River Basin, Afghanistan under representative concentration pathways. GRD Journals – Global Research and Development Journal for Engineering, 2 (5), 69-78.

IPCC, 2007a, Climate Change 2007: Impacts, Adaptation, and Vulnerability, Contribution of Working Group II to the Fourth Assessment Report of the Intergovernmental Panel on Climate Change, Cambridge University Press, 976 pp.

IPCC, 2007b, Climate Change 2007: The Physical Science Basis, Contribution of Working Group I to the Fourth Assessment Report of the Intergovernmental Panel on Climate Change, Cambridge University Press, 987 pp.

IPCC, 2014, Climate Change 2014: The Physical Science Basis – Summary for Policymakers, Contribution of Working Group I to the Fifth Assessment Report of the Intergovernmental Panel on Climate Change.

IPCC, 2022, Technical Summary, [in:] Climate Change 2022: Impacts, Adaptation and Vulnerability, Contribution of Working Group II to the Sixth Assessment Report of the Intergovernmental Panel on Climate Change, 37-118, DOI: 10.1017/9781009325844.002.

Javadinejad S., Eslamian S., Ostad-Ali-Aaskari K., 2021, The analysis of the most important climatic parameters affecting the performance of crop variability in a changing climate, International Journal of Hydrology Science and Technology, 11 (1), DOI: 10.1504/IJHST.2021.112651.

Jawid A., 2020, A Ricardian analysis of the economic impact of climate change on agriculture: Evidence from the farms in the central highlands of Afghanistan, Journal of Asian Economics, 67, DOI: 10.1016/j.asieco.2020.101177.

Kadiyala M.D.M., Nedumaran S., Padmanabhan J., Gumma M.K., Gummadi S., Srigiri S.R., Robertson R., Whitbread A., 2021, Modeling the potential impacts of climate change and adaptation strategies on groundnut production in India, Science of the Total Environment, 776, DOI: 10.1016/j.scitotenv.2021.145996.

Kounani Z., Ildoromi A., Zenivand H., Nouri H., 2021, Impact of climate change on runoff of Silakhor-Rahimabad Basin in Lorestan, Journal of Hydrogeomorphology, 7 (25), DOI: 10.22034/hyd.2021.32443.1474.

Lavalle C., Micale F., Houston T.D., Camia A., Hiederer R., Lazar C., Conte C., Amatulli G., Genovese G., 2009, Climate change in Europe: 3. Impact on agriculture and forestry. A review, Agronomy for Sustainable Development, 29, 433-446, DOI: 10.1051/agro/2008068.

Lee J.-Y., Marotzke J., Bala G., Cao L., Corti S., Dunne J.P., Engelbrecht F., Fischer E., Fyfe J.C., Jones C., Maycock A., Mutemi J., Ndiaye O., Panickal S., Zhou T., 2021, Future global climate: scenario-based projections and near term information, [in:] Climate Change 2021: The Physical Science Basis, Contribution of Working Group I to the Sixth Assessment Report of the Intergovernmental Panel on Climate Change, 553-672, DOI: 10.1017/9781009157896.006.

MAIL, 2022, Ministry of Agriculture, Irrigation & Livestock, Kabul, Government of Afghanistan.

MDA, 2022, Meteorological Department of Afghanistan. Kabul, Government of Afghanistan.

MEW, 2022, Ministry of Energy and Water, Kabul, Government of Afghanistan.

Munawar S., Rahman G., Moazzam M.F.U., Miandad M., Ullah K., Al-Ansari N., Linh N.T.T., 2022, Future climate projections using SDSM and LARS-WG downscaling methods for CMIP5 GCMs over the Transboundary Jhelum River Basin of the Himalayas region, Atmosphere, 13 (6), DOI: 10.3390/atmos13060898.

Nazari M., Mirgol B., Salehi H., 2021, Climate Change impact assessment and adaptation strategies for rainfed wheat in contrasting climatic regions of Iran, Frontiers in Agronomy, 3, DOI: 10.3389/fagro.2021.806146.

NEPA, 2018, Second National Communication under UNFCCC, Kabul, Afghanistan, National Environmental Protection Agency, https://www.nepa.gov.af/service3.

NEPA & UNEP, 2015, Climate Change and Governance in Afghanistan, National Environmental Protection Agency and United Nations Environment Programme.

Rasouli H., 2022, Climate change impacts on water resource and air pollution in Kabul sub-basins, Afghanistan, Advances in Geological and Geotechnical Engineering Research, 4 (1), 11-27, DOI: 10.30564/agger.v4i1.4312.

Saddique N., Bernhofer C., Kronenberg R., Usman M., 2019, Downscaling of CMIP5 models output by using statistical models in a data-scarce mountain environment (Mangla Dam Watershed), Northern Pakistan, Asia-Pacific Journal of Atmospheric Sciences, 55, 719-735, DOI: 10.1007/s13143-019-00111-2.

Sarwary M., Samiappan S., Khan G.D., Moahid M., 2023, Climate change and cereal crop productivity in Afghanistan: evidence based on panel regression model, Sustainability, 15 (14), DOI: 10.3390/su151410963.

Sayed A., Raza T., Bhatti T.T., Eash N.S., 2022, Climate impacts on the agricultural sector of Pakistan: risks and solutions, Environmental Challenges, 6, DOI: 10.1016/j.envc.2021.100433.

Solomon S., Plattner G.-K., Knutti R., Friedlingstein P., 2009, Irreversible climate change due to carbon dioxide emissions, PNAS, 106 (6), 1704-1709, DOI: 10.1073/pnas.0812721106.

UNDP, 2017, Climate Change Adaptation Project: Climate Change Scenarios for Agriculture of Afghanistan, The Islamic Republic of Afghanistan, Ministry of Agriculture, Irrigation and Livestock, 280 pp.

USAID, 2016, Climate Change Risk Profile Afghanistan, available on line at https://www.climatelinks.org/resources/climate-risk-profile-afghanistan (data access 14.10.2024).

Wayne G., 2013, The Beginner's Guide to Representative Concentration Pathways, Version 1.0., available online at http://climate.calcommons.org/sites/default/files/RCP_Guide.pdf (data access 25.11.2024).

WBG, 2021, Climate Risk Country Profile: Afghanistan, The World Bank Group and the Asian Development Bank.

# Changes in the seasonal cycles of extreme temperatures in the Sudano-Sahelian domain in West Africa: a case study from Burkina Faso

Joseph Yaméogo[1,2]

[1] Norbert ZONGO University, Burkina Faso

[2] Postdoc African Cluster Centers of Joseph Ki-ZERBO University, Burkina Faso

Abstract

Temperature is a key variable in understanding climate change. In tropical West Africa, however, temperature has been neglected because it is always hot because of the sun. Studying extreme temperatures can be a way to better understand climate change in the Sudano-Sahelian region of West Africa. The main objective of this study is to analyze changes in extreme temperatures. To this end, temperature data were obtained from Power NASA over the period 1981-2022 at monthly time steps. The methods used to analyze the data were normality and homogeneity statistics, linear regression, Mann-Kendall tests, and Spearman's *r* test. Tests of Sen's slope estimator, moving averages, and z-score. The study shows that maximum temperatures are normally distributed, unlike minimum temperatures, and that maximum temperature data are homogeneous, with breaks in the periods 1998, 2000, 2006, and 2010 before, during, and after the rainy seasons. On the other hand, minimum temperature data are generally not homogeneous and do not show many breaks. The study also shows that extreme temperatures tend to increase before, during, and after the rainy season, according to Spearman's r test. However, the Mann-Kendall test shows that extreme temperatures generally do not show trends. Furthermore, temperatures are continuously variable, with an increase in temperature anomalies in the 1980s, 2000s, and 2020s.

Keywords

Extreme temperature, variability, trend, temperature anomaly, Burkina Faso.

Submitted 17 June 2024, revised 11 September 2024, accepted 10 October 2024

DOI: 10.26491/mhwm/194451

## 1. Introduction

Global warming as a result of greenhouse gas emissions is now undeniable, and there has been a significant increase in the atmospheric concentration of $CO_2$ over the last century (Alemu, Dioha 2020). The increase in average and extreme temperatures in Africa can be attributed to climate change caused by human activity (Trisos et al. 2022). Several studies have found that temperatures are changing in Africa. Muthoni et al. (2019) studied the extent and significance of spatio-temporal trends in rainfall, maximum ($T_{max}$) and minimum ($T_{min}$) temperatures for West Africa. In northern Ghana, De Pinto et al. (2012) found that temperatures were higher than in any other part of Ghana and that they could increase between 1.0°C and 3.0°C by 2060 and between 1.5°C and 5.2°C by 2090. In Mali, Kouressy et al. (2019) report that between 1951 and 2010, maximum temperatures increased significantly by 0.44°C to 1.53°C and minimum temperatures by 1.05°C to 1.93°C, depending on the location. In Benin, Senegal, and Niger, mean annual minimum temperature increased significantly between 1965 and 2013: in less than 50 years, minimum temperature increased by 1.2°C in Djougou (Benin), 1.8°C in Bambey (Senegal) and 1.4°C in Niamey (Niger) (Kosmowski et al. 2015).

Few statistical studies have been carried out in Burkina Faso on the trend and variability of extreme temperature (Bambara et al. 2018; Rouamba et al. 2023), and even fewer on the seasonal analysis of extreme temperature in the Sudano-Sahelian part of Burkina Faso. It is very important to gain a better understanding of the seasonal occurrence of extreme temperatures because they cause illness and even death in young children and the elderly (Arisco et al. 2023). In this article, seasonality is based on rainfall, as temperatures change before, during, and after the rainy season. Three periods can be distinguished: the pre-wet period (January to May), the wet period (June to October) and the post-wet period (November to December). In this study, we analyze the seasonal trends in extreme temperatures over the past few decades.

## 2. Materials and methods

### 2.1. Data and methods

Burkina Faso is located in West Africa, where Sahelian, Sudano-Sahelian, and Sudanian climatic domains dominate (Fig. 1).

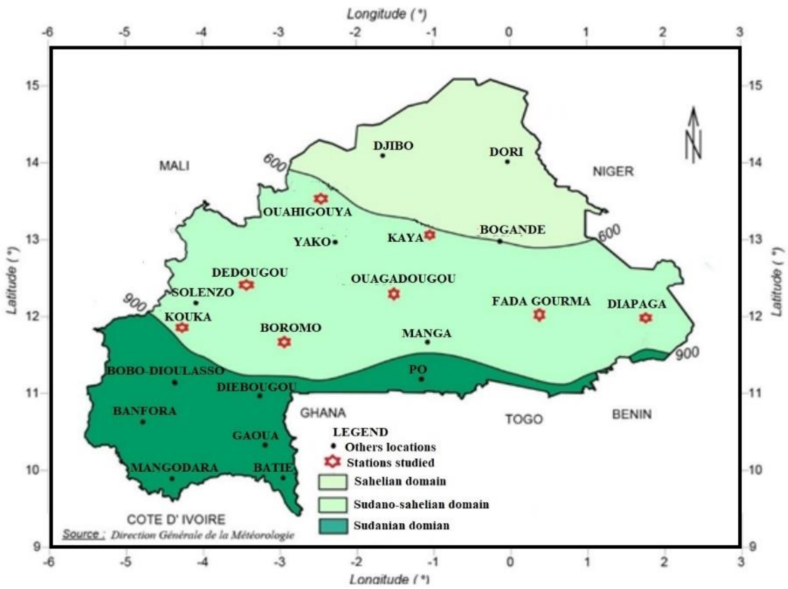


Fig. 1. Climatic zones and study stations in Burkina Faso.

The raw data used to assess extreme temperatures came from NASA's POWER (National Aeronautics and Space Administration Prediction of Worldwide Energy Resource) online public database (https://power.larc.nasa.gov/data-access-viewer). Power data are based on satellite observations from which surface insolation values are derived. The meteorological parameters are based on the MERRA-2 assimilation model. The database has the advantage of being generally continuous over time and is based on a global grid with a resolution of 0.5° latitude by 0.5° longitude (Marzouk 2021). Numerous studies have assessed the accuracy of the data and found that the source of the data (NASA POWER) is sufficiently accurate to allow valid interpretation (Jiménez-Jiménez et al. 2021; Marzouk 2021; Ahmed et al. 2022; Kwawuvi et al. 2022; Oloyede et al. 2023; Darman et al. 2024; Kheyruri et al. 2024).

Data for Burkina Faso from NASA's power data access viewer was collected at monthly intervals over the period 1981 to 2022. The characteristics of the localities selected are shown in Table 1 below (Table 1).

Table 1. Characteristics of the selected stations, all within the Sudan-Sahelian.

| Station names | Type of climate domain | Regions concerned | Period selected | Latitude | Longitude | Altitudes |
|---|---|---|---|---|---|---|
| Ouagadougou | Sudan-Sahelian | Centre | 1981-2022 | 12.3489 | –1.5197 | 303.27 m |
| Kaya | Sudan-Sahelian | North-East | 1981-2022 | 13.0856 | –1.0583 | 313.72 m |
| Ouhigouya | Sudan-Sahelian | North | 1981-2022 | 13.5614 | –2.4014 | 319.61 m |
| Fada Gourma | Sudan-Sahelian | East | 1981-2022 | 12.22 | 0.6308 | 269.06 m |
| Diapaga | Sudan-Sahelian | | 1981-2022 | 12.0804 | 1.8476 | 260.2 m |
| Dedougou | Sudan-Sahelian | Boucle du Mouhoun | 1981-2022 | 12.4454 | –3.3764 | 283.4 m |
| Boromo | Sudan-Sahelian | | 1981-2022 | 11.7446 | –2.9351 | 288.65m |
| Kouka | Sudan-Sahelian | | 1981-2022 | 11.8641 | –4.3213 | 346 m |

Source: https://power.larc.nasa.gov/data-access-viewer/.

### 2.1.1. Statistical normality and homogeneity

The normality test is important for determining appropriate methods for the assessment of significant trends in time series of precipitation data, using parametric or non-parametric methods of trend analysis (Talib et al. 2024). Normality tests, including Shapiro-Wilk W, Anderson-Darling, Lilliefors, and Jarque-Bera tests, were applied to the annual time series to evaluate the normal distribution of time series data. For all four tests, the null hypothesis is as follows:

$H_0$: the temperature time series has a normal distribution; if the p-value is less than 5%, the normal distribution can be rejected, and the alternative hypothesis ($H_1$) can be accepted. Among the tests proposed, the Shapiro-Wilk and Anderson-Darling tests are considered the most accurate, while the Lilliefors and Jarque-Bera tests are given for reference (Hammer 2024). Only the first two tests have been considered in this study. Thus, the mathematical formula for the calculation of Shapiro-Wilk ($W$) is (Asamoah, Ansah-Mensah 2020):

$$W = \frac{\left(\sum_{i=1}^{n} a_i x_{(i)}\right)^2}{\sum_{i=1}^{n} (x_i - \overline{x})^2}; \tag{1}$$

where $x_i$ is the value of the ordered sample, $a_i$ is a constant generated from the means, variances and covariances of the ordered statistics, $n$ is the number of observations, and $\overline{x}$ is the sample mean.

The Anderson-Darling ($AD$) test uses the cumulative distribution function to determine normality, and its formula is as follows (Asamoah, Ansah-Mensah 2020):

$$AD = -n - \frac{1}{2}\sum_{i=1}^{n}(2i-1)\left[\ln F(x_i) + \ln(1 - F(x_{n-i+1}))\right]; \tag{2}$$

where $n$ is the sample size, $F(x)$ is the cumulative distribution function for the specified distribution, and $i$ the $i^{th}$ sample for an ascending order.

The Buishand test was used to determine the homogeneity of the temperature data. The Buishand test, like the Petitt test, is more sensitive to breaks in the middle of the time series. (Wijngaard et al. 2003). In the Buishand test, the assumption is that the data are normally distributed and that the data are independently and randomly distributed (Bickici Arikan, Kahya 2019). The adjusted partial sums are defined as (Lin et al. 2015):

$$S^*_0 = 0 \text{ and } S^*_K = \sum_{i=1}^{k}(\bar{X}_i - \bar{X}) \quad k=1,2,3,......,n \tag{3}$$

There will be no systematic deviation of $\bar{X}_i$ values from their mean, and $S_{K^*}$ values will fluctuate around zero if the series is homogeneous. The 'rescaled adjusted interval' $R$ can be used to test the significance of the change in the mean. The value of $R$ is given by:

$$R= \frac{(\max S^*_K - \min S^*_K)}{S}, \text{ with } 0 \le k \le n \tag{4}$$

The Von Neumann test ($VNT$) examines the randomness and change point detection of the time series. The $VNT$ test statistic can be computed as (Lebeza et al. 2023):

$$N = \frac{\sum_{i=1}^{n-1}(X_{i-1} - X_{i-1})^2}{\sum_{i=1}^{n}(X_i - \bar{X})^2}; \tag{5}$$

where $N$ is the test static value of $VNT$, $X$ is observed time-series data and $\bar{X}$ refers to the mean of observed time-series data. Homogenous time series data can be found if the expected value of $N$ is 2. The value of $N$ is less than 2 can show a break pattern.

### 2.1.2. Method of trend analysis

Trends in hydro-climatological variables are generally evaluated using a variety of statistical tests, such as linear regression, Mann-Kendall (MK) and modified MK tests, with non-trending pre-whitening and Sen Slope (SS) estimators (Xu et al. 2007; Longobardi, Villani 2010; Nisansala et al. 2020; Ay 2021); other authors add the Spearman's *r* test (Yue et al. 2002; Yacoub, Tayfur 2019). The Mann-Kendall test, Spearman's *r* test and Sen's slope estimator were used to assess the trend and magnitude of seasonal temperature extremes in Burkina Faso.

- Linear Regression Analysis.

  Linear Regression is a parametric method used to estimate linear trends in time series (Rahmani et al. 2015; Esit, Yuce 2022):

$$Y = \beta_0 + \beta_1 X + \varepsilon \tag{6}$$

where $Y$ is the temperature time series, $X$ is the year or time, $\beta_0$ = Intercept, $\beta_1$ = Slope, and ε is the residual error.

- Mann-Kendall Trend Test.

  Mann-Kendall (MK) is a non-parametric test (Mann 1945). It is specifically used to detect trends in environmental, climatic, and hydrological time series (Aditya et al. 2021; Lornezhad et al. 2023). According to Ahmad et al. (2015), the null hypothesis ($H_0$) of this test is that there is no monotonic trend in the time series. The alternative hypothesis ($H_a$) is that there is a trend. The MK test is based on the calculation of the variance ($S$) and is obtained by the following equation (Mirabbasi et al. 2020):

$$S = \sum_{k=1}^{n-1} \sum_{j=k+1}^{n} \operatorname{sgn}(x_j - x_k) \tag{7}$$

The $sgn$ function is calculated as follows:

$$\begin{cases} \operatorname{sgn}(x_j - x_i) = 1 \ \text{ si } (x_j - x_i) > 1 \\ \operatorname{sgn}(x_j - x_i) = 0 \ \text{ si } (x_j - x_i) = 1 \\ \operatorname{sgn}(x_j - x_i) = -1 \ \text{ si } (x_j - x_i) < 1 \end{cases} \tag{8}$$

where $n$ is the length of the sample, $x_k$ and $x_j$ come from $k = 1, 2, ..., n - 1$ and $j = k + 1, ..., n$. If $n$ is greater than 8, the $S$ statistic approximates the normal distribution. The mean of $S$ is 0 and the variance of $S$ can be obtained as follows:

$$Var(S) = \frac{1}{18}\left[ n(n-1)(2n+5) - \sum_{i=1}^{m}(t_i - 1)(2t_i + 5) \right] \tag{9}$$

The $Z$ statistic is calculated using the formula:

$$Z = \begin{cases} \dfrac{s-1}{\sqrt{Var(s)}}, & \text{si } s > 0 \\ 0 & \text{si } s = 0 \\ \dfrac{s-1}{\sqrt{Var(s)}}, & \text{si } s < 0 \end{cases} \tag{10}$$

The null hypothesis $H_0$ (no trend) is rejected if the significance level or p-value is <5%. Table 2 below shows the level of significance.

Table 2. Interpretation of the meaning of the trend in the MK.

| Mann-Kendall test (p-value) | Significance of the trend |
|---|---|
| <0.01 | Very significant |
| 0.01≤ p <0.05 | Significant |
| ≥0.05 | Not significant |

Source: Author

- Spearman's $r$ Test (SR).

  Spearman's $r$ (SR) is a powerful method for detecting linear and non-linear trends and is frequently used to test for the absence of trends (Rahman et al. 2017). In this test, the null hypothesis ($H_0$) of the test is that all the data in the time series are independent and identically distributed, while the alternative hypothesis ($H_1$) is that there are upward or downward trends. Positive values of the SRZ standardized test statistic indicate upward trends, while negative values indicate downward trends in the time series (Zakwan 2021). The test statistics $r_{sp}$ and standardized statistics $Z_{sp}$ are defined as (Ahmed et al. 2022):

$$\mathrm{R}_{sp} = 1 - \frac{6\sum_{i=1}^{n} D_i - i)^2}{n(n^2-1)} \tag{11}$$

$$\mathrm{Z}_{sp} = R_{sp}\sqrt{\frac{n-2}{1-R_{sp}}}\ ; \tag{12}$$

where $D_i$ is the rank of $i^{\text{th}}$ observation, $I$ is the chronological order number, $n$ is the total length of the time series data, and $Z_{sp}$ is Student's $t$-distribution with $(n-2)$ degree of freedom. The positive values of $Z_{sp}$ represent an increasing trend across the hydrologic time series, and negative values represent the decreasing trends.

- Sen's slope estimator test.

  The non-parametric Sen test (Sen 1968) is commonly used for the estimation of the magnitude of trends in time series data. The Sen test for the slope assumes a linear trend and is a quantification of the change over time (Muia et al. 2024). The slope of Sen is calculated according to the following equation (Frimpong et al. 2022):

$$Q_i = \frac{x_j + x_k}{j-k} \ \ \textbf{for i=1,....,N}; \tag{13}$$

where, $x_j$ and $i_k$ = the data values at times j and $k\,(j > k)$.

If there is only one datum in each period, then:

$$N = \frac{n\ (n-1)}{2}\ ; \tag{14}$$

where $n$ = total number of observations.

The $N$ values of $Q_i$ have been ranked from the lowest to the highest, and the median slope or Sen's slope estimator has been calculated as follows:

$$Q_i = \begin{cases} Q_{\left[\frac{N+1}{2}\right]} & \text{N is odd} \\ Q_{\frac{n}{2}} + Q_{\left[\frac{N+2}{2}\right]} & \text{N is even} \end{cases} \quad (15)$$

A positive value of $Q_i$ represents an upward trend; a negative value of $Q_i$ represents a downward trend, over time (Ahmad et al. 2015).

2.1.3. Method analysis variability

- The moving average method

  The moving average is the most widely used method for the measurement of seasonal fluctuations (Bacescu-Carbunaru, Condruz-Bacescu 2013). In this study, moving averages (*MA*) have been used for the assessment of the overall trend in the variation of extreme temperatures (Zeitoun 2024):

$$MA = \frac{\sum_{i=1}^{n} M(d-i)+1}{n}\ ; \quad (16)$$

where $n$ is the number of data points, $d$ is the moving average, and $M$ is the data calculated as the simple moving average with the period is 3, *MA*: moving average.

- The Fligner Killeen test

  This non-parametric test (Conover et al. 1981) indicated significant differences in variability by testing the equality of the coefficients of variation of two samples. The coefficient of variation (or relative variation) is defined as the ratio of standard deviation to the mean in percent, and is computed as (Hammer 2024):

$$CV = \frac{\sigma}{\bar{X}} * 100 = \frac{\sqrt{\frac{1}{n-1}\sum (x_i - \bar{x})^2}}{\bar{x}} * 100 \quad (17)$$

The null hypothesis of the statistical test is $H_0$: the samples were taken from populations with the same coefficient of variation. However, when the p-value is less than 5%, the null hypothesis is rejected, and the alternative hypothesis is supported.

- Temperature Anomaly Detection Method

  Anomaly detection is a popular research area in time series data mining, where data points that don't conform to other data are referred to as anomalies (Wickramasinghe et al. 2023). Z-score is used to detect temperature anomalies, so the hypothesis is that the temperature data either contain anomalies or they do not (Zeitoun 2024). The formulas for a z-score transformation are (Jackson 2009):

$$Z = \frac{x-\mu}{\sigma}\ ; \quad (18)$$

where $z$ is the symbol for the standard score, $\mu$ is the mean, $\sigma$ is the standard deviation. The significant level is 0.95, with alpha (α) equal to 0.05, and the critical value of the Z-score is +1.96 and –1.96 (Zeitoun 2024). According to Pandey et al. (2023), the value of the z-score indicates the number of standard deviations the variables are from the mean. If a z-score is equal to 0, then the mean is on the mean. A positive z-score indicates that the raw score is comparatively higher than the mean and a negative z and a negative z-score indicates that the raw score is lower than the mean.

## 3. Results

### 3.1. Statistical normality and homogeneity in the study area

Table 3 below shows that the maximum temperature data for Ouahigouya, Diapaga, Dédougou, Ouagadougou, Kaya, and Kouka sites are normally distributed. On the other hand, the Shapiro-Wilk and Anderson-Darling statistics imply a lack of normality in the minimum temperature data.

The temperature data (maximum, minimum) were also subjected to homogeneity tests. The Buishand test shows that there is a change in both the maximum and minimum temperature data. The Von Neumann test was also applied to the temperature data. Table 4 shows the results of the two homogeneity tests.

Table 4 shows that temperature data change with the seasons. The change in maximum temperature data occurred in 2000 in Diapaga during the rainy season. In Kaya, the changes occurred before, during and after the rainy season in 1998, 2006, and 2010 respectively. In Ouahigouya, the change occurred during the pre-rainy season, as it did at Fada Gourma and Boromo. In Ouagadougou and Dédougou, however, the changes affected both the pre-rainy season and the rainy and post-rainy seasons. Overall, there has been an increase in maximum temperatures following the changes that occurred between 1998 and 2010. However, there has been very little change in the minimum temperature data. In Diapaga and Fada Gourma, the minimum temperature data were disrupted, especially during the wet and humid pre-season in 2004 and 1992 in Diapaga.

In Fada Gourma the change occurred in 1998. The minimum temperature increased significantly in the following years.

### 3.2. Statistical trends in extreme temperatures in the Sudano-Sahelian zone of Burkina Faso

#### 3.2.1. Analysis of maximum temperature trends using linear regression methods

The results of the normality test revealed that the maximum temperature data are normally distributed, allowing for trend analysis using parametric tests, particularly linear regression. The table below shows the seasonal trends over the period 1981-2020 (Table 5).

Table 3. The normality of extreme temperature data.

| Stations | Maximum temperature | | | Minimum temperature | | |
|---|---|---|---|---|---|---|
| Ouahigouya | Period | Shapiro-Wilk | Anderson-Darling | Period | Shapiro-Wilk | Anderson-Darling |
| | V1 | **0.007** | **0.001** | V1 | 0.571 | 0.38 |
| | V2 | 0.627 | 0.282 | V2 | 0.865 | 0.53 |
| | V3 | 0.812 | 0.850 | V3 | 0.94 | 0.89 |
| Diapaga | Period | Shapiro-Wilk | Anderson-Darling | Period | Shapiro-Wilk | Anderson-Darling |
| | V1 | **0.040** | 0.067 | V1 | 0.381 | 0.368 |
| | V2 | 0.258 | 0.215 | V2 | 0.482 | 0.502 |
| | V3 | 0.236 | 0.400 | V3 | 0.509 | 0.661 |
| Dédougou | Period | Shapiro-Wilk | Anderson-Darling | Period | Shapiro-Wilk | Anderson-Darling |
| | V1 | **0.037** | **0.026** | V1 | 0.902 | 0.912 |
| | V2 | 0.836 | 0.923 | V2 | 0.762 | 0.890 |
| | V3 | 0.237 | 0.490 | V3 | 0.644 | 0.558 |
| Ouagadougou | Period | Shapiro-Wilk | Anderson-Darling | Period | Shapiro-Wilk | Anderson-Darling |
| | V1 | 0.061 | **0.035** | V1 | 0.949 | 0.923 |
| | V2 | 0.126 | 0.150 | V2 | 0.739 | 0.829 |
| | V1 | 0.608 | 0.802 | V3 | 0.809 | 0.881 |
| Kaya | Period | Shapiro-Wilk | Anderson-Darling | Period | Shapiro-Wilk | Anderson-Darling |
| | V1 | 0.068 | **0.021** | V1 | 0.889 | 0.866 |
| | V2 | 0.093 | **0.049** | V2 | 0.399 | 0.417 |
| | V1 | 0.631 | 0.664 | V3 | 0.944 | 0.919 |
| Kouka | Period | Shapiro-Wilk | Anderson-Darling | Period | Shapiro-Wilk | Anderson-Darling |
| | V1 | 0.009 | **0.025** | V1 | 0.884 | 0.584 |
| | V2 | 0.736 | 0.795 | V2 | 0.895 | 0.685 |
| | V3 | 0.155 | 0.220 | V3 | 0.750 | 0.524 |
| Fada Gourma | Period | Shapiro-Wilk | Anderson-Darling | Period | Shapiro-Wilk | Anderson-Darling |
| | V1 | 0.142 | 0.125 | V1 | 0.177 | 0.313 |
| | V2 | 0.286 | 0.204 | V2 | 0.854 | 0.952 |
| | V3 | 0.163 | 0.201 | V3 | 0.847 | 0.808 |
| Boromo | Period | Shapiro-Wilk | Anderson-Darling | Period | Shapiro-Wilk | Anderson-Darling |
| | V1 | 0.003 | **0.006** | V1 | 0.500 | 0.384 |
| | V2 | 0.279 | 0.392 | V2 | 0.332 | 0.143 |
| | V3 | 0.073 | 0.258 | V3 | 0.135 | 0.147 |

Source: Power NASA, 1981-2022, v1 = rainy pre-season; v2 = rainy season; v3 = post-rainy season.

Table 4. Homogeneity of extreme temperature data.

| Stations | Maximum temperature | | | | | | Minimum temperature | | | | |
|---|---|---|---|---|---|---|---|---|---|---|---|
| Diapaga | Period | Buishand | Von Neumann | Period change | Before | After | Buishand | Von Neumann | Period change | Before | After |
| | V1 | **0.001** | **0.001** | 2000 | 40.17 | 41.2 | **0.014** | 0.316 | 2004 | 18.38 | 19.09 |
| | V2 | 0.263 | 0.375 | - | - | - | **0.005** | 0.248 | 1992 | 20.75 | 21.3 |
| | V3 | 0.182 | 0.227 | - | - | - | 0.500 | 0.676 | - | - | - |
| Kaya | Period | Buishand | Von Neumann | Period change | Before | After | Buishand | Von Neumann | Period change | before | after |
| | V1 | **0.014** | 0.424 | 1998 | 40.21 | 40.8 | 0.360 | 0.242 | - | - | - |
| | V2 | **0.021** | 0.616 | 2006 | 37.6 | 36.6 | 0.334 | 0.680 | - | - | - |
| | V3 | **0.015** | 0.418 | 2010 | 36.44 | 35.21 | 0.061 | 0.719 | - | - | - |
| Ouahigouya | Period | Buishand | Von Neumann | Period change | Before | After | Buishand | Von Neumann | Period change | before | after |
| | V1 | **0.001** | 0.584 | 1998 | 40.36 | 41.1 | 0.271 | 0.478 | - | - | - |
| | V2 | 0.071 | 0.876 | - | - | - | 0.356 | 0.522 | - | - | - |
| | V3 | 0.270 | 0.839 | - | - | - | 0.139 | 0.408 | - | - | - |
| Ouagadougou | Period | Buishand | Von Neumann | Period change | Before | After | Buishand | Von Neumann | Period change | before | after |
| | V1 | **0.018** | 0.212 | 1998 | 40 | 40.6 | 0.485 | 0.302 | - | - | - |
| | V2 | 0.189 | 0.281 | - | - | - | 0.057 | 0.423 | - | - | - |
| | V3 | **0.033** | 0.304 | 2010 | 36.6 | 35.4 | 0.063 | 0.544 | - | - | - |
| Kouka | Period | Buishand | Von Neumann | Period change | Before | After | Buishand | Von Neumann | Period change | before | after |
| | V1 | 0.300 | 0.109 | - | - | - | 0.294 | 0.115 | - | - | - |
| | V2 | 0.124 | 0.106 | - | - | - | 0.125 | 0.109 | - | - | - |
| | V3 | 0.427 | 0.159 | - | - | - | 0.427 | 0.166 | - | - | - |
| Fada Gournma | Period | Buishand | Von Neumann | Period change | Before | After | Buishand | Von Neumann | Period change | before | after |
| | V1 | **0.004** | 0.0723 | 1998 | 40.04 | 40.8 | 0.294 | **0.040** | - | - | - |
| | V2 | 0.28 | 0.2881 | - | - | - | **0.012** | 0.107 | 1998 | 20.70 | 21.08 |
| | V3 | 0.064 | 0.0534 | - | - | - | 0.250 | 0.394 | - | - | - |
| Boromo | Period | Buishand | Von Neumann | Period change | Before | After | Buishand | Von Neumann | Period change | before | after |
| | V1 | **0.003** | 0.072 | 1998 | 40.74 | 41.5 | 0.291 | **0.039** | - | - | - |
| | V2 | 0.278 | 0.278 | - | - | - | **0.012** | 0.102 | 2001 | 20.70 | 21.08 |
| | V3 | 0.060 | **0.057** | - | - | - | 0.248 | 0.398 | - | - | - |
| Dédougou | Period | Buishand | Von Neumann | Period change | Before | After | Buishand | Von Neumann | Period change | before | after |
| | V1 | **0.001** | 0.499 | 1998 | 40.7 | 41.5 | 0.665 | 0.147 | - | - | - |
| | V2 | **0.010** | 0,292 | 2002 | 36.2 | 35.2 | 0.117 | 0.122 | - | - | - |
| | V3 | 0.056 | 0,222 | - | - | - | 0.256 | 0.129 | - | - | - |

Source: Power NASA, 1981-2022, v1 = rainy pre-season; v2 = rainy season; v3 = post-season rainy.

Table 5. Trends in maximum temperatures over the period 1981-2022.

| Stations | Seasonal | Source | Value | Standard error | t | p-value | Trend |
|---|---|---|---|---|---|---|---|
| Ouahigouya | V1 | Constant value | –3.206 | 15.719 | –0.204 | 0.839 | |
| | | Year | 0.022 | 0.008 | 2.799 | **0.008**** | Increasing |
| | V2 | Constant value | 73.201 | 24.794 | 2.952 | 0.005 | |
| | | Year | –0.018 | 0.012 | –1.457 | 0.153 | - |
| | V3 | Constant value | 55.823 | 27.356 | 2.041 | 0.048 | |
| | | Year | –0.010 | 0.014 | –0.706 | 0.484 | - |
| Diapaga | V1 | Constant value | –19.877 | 17.091 | –1.163 | 0.252 | |
| | | Year | 0.030 | 0.009 | 3.543 | **0.001**** | Increasing |
| | V2 | Constant value | 1.648 | 23.331 | 0.071 | 0.944 | |
| | | Year | 0.017 | 0.012 | 1.446 | 0.156 | - |
| | V3 | Constant value | –4.381 | 28.378 | –0.154 | 0.878 | |
| | | Year | 0.021 | 0.014 | 1.459 | 0.152 | - |
| Dédougou | V1 | Constant value | –4.358 | 16.020 | –0.272 | 0.787 | |
| | | Year | 0.023 | 0.008 | 2.842 | **0.007**** | Increasing |
| | V2 | Constant value | 77.700 | 24.481 | 3.174 | 0.003 | |
| | | Year | –0.021 | 0.012 | –1.711 | **0.095*** | Increasing |
| | V3 | Constant value | 85.342 | 35.031 | 2.436 | 0.019 | |
| | | Year | –0.024 | 0.018 | –1.383 | 0.174 | - |
| Ouagadougou | V1 | Constant value | 9.861 | 17.620 | 0.560 | 0.579 | |
| | | Year | 0.015 | 0.009 | 1.732 | **0.091*** | Increasing |
| | V2 | Constant value | 52.184 | 21.930 | 2.380 | 0.022 | |
| | | Year | –0.008 | 0.011 | –0.713 | 0.480 | - |
| | V3 | Constant value | 78.357 | 31.276 | 2.505 | 0.016 | |
| | | Year | –0.021 | 0.016 | –1.347 | 0.185 | - |
| Kaya | V1 | Constant value | 11.060 | 16.779 | 0.659 | 0.514 | |
| | | Year | 0.015 | 0.008 | 1.759 | **0.086*** | Increasing |
| | V2 | Constant value | 83.043 | 20.502 | 4.050 | 0.000 | |
| | | Year | –0.023 | 0.010 | –2.242 | **0.031**** | Increasing |
| | V3 | Constant value | 95.886 | 29.626 | 3.237 | 0.002 | |
| | | Year | –0.030 | 0.015 | –2.019 | **0.049**** | Decreasing |
| Kouka | V1 | Constant value | –4.051 | 16.789 | –0.241 | 0.811 | - |
| | | Year | 0.022 | 0.008 | 2.653 | **0.011**** | Increasing |
| | V2 | Constant value | 46.538 | 23.921 | 1.946 | 0.059 | |
| | | Year | –0.006 | 0.012 | –0.495 | 0.623 | - |
| | V3 | Constant value | 79.900 | 37.371 | 2.138 | 0.039 | |
| | | Year | –0.022 | 0.019 | –1.179 | 0.245 | - |
| Fada Gourma | V1 | Constant value | –14.090 | 15.291 | –0.921 | 0.362 | |
| | | Year | 0.027 | 0.008 | 3.578 | **0.001**** | Increasing |
| | V2 | Constant value | 25.302 | 22.803 | 1.110 | 0.274 | |
| | | Year | 0.005 | 0.011 | 0.441 | 0.662 | - |
| | V3 | Constant value | 28.307 | 30.599 | 0.925 | 0.360 | |
| | | Year | 0.004 | 0.015 | 0.283 | 0.779 | - |
| Boromo | V1 | Constant value | –6.227 | 17.707 | –0.352 | 0.727 | |
| | | Year | 0.023 | 0.009 | 2.638 | **0.012**** | Increasing |
| | V2 | Constant value | 46.023 | 26.669 | 1.726 | 0.092 | |
| | | Year | –0.006 | 0.013 | –0.426 | 0.673 | - |
| | V3 | Constant value | 77.123 | 39.641 | 1.946 | 0.059 | |
| | | Year | –0.020 | 0.020 | –1.028 | 0.310 | - |

Source: Power NASA, 1981-2022, ***Significance at 1% level, **Significance at 5% level, Significance at 10% level; -: no trend

### 3.2.2. Minimum temperature trends using Mann-Kendall and Spearman's *r* tests and Sen's slope estimator

The minimum temperature trend time series data were examined using the Mann-Kendall (MK), Spearman's *r* and Sen (SS) slope tests, as the results of the normality test indicated that these data are not normally distributed, requiring non-parametric tests for trend analysis.

- Mann-Kendall trend test and Sen's estimator of the slope

  Table 6 below shows that, on the whole, the extreme temperatures at the different sites studied do not show any trend in the temperature series. However, in Diapaga, Kouka, Fada Gourma, and Dédougou, positive trends were observed in the period before the rainy season. On the other hand, negative trends before and during the rainy season were observed in Ouahigouya and Kaya.

Table 6. Trends and amplitudes of minimum temperatures between 1981 and 2022.

| | Minimum temperature | | | |
|---|---|---|---|---|
| Diapaga | Period | Kendall's Tau | p-value | Sen's slope |
| | v1 | 0.323 | **0.003** | 0.032 |
| | v2 | 0.231 | **0.032** | 0.014 |
| | v3 | 0.089 | 0.41 | 0.013 |
| Kaya | Period | Kendall's Tau | p-value | Sen's slope |
| | v1 | 0.151 | 0.162 | 0.011 |
| | v2 | 0.152 | 0.159 | 0.009 |
| | v3 | –0.148 | 0.172 | -0.021 |
| Ouahigouya | Period | Kendall's Tau | p-value | Sen's slope |
| | v1 | 0.148 | 0.172 | 0.016 |
| | v2 | 0.092 | 0.398 | 0.006 |
| | v3 | 0.089 | 0.41 | 0.016 |
| Ouagadougou | Period | Kendall's Tau | p-value | Sen's slope |
| | v1 | 0.096 | 0.374 | 0.007 |
| | v2 | 0.192 | 0.076 | 0.012 |
| | v3 | –0.124 | 0.251 | -0.018 |
| Kouka | Period | Kendall's Tau | p-value | Sen's slope |
| | v1 | 0.064 | 0.558 | 0.005 |
| | v2 | 0.154 | 0.153 | 0.009 |
| | v3 | 0.036 | 0.745 | 0.007 |
| Fada Gourma | Period | Kendall's Tau | p-value | Sen's slope |
| | V1 | 0.250 | **0.020** | 0.025 |
| | v2 | 0.287 | **0.008** | 0.016 |
| | v3 | 0.033 | 0.770 | 0.005 |
| Boromo | Period | Kendall's Tau | p-value | Sen's slope |
| | v1 | 0.034 | 0.762 | 0.002 |
| | v2 | 0.272 | **0.012** | 0.014 |
| | v3 | –0.045 | 0.680 | -0.005 |
| Dédougou | Period | Kendall's Tau | p-value | Sen's slope |
| | v1 | 0.066 | 0.544 | 0.007 |
| | v2 | 0.128 | 0.237 | 0.008 |
| | v3 | 0.002 | 0.991 | 0.000 |

Source: Power NASA, 1981-2022, v1 = rainy pre-season; v2 = rainy season; v3 = post-season rainy.

- Spearman's *r* test

  This test was also applied to the temperature data. It was found that the pre-wet season (January to May) shows positive trends, with positive correlation coefficients for maximum and minimum temperatures in Diapaga, Kaya, Ouahigouya, Ouagadougou, Kouka, Fada Gourma, Boromo and Dédougou. During the rainy season, the trend in extreme temperatures is also upward in all the locations studied, with a very high degree of significance. However, the minimum temperatures in Boromo and Dédougou show no trend between 1981 and 2022. On the other hand, in the period after the rainy season, temperature trends are significant over the period 1981-2022. Table 7 below gives details by season and month of the extreme temperature trends over the period 1981-2022.

Table 7. The upward trend in extreme temperatures in Burkina Faso between 1981 and 2022.

| | **Diapaga** | | | **Kaya** | | | | **Ouahigouya** | | | |
|---|---|---|---|---|---|---|---|---|---|---|---|
| | $T_{min}$ | | ANN | $T_{min}$ | | | ANN | $T_{min}$ | | | ANN |
| | | CC | **.557**** | | | CC | **.388*** | | | CC | **.513**** |
| | JAN | Sig | 0.000 | | JAN | Sig | 0.011 | | JAN | Sig | 0.001 |
| | | N | 42 | | | N | 42 | | | N | 42 |
| | | CC | **.441**** | | | CC | **.418**** | | | CC | .364* |
| | FEB | Sig | 0.003 | | FEB | Sig | 0.006 | | FEB | Sig | 0.018 |
| | | N | 42 | | | N | 42 | | | N | 42 |
| | | CC | 0.264 | | | CC | 0.094 | | | CC | 0.283 |
| V1 | MAR | Sig | 0.091 | V1 | MAR | Sig | 0.554 | V1 | MAR | Sig | 0.069 |
| | | N | 42 | | | N | 42 | | | N | 42 |
| | | CC | **.393**** | | | CC | 0.191 | | | CC | **.385*** |
| | APR | Sig | 0.010 | | APR | Sig | 0.227 | | APR | Sig | 0.012 |
| | | N | 42 | | | N | 42 | | | N | 42 |
| | | CC | **.413**** | | | CC | **.624**** | | | CC | **.591**** |
| | MAY | Sig | 0.007 | | MAY | Sig | 0.000 | | MAY | Sig | 0.000 |
| | | N | 42 | | | N | 42 | | | N | 42 |
| | | CC | **.544**** | | | CC | **.554**** | | | CC | **.310*** |
| | JUN | Sig | 0.000 | | JUN | Sig | 0.000 | | JUN | Sig | 0.045 |
| | | N | 42 | | | N | 42 | | | N | 42 |
| | | CC | **.595**** | | | CC | 0.190 | | | CC | 0.173 |
| | JUL | Sig | 0.000 | | JUL | Sig | 0.227 | | JUL | Sig | 0.274 |
| | | N | 42 | | | N | 42 | | | N | 42 |
| | | CC | **.455**** | | | CC | 0.173 | | | CC | 0.091 |
| V2 | AUG | Sig | 0.002 | V2 | AUG | Sig | 0.274 | | AUG | Sig | 0.566 |
| | | N | 42 | | | N | 42 | V2 | | N | 42 |
| | | CC | **.493**** | | | CC | **.479**** | | | CC | **.307*** |
| | SEP | Sig | 0.001 | | SEP | Sig | 0.001 | | SEP | Sig | 0.048 |
| | | N | 42 | | | N | 42 | | | N | 42 |
| | | CC | **.395**** | | | CC | **.327*** | | | CC | 0.176 |
| | OCT | Sig | 0.010 | | OCT | Sig | 0.035 | | OCT | Sig | 0.264 |
| | | N | 42 | | | N | 42 | | | N | 42 |
| V3 | NOV | CC | **.455**** | V3 | NOV | CC | **.388*** | | NOV | CC | **.313*** |
| | | Sig | 0.002 | | | Sig | 0.011 | | | Sig | 0.044 |

| | | | | | | | | | | | |
|---|---|---|---|---|---|---|---|---|---|---|---|
| | | N | 42 | | | N | 42 | | | N | 42 |
| | DEC | CC | 0.080 | | DEC | CC | .502** | | DEC | CC | .643** |
| | | Sig | 0.616 | | | Sig | 0.001 | | | Sig | 0.000 |
| | | N | 42 | | | N | 42 | | | N | 42 |
| Ouagadougou | | | | Kouka | | | | Fada Gourma | | | |
| $T_{min}$ | | | ANN | $T_{min}$ | | | ANN | $T_{min}$ | | | ANN |
| V1 | JAN | CC | .488** | V1 | JAN | CC | .563** | V1 | JAN | CC | .490** |
| | | Sig | 0.001 | | | Sig | 0.000 | | | Sig | 0.001 |
| | | N | 42 | | | N | 42 | | | N | 42 |
| | FEB | CC | .496** | | FEB | CC | .376* | | FEB | CC | .502** |
| | | Sig | 0.001 | | | Sig | 0.014 | | | Sig | 0.001 |
| | | N | 42 | | | N | 42 | | | N | 42 |
| | MAR | CC | -0.009 | | MAR | CC | 0.114 | | MAR | CC | 0.198 |
| | | Sig | 0.957 | | | Sig | 0.472 | | | Sig | 0.208 |
| | | N | 42 | | | N | 42 | | | N | 42 |
| | APR | CC | 0.160 | | APR | CC | 0.180 | | APR | CC | .370* |
| | | Sig | 0.311 | | | Sig | 0.254 | | | Sig | 0.016 |
| | | N | 42 | | | N | 42 | | | N | 42 |
| | MAY | CC | .579** | | MAY | CC | .448** | | MAY | CC | 0.188 |
| | | Sig | 0.000 | | | Sig | 0.003 | | | Sig | 0.234 |
| | | N | 42 | | | N | 42 | | | N | 42 |
| V2 | JUN | CC | .469** | V2 | JUN | CC | 0.274 | V2 | JUN | CC | .433** |
| | | Sig | 0.002 | | | Sig | 0.079 | | | Sig | 0.004 |
| | | N | 42 | | | N | 42 | | | N | 42 |
| | JUL | CC | 0.226 | | JUL | CC | .361* | | JUL | CC | .468** |
| | | Sig | 0.149 | | | Sig | 0.019 | | | Sig | 0.002 |
| | | N | 42 | | | N | 42 | | | N | 42 |
| | AUG | CC | 0.230 | | AUG | CC | 0.243 | | AUG | CC | .364* |
| | | Sig | 0.143 | | | Sig | 0.121 | | | Sig | 0.018 |
| | | N | 42 | | | N | 42 | | | N | 42 |
| | SEP | CC | .457** | | SEP | CC | 0.221 | | SEP | CC | .398** |
| | | Sig | 0.002 | | | Sig | 0.159 | | | Sig | 0.009 |
| | | N | 42 | | | N | 42 | | | N | 42 |
| | OCT | CC | .357* | | OCT | CC | 0.126 | | OCT | CC | .381* |
| | | Sig | 0.020 | | | Sig | 0.425 | | | Sig | 0.013 |
| | | N | 42 | | | N | 42 | | | N | 42 |
| V3 | NOV | CC | .457** | V3 | NOV | CC | .490** | V3 | NOV | CC | .380* |
| | | Sig | 0.002 | | | Sig | 0.001 | | | Sig | 0.013 |
| | | N | 42 | | | N | 42 | | | N | 42 |
| | DEC | CC | .438** | | DEC | CC | .497** | | DEC | CC | 0.130 |
| | | Sig | 0.004 | | | Sig | 0.001 | | | Sig | 0.413 |
| | | N | 42 | | | N | 42 | | | N | 42 |
| Boromo | | | | Dédougou | | | | | | | |
| $T_{min}$ | | | ANN | $T_{min}$ | | | ANN | | | | |
| V1 | JAN | CC | .516** | V1 | JAN | CC | .430** | | | | |
| | | Sig | 0.000 | | | Sig | 0.005 | | | | |
| | | N | 42 | | | N | 42 | | | | |

| | | | | | | | |
|---|---|---|---|---|---|---|---|
| | FEB | CC | **.443**** | | FEB | CC | .400** |
| | | Sig | 0.003 | | | Sig | 0.009 |
| | | N | 42 | | | N | 42 |
| | MAR | CC | 0.058 | | MAR | CC | 0.112 |
| | | Sig | 0.715 | | | Sig | 0.481 |
| | | N | 42 | | | N | 42 |
| | APR | CC | **.344*** | | APR | CC | 0.192 |
| | | Sig | 0.026 | | | Sig | 0.223 |
| | | N | 42 | | | N | 42 |
| | MAY | CC | **.384*** | | MAY | CC | **.558**** |
| | | Sig | 0.012 | | | Sig | 0.000 |
| | | N | 42 | | | N | 42 |
| V2 | JUN | CC | 0.210 | V2 | JUN | CC | **.374*** |
| | | Sig | 0.181 | | | Sig | 0.015 |
| | | N | 42 | | | N | 42 |
| | JUL | CC | 0.168 | | JUL | CC | 0.103 |
| | | Sig | 0.289 | | | Sig | 0.517 |
| | | N | 42 | | | N | 42 |
| | AUG | CC | 0.298 | | AUG | CC | 0.252 |
| | | Sig | 0.055 | | | Sig | 0.108 |
| | | N | 42 | | | N | 42 |
| | SEP | CC | 0.246 | | SEP | CC | 0.240 |
| | | Sig | 0.117 | | | Sig | 0.127 |
| | | N | 42 | | | N | 42 |
| | OCT | CC | **.558**** | | OCT | CC | 0.123 |
| | | Sig | 0.000 | | | Sig | 0.437 |
| | | N | 42 | | | N | 42 |
| V3 | NOV | CC | **.606**** | V3 | NOV | CC | **.497**** |
| | | Sig | 0.000 | | | Sig | 0.001 |
| | | N | 42 | | | N | 42 |
| | DEC | CC | **.588**** | | DEC | CC | **.535**** |
| | | Sig | 0.000 | | | Sig | 0.000 |
| | | N | 42 | | | N | 42 |

Source: Power NASA, 1981-2022, coefficient of correlation = CC. **CC is significant at the 0.01 level (two-tailed), *CC is significant at the 0.05 level.

## 3.3. Extreme temperature variability in the Sudano-Sahelian domain of Burkina Faso

In this study, the variability of extreme temperatures was analyzed by moving averages, the anomaly method, and the Fligner-Killeen test.

### 3.3.1. Analysis of variability in extreme temperatures using moving averages and Fligner-Killeen test

The moving averages show a fluctuating trend in extreme temperatures, reflecting the variability of the time series from 1981 to 2022. Overall, there is a four-stage trend in maximum temperatures, with a decrease between 1981 and 1998, an increase between 1999 and 2001, a decrease between 2022 and 2011, and an increase between 2012 and 2022. However, the behavior of minimum temperatures is different. There is no phase of change, but rather a continuous sawtooth pattern. This means that the variability of minimum temperatures is even greater than that of maximum temperatures. The stations close to the Sahelian domains (Ouahigouya, Kaya) and the Sudanian domains (Kouka, Boromo) have strong fluctuations in minimum temperatures, compared with the stations in Ougadougou, Fada Gourma, and Diapaga, which are in the center of the Sudano-Sahelian zone. Figure 2 shows the changes in temperature variability between 1981 and 2022 for the selected study regions. In the northeast region, the Kaya station was chosen. Similarly, in the north and central regions, the Ouahigouya and Ouagadougou stations were chosen because of their different variation. The Dédougou station in the Boucle du Mouhoun region was chosen because the other stations (Boromo, Kouka) are similar in terms of temperature variation. The same is true for the Fada Gourma station in the eastern region.

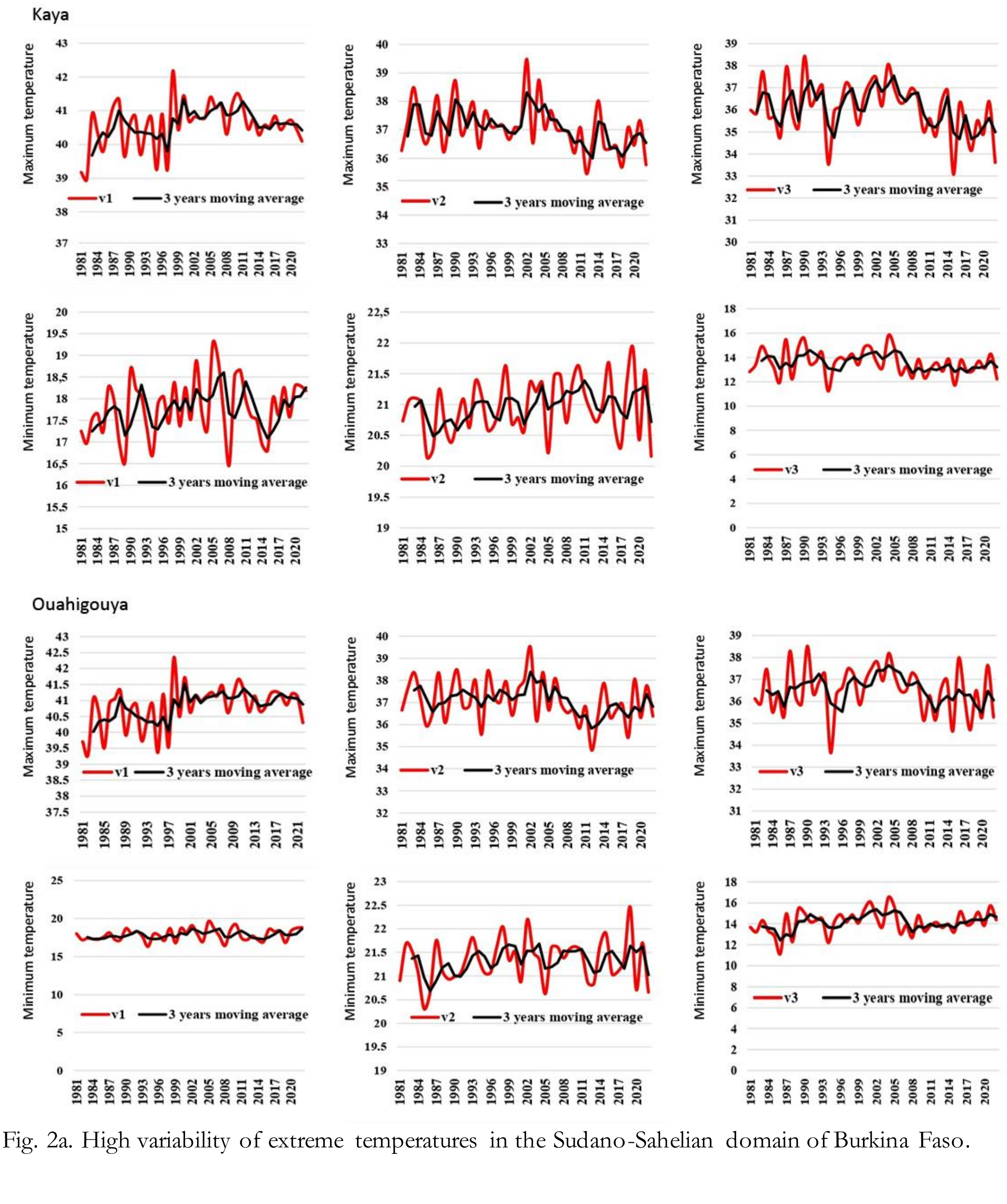


Fig. 2a. High variability of extreme temperatures in the Sudano-Sahelian domain of Burkina Faso.

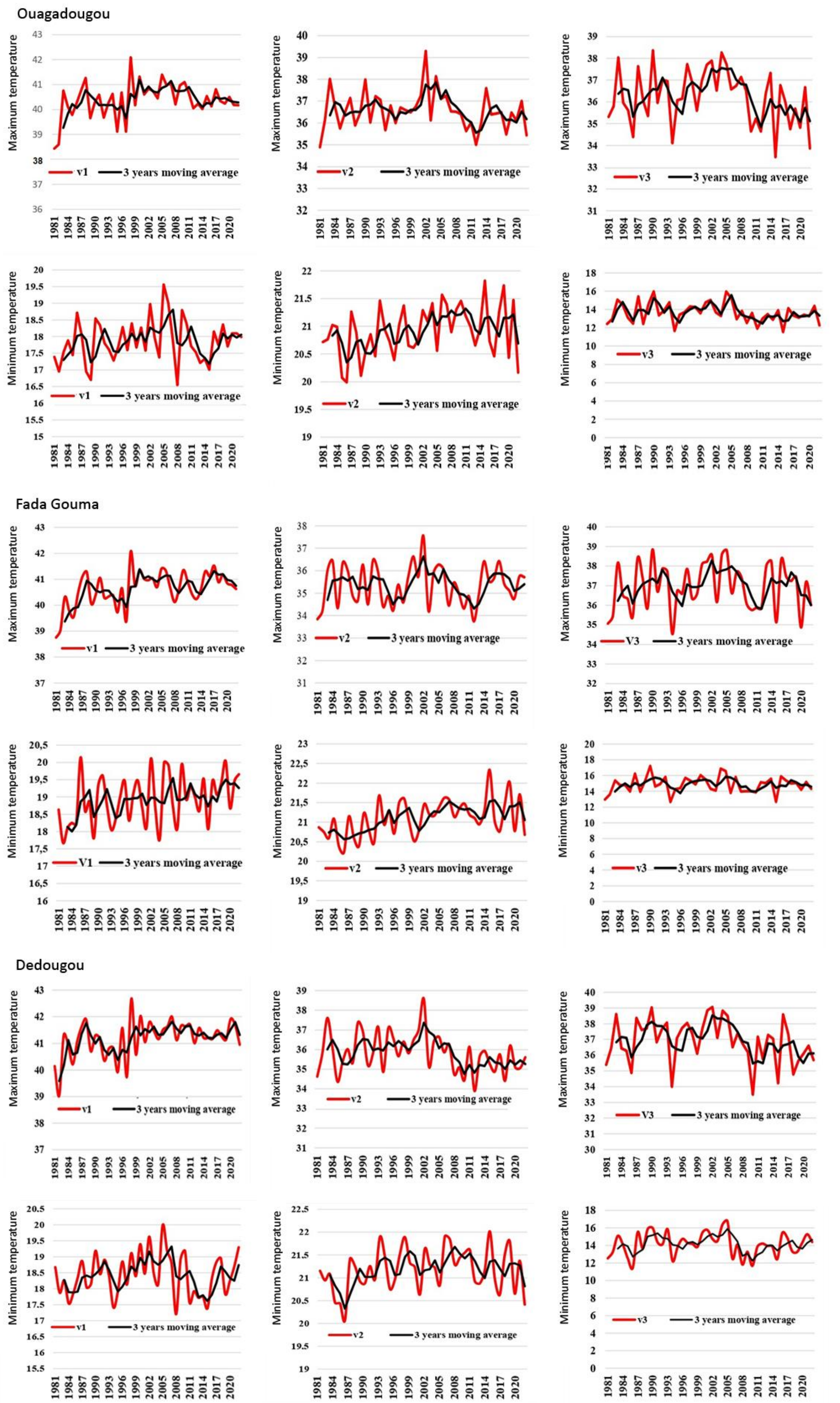


Fig. 2b. High variability of extreme temperatures in the Sudano-Sahelian domain of Burkina Faso.

These variations are quite large in comparison with the pre-rainy season, the rainy, and the post-rainy season (Table 8).

Table 8. Comparative variability of extreme temperatures for the periods before the rainy season, during the rainy season and after the rainy season.

| Localities | Compared seasonality | T | Expected T | z | p (one-tailed): | p (two-tailed): | Type of temperature |
|---|---|---|---|---|---|---|---|
| Diapaga | v1-v2 | 50.078 | 39.092 | 1.9382 | **0.026297** | **0.052595** | maximum temperature |
| | v2-v3 | 43.881 | 39.092 | 0.84492 | 0.19908 | 0.39816 | |
| | v1-v3 | 56.052 | 39.092 | 2.9921 | **0.0013852** | **0.0027704** | |
| | v1-v2 | 20.696 | 39.092 | –3.247 | **0.00058319** | **0.0011664** | minimum temperature |
| | v2-v3 | 64.955 | 39.092 | 4.5629 | **2.52E-06** | **5.04E-06** | |
| | v1-v3 | 58.715 | 39.092 | 3.4621 | **0.00026795** | **0.0005359** | |
| Kaya | v1-v2 | 49.298 | 39.092 | 1.8006 | **0.035882** | **0.071765** | maximum temperature |
| | v2-v3 | 50.727 | 39.092 | 2.0527 | **0.020053** | **0.040106** | |
| | v1-v3 | 57.344 | 39.092 | 3.2201 | **0.00064068** | **0.0012814** | |
| | v1-v2 | 20.696 | 39.092 | –3.247 | **0.00058319** | **0.0011664** | minimum temperature |
| | v2-v3 | 64.955 | 39.092 | 4.5629 | **2.52E-06** | **5.04E-06** | |
| | v1-v3 | 58.715 | 39.092 | 3.4621 | **0.00026795** | **0.0005359** | |
| ouahigouga | v1-v2 | 54.215 | 39.092 | 2.668 | **0.0038155** | **0.007631** | maximum temperature |
| | v2-v3 | 41.895 | 39.092 | 0.49457 | **0.31045** | **0.6209** | |
| | v1-v3 | 56.246 | 39.092 | 3.0264 | **0.0012373** | **0.0024746** | |
| | v1-v2 | 16.224 | 39.092 | –4.0344 | **2.74E-05** | **5.47E-05** | minimum temperature |
| | v2-v3 | 64.549 | 39.092 | 4.4912 | **3.54E-06** | **7.08E-06** | |
| | v1-v3 | 54.952 | 39.092 | 2.7981 | **0.0025699** | **0.0051399** | |
| Ouagadougou | v1-v2 | 45.533 | 39.092 | 1.1364 | **0.12789** | **0.25578** | maximum temperature |
| | v2-v3 | 52.662 | 39.092 | 2.3941 | **0.0083303** | **0.016661** | |
| | v1-v3 | 59.393 | 39.092 | 3.5816 | **0.00017078** | **0.00034156** | |
| | v1-v2 | 23.671 | 39.092 | –2.7206 | **0.003258** | **0.006516** | minimum temperature |
| | v2-v3 | 65.605 | 39.092 | 4.6776 | **1.45E-06** | **2.90E-06** | |
| | v1-v3 | 60.4 | 39.092 | 3.7592 | **8.52E-05** | **0.00017046** | |
| Kouka | v1-v2 | 53.249 | 39.092 | 2.4977 | **0.0062506** | **0.012501** | maximum temperature |
| | v2-v3 | 54.39 | 39.092 | 2.699 | **0.0034775** | **0.0069549** | |
| | v1-v3 | 62.319 | 39.092 | 4.0978 | **2.09E-05** | **4.17E-05** | |
| | v1-v2 | 23.43 | 39.092 | –2.763 | **0.0028634** | **0.0057267** | minimum temperature |
| | v2-v3 | 66.219 | 39.092 | 4.786 | **8.51E-07** | **1.70E-06** | |
| | v1-v3 | 61.193 | 39.092 | 3.8993 | **4.82E-05** | **9.65E-05** | |
| Fada Gourma | v1-v2 | 53.892 | 39.092 | 2.6114 | **0.0045088** | **0.0090176** | maximum temperature |
| | v2-v3 | 51.039 | 39.092 | 2.1077 | **0.017527** | **0.035054** | |
| | v1-v3 | 61.1 | 39.092 | 3.8828 | **5.16E-05** | **0.00010324** | |
| | v1-v2 | 18.835 | 39.092 | –3.5737 | **0.00017597** | **0.00035194** | minimum temperature |
| | v2-v3 | 66.235 | 39.092 | 4.7888 | **8.39E-07** | **1.68E-06** | |
| | v1-v3 | 59.158 | 39.092 | 3.5401 | **0.00019998** | **0.00039996** | |
| Boromo | v1-v2 | 54.152 | 39.092 | 2.657 | **0.0039418** | **0.0078835** | maximum temperature |
| | v2-v3 | 51.48 | 39.092 | 2.1855 | **0.014425** | **0.028851** | |
| | v1-v3 | 61.938 | 39.092 | 4.0305 | **2.78E-05** | **5.57E-05** | |
| | v1-v2 | 24.94 | 39.09 | –2.50 | **0.0062515** | **0.012503** | minimum temperature |
| | v2-v3 | 65.59 | 39.09 | 4.675 | **1.47E-06** | **2.94E-06** | |
| | v1-v3 | 64.52 | 39.09 | 2.345 | **0.000198** | **0.0003696** | |
| Dédougou | v1-v2 | 50.34 | 39.092 | 2.699 | **0.0054792** | **0.0061521** | maximum temperature |
| | v2-v3 | 62.24 | 39.09 | 4.08 | **2.21E-05** | **4.42E-05** | |
| | v1-v3 | 55.118 | 39.092 | 2.8274 | **0.0023463** | **0.0046925** | |
| | v1-v2 | 50.061 | 39.092 | 1.9353 | **0.026479** | **0.052958** | minimum temperature |
| | v2-v3 | 54.94 | 39.09 | 2.50 | **0.0032515** | **0.032503** | |
| | v1-v3 | 60.694 | 39.092 | 3.8111 | 6.92E-05 | 0.00013836 | |

Source: Power NASA, 1981-2022, v1 = rainy pre-season; v2 = rainy season; v3 = post-season rainy.

### 3.3.2. Analysis of anomalies as a factor in temperature variability in Burkina Faso

Extreme temperatures are anomalies that develop decade by decade over the period 1981 to 2022. Indeed, in the 1980s, especially in 1981, 1982, 1983, and 1987, extreme temperature anomalies (maximum, minimum) exceeding z = 1.96 were recorded during the pre-rainy season at all the sites studied. Further temperature anomalies occurred in 1994, 1995, and 1998, mainly during the rainy and post-rainy seasons. From 2000 onward, the occurrence of extreme temperature anomalies increased significantly: the number of years in which anomalies occurred increased over the period 2000-2022, with anomalies occurring in 2000, 2001, 2002, 2003, 2005, 2009, 2011, 2013, 2015, 2019, and 2021. Extreme temperature anomalies occur during the rainy season, the post-rainy season and, to a lesser extent, the pre-rainy season. This indicates an increase in temperature variability at the study sites. Figure 3 shows temperature anomalies from 1981 to 2022.

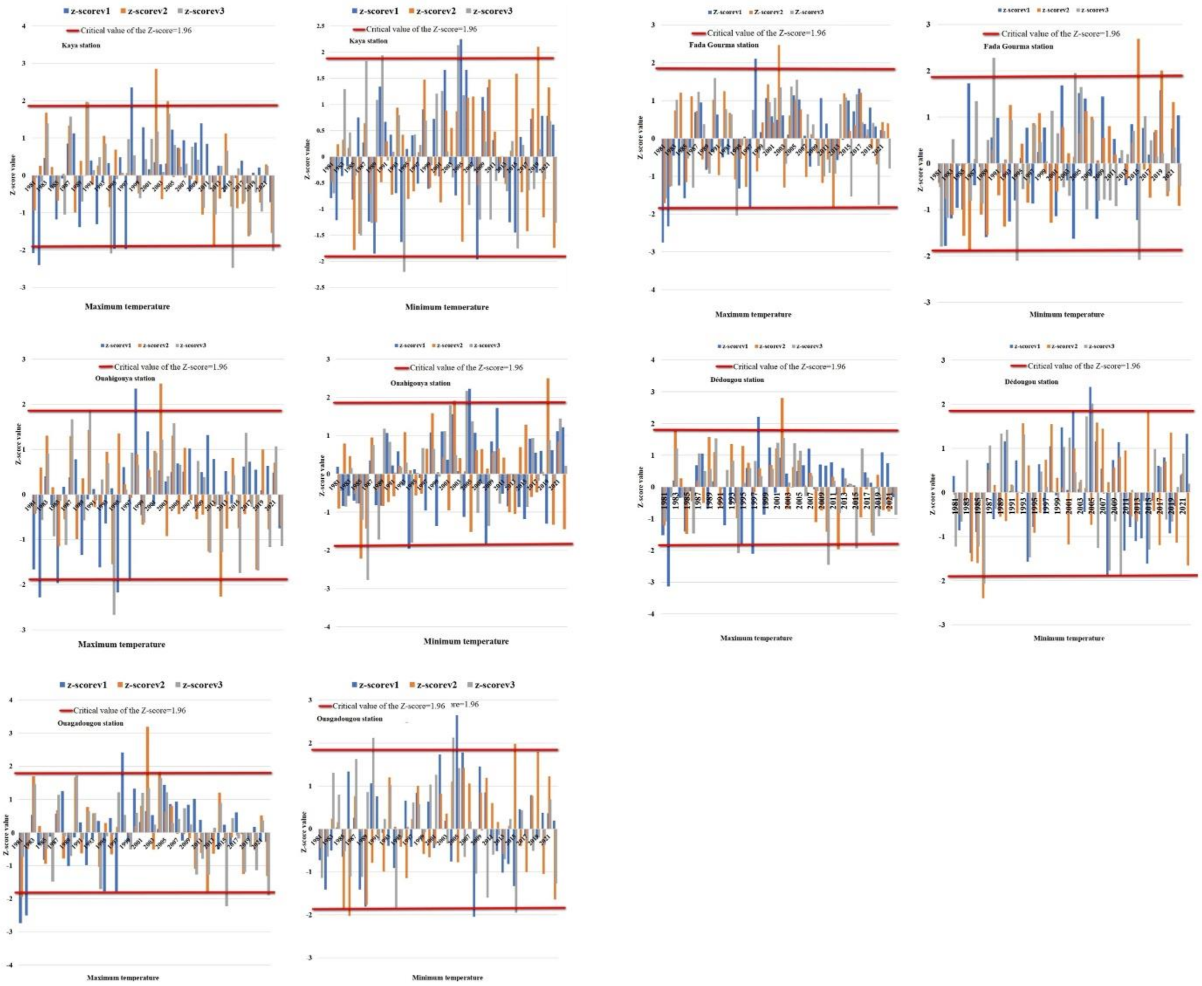


Fig. 3. Seasonal anomalies of extreme temperatures in the Sudano-Sahelian zone of Burkina Faso.

# 4. Discussion

## 4.1. Temperature trends in Burkina Faso and Africa

The results of the study are quite remarkable. Extreme temperatures (maximum and minimum) show a change in the 2000s compared to the period 1981-2022 period. Furthermore, extreme temperatures show an upward trend according to Spearman's *r*, regardless of seasonality. Temperature variability was also strong and increasing over the period 2000-2022. However, the trends vary from station to station. This could be explained by a general variation in rainfall and temperature across the country. Indeed, the area occupied by the Sahelian and Sudano-Sahelian domains has increased over time (1931-2010) to the detriment of the Sudanese domain (Rouamba 2017). Furthermore, isotherms have also shifted from north to south from 1971 to the present day, reflecting temperature dynamics across the country (Dipama 2014). Yaméogo and Rouamba (2023) also found an increase and change in maximum temperatures in the Sahelian, Sudano-Sahelian, and Sudanese domains over the period 1960-2019. Other studies in the Sudano-Sahelian domain (Rouamba et al. 2023) found similar results. Yanogo and Yaméogo (2023) also note that temperatures in the Sudano-Sahelian region of Burkina Faso are changing, particularly in the 2000s over the period 1990-2020. Several other studies carried out in West Africa and Africa as a whole corroborate the results of this study. For example, Sanogo et al. (2023) found that maximum temperatures in Mali are increasing, but that the trend was also upward for the period 1991-2020. Similar studies have confirmed the findings of previous studies. For example, Musa et al. (2021) found an increasing trend and high variability in extreme temperatures in north-central Nigeria. Other studies conducted in Nigeria (Ogunrayi et al. 2016; Ekwueme, Agunwamba 2021; Dan'azumi, Ibrahim 2023), Mauritania (Yacoub, Tayfur 2019), Senegal (Djaman et al. 2017) and Gambia (Jabbi et al. 2021) have made similar observations. According to Ilori and Ajayi (2020), extreme temperatures are evolving due to temporal breaks in temperature data in the 1980s, which then show an upward trend until 2010. Other regions of Africa are affected by changes in seasonal temperature cycles. In East Africa, particularly Ethiopia and South Africa, extreme temperatures are increasing (Worku et al. 2022; Chapungu et al. 2024). The same trends have also been observed in Central Africa, such as the Democratic Republic of Congo (Posite et al. 2024) and Burundi (Niyongendako et al. 2020). The work of Umeh et al. (2024) on 48 African countries shows an overall trend toward rising temperatures in all countries except Madagascar and Niger.

### 4.2. Seasonal temperature variability in Burkina Faso and West Africa

Maximum and minimum temperatures show inter-seasonal variability in the eight (08) stations in the Sudano-Sahelian region. This could be explained by the fact that in the arid tropical region of Africa where Burkina Faso is located, temperature is modulated by rainfall. Thus, the temperature is very high as the rainy season approaches, then moderately high during the rainy season, and the temperature drops just after the rainy season, i.e., in November, December, and January. This situation could influence the seasonal variability of extreme temperatures. In addition, in other studies in Burkina Faso, Yaméogo and Rouamba (2023), and Koala et al. (2023a), add that seasonal variability in maximum temperatures is observed across the country. Koala et al. (2023b) predict that a continuous trend in temperature variability in the Sudano-Sahelian zone (from the Nakambè catchment) will continue until 2050. Studies carried out in West Africa confirm these results. In Nigeria, maximum, minimum, and mean temperatures in the Niger basin over the period 1948-2008 (Oloruntade et al. 2016), as well as in the coastal region of Nigeria (Agbonaye, Okonofua 2024), have been rising steadily. In Mali and northern Togo they increased over the period 1951-2010 (Kouressy et al. 2019l; Gadedjisso-Tossou et al. 2021). According to Ringard et al. (2016) and Asamoah and Ansah-Mensah (2020), there has been an increase in extreme variability across the West African region (Sahel and Gulf of Guinea). There has also been an increase in extreme temperature anomalies. The various results show a general increase in temperatures, interspersed with a high-temperature variability according to season (wet and dry). This seasonal temperature variability results from the hydrological cycle (Diba et al. 2022).

## 5. Conclusion

Temperature extremes in the Sudano-Sahelian region of Burkina Faso were analyzed using normality, homogeneity, trend, and anomaly statistics. The normality tests showed that the maximum temperature data generally followed a normal distribution, while the minimum temperature data did not follow a normal distribution. Homogeneity tests of the temperature data reveal temperature breaks in the 2000s before, during, and after the rainy season for maximum temperature data. However, minimum temperatures showed little change. The study shows that temperatures change seasonally, with maximum temperatures changing more markedly than minimum temperatures during the pre-rainy season, the rainy season, and the post-rainy seasons. Temperatures are also highly variable, with anomalies observed in the pre-rainy season, the rainy season, and the post-rainy season in the 2000s. Local and regional authorities must, therefore, take urgent action to protect vulnerable groups.

## References


Aditya F., Gusmayanti E., Sudrajat J., 2021, Rainfall trend analysis using Mann-Kendall and Sen's slope estimator test in West Kalimantan, IOP Conference Series: Earth and Environmental Science, DOI: 10.1088/1755-1315/893/1/012006.

Agbonaye A.I., Okonofua E.S., 2024, Trends and spatial variability of climate change in Nigeria's coastal region. Malaysian Journal of Civil Engineering, 36 (2), 19-32, DOI: 10.11113/mjce.v36.21861.

Ahmad I., Tang D., Wang T., Wang M., Wagan B., 2015, Precipitation trends over time using Mann-Kendall and spearman's rho tests in Swat River Basin, Pakistan, Advances in Meteorology, 1, DOI: 10.1155/2015/431860.

Ahmed M., Hoque A., Islam M.K., 2022, A trend analysis of climatic variables in the Karimganj District of Assam, India, Indian Journal of Science and Technology, 15 (10), 442-450, DOI: 10.17485/IJST/v15i10.109.

Alemu Z.A., Dioha M.O., 2020, Climate change and trend analysis of temperature: the case of Addis Ababa, Ethiopia, Environmental Systems Research, 9, 1-15, DOI: 10.1186/s40068-020-00190-5.

Asamoah Y., Ansah-Mensah K., 2020, Temporal description of annual temperature and rainfall in the Bawku area of Ghana, Advanced in Meteorology, 1, DOI: 10.1155/2020/3402178.

Arisco N.J., Sewe M.O., Bärnighausen T., Sié A., Zabre P., Bunker A., 2023, The effect of extreme temperature and precipitation on cause-specific deaths in rural Burkina Faso: a longitudinal study, The Lancet Planetary Health, 7 (6), 4780489, DOI: 10.1016/S2542-5196(23)00027-X.

Ay M., 2021, Trend tests on maximum rainfall series by a novel approach in the Aegean region, Turkey, Meteorology and Atmospheric Physics, 133 (4), 1041-1055, DOI: 10.1007/s00703-021-00795-0.

Bacescu-Carbunaru A., Condruz-Bacescu M., 2013, Methods used in the seasonal variations analysis of time series, Romanian Statistical Review, 61 (3), 12-18.

Bambara D., Compaoré H., Bilgo A., 2018, Évolution des températures au Burkina Faso entre 1956 et 2015: cas de Ouagadougou et de Ouahigouya, Physio-Géo. Géographie Physique et Environnement, 12, 23-41, DOI: 10.4000/physio-geo.5688.

Bickici Arikan B., Kahya E., 2019, Homogeneity revisited: analysis of updated precipitation series in Turkey, Theoretical and Applied Climatology, 135 (1), 211-220, DOI: 10.1007/s00704-018-2368-x.

Chapungu L., Nhamo G., Chikodzi D., Dube K., 2024, Trends and impacts of temperature and fire regimes in South Africa's coastal national parks: implications for tourism, Natural Hazards, 120, DOI: 10.1007/s11069-023-06384-1.

Conover W.J., Johnson M.E., Johnson M.M., 1981, A comparative study of tests for homogeneity of variances, with applications to the outer continental shelf bidding data, Technometrics, 23, 351-361, DOI: 10.2307/1268225.

Dan'azumi S., Ibrahim U.A., 2023, Trend analysis of observed precipitation, temperature, and streamflow for Hadejia-Nguru wetlands catchment, Nigeria, Theoretical and Applied Climatology, 151 (1), 195-207, DOI: 10.1007/s00704-022-04270-7.

Darman L.P., Januhariadi J., Yudha M.P., Aslan A., 2024, Assessment of NASA POWER reanalysis products as data resources alternative for weather monitoring in West Sumbawa, Indonesia, E3S Web of Conferences, 485, DOI: 10.1051/e3sconf/202448506006.

De Pinto A., Demirag U., Haruna A., Koo J., Asamoah M., 2012, Climate change, agriculture, and food crop production in Ghana. IFPRI Policy Note No. 3., Washington, DC, USA: International Food Policy Research Institute (IFPRI).

Diba I., Diedhiou A., Famien A.M., Camara M., Fotso-Nguemo T.C., 2022, Changes in compound extremes of rainfall and temperature over West Africa using CMIP5 simulations, Environmental Research Communications, 4 (10), DOI: 10.1088/2515-7620/ac9aa7.

Dipama J.M., 2014, Approche spatiale du phénomène du réchauffement climatique à l'échelle du Burkina Faso et perceptions des populations, Climat et Développement, 16, 36-49.

Djaman K., Balde A.B., Rudnick D.R., Ndiaye O., Irmak S., 2017, Long-term trend analysis in climate variables and agricultural adaptation strategies to climate change in the Senegal River Basin, International Journal of Climatology, 37 (6), 2873-2888, DOI: 10.1002/joc.4885.

Ekwueme B.N., Agunwamba J.C., 2021, Trend analysis and variability of air temperature and rainfall in regional river basins, Civil Engineering Journal, 7 (5), 816-826, DOI: 10.28991/cej-2021-03091692.

Esit M., Yuce M.I., 2022, Comprehensive evaluation of trend analysis of extreme drought events in the Ceyhan River Basin, Turkey, Meteorology Hydrology and Water Management, 11 (1), 22-43, DOI: 10.26491/mhwm/154573.

Frimpong B.F., Koranteng A., Molkenthin F., 2022, Analysis of temperature variability utilising Mann-Kendall and Sen's slope estimator tests in the Accra and Kumasi Metropolises in Ghana, Environmental Systems Research, 11 (1), DOI: 10.1186/s40068-022-00269-1.

Gadedjisso-Tossou A., Adjegan K.I., Kablan A.K.M., 2021, Rainfall and temperature trend analysis by Mann–Kendall test and significance for Rainfed Cereal Yields in Northern Togo, Science, 3 (1), DOI: 10.3390/sci3010017.

Hammer Ø., 2024, PAST: PAleontological STatistics. Version 4.17, Reference Manual, Natural History Museum, University of Oslo, 315 pp.

Ilori O.W., Ajayi V.O., 2020, Change detection and trend analysis of future temperature and rainfall over West Africa, Earth Systems and Environment, 4, 493-512, DOI: 10.1007/s41748-020-00174-6.

Jabbi F.F., Li Y.E., Zhang T., Bin W., Hassan W., Songcai Y., 2021, Impacts of temperature trends and SPEI on yields of major cereal crops in the Gambia, Sustainability, 13 (22), DOI: 10.3390/su132212480.

Jackson S.L., 2009, Research Methods and Statistics: A Critical Thinking Approach, 3rd edition, Wadsworth Publishing, 430 pp.

Jiménez-Jiménez S.I., Ojeda-Bustamante W., Inzunza-Ibarra M.A., Marcial-Pablo M.D.J., 2021, Analysis of the NASA-POWER system for estimating reference evapotranspiration in the Comarca Lagunera, Mexico, Ingeniería Agrícola y Biosistemas, 13 (2), 201-226, DOI: 10.5154/r.inagbi.2021.03.050.

Kheyruri Y., Sharafati A., Ahmadi Lavin J., 2024, Performance assessment of NASA POWER temperature product with different time scales in Iran, Acta Geophysica, 72, 1175-1189, DOI: 10.1007/s11600-023-01186-2.

Koala S., Dipama J.M., Vissin E.W., 2023a, Evolution of extreme rainfall and temperature indices in the Nakambé Watershed at the Bagré outflow (Burkina Faso), International Journal of Advanced Engineering and Management Research, 8 (02), 154-169, DOI: 10.51505/ijaemr.2023.8214.

Koala S., Nakoulma G., Dipama, J.-M., 2023b, Évolution des Précipitations et de la Température a l'Horizon 2050 avec les modèles climatiques CMIP5 dans le bassin versant du Nakambé (Burkina Faso), International Journal of Progressive Sciences and Technologies, 37 (2), 110-124, DOI: 10.52155/ijpsat.v37.2.5133.

Kosmowski F., Lalou R., Sultan B., Ndiaye O., Muller B., Galle S., Seguis L., 2015, Observations et perceptions des changements climatiques: Analyse comparée dans trois pays d'Afrique de l'Ouest, [in:] Les Sociétés Rurales Face aux Changements Climatiques et Environnementaux en Afrique de l'Oues, B. Sultan, R. Lalou, M.A. Sanni, Z. Oumarou, M.A. Soumaré (eds.), IRD Éditions, 89-111.

Kouressy M., Sultan B., Vaksmann M., Bélières J.F., Claessens L., Dingkuhn M., Teme N., 2019, Climate change and cereal production evolution trend in the Sahel: case study in Mali from 1951 to 2010, Sustainable Agriculture Research, 8 (2), 68-89, DOI: 10.22004/ag.econ.301883.

Kwawuvi D., Mama D., Agodzo S.K., Hartmann A., Larbi I., Bessah E., Abraham T., Dotse S.-Q., Limantol A.M., 2022, An investigation into the future changes in rainfall onset, cessation and length of rainy season in the Oti River Basin, West Africa, Modeling Earth Systems and Environment, 8 (4), 5077-5095, DOI: 10.1007/s40808-022-01410-w.

Lebeza T.M., Gashaw T., Tefera G.W., Mohammed J.A., 2023, Trend analysis of hydro-climate variables in the Jemma sub-basin of Upper Blue Nile (Abbay) Basin, Ethiopia, SN Applied Sciences, 5 (5), DOI: 10.1007/s42452-023-05345-4.

Lin N.J., Abd Aziz S., Feng H.Y., Wayayok A., Kamal M.R., 2015, Homogeneity analysis of rainfall in Kelantan, Malaysia, Jurnal Teknologi, 76 (15), DOI: 10.11113/jt.v76.5944.

Longobardi A., Villani P., 2010, Trend analysis of annual and seasonal rainfall time series in the Mediterranean area, International journal of Climatology, 30 (10), 1538-1546, DOI: 10.1002/joc.2001.

Lornezhad E., Ebrahimi H., Rabieifar H.R., 2023, Analysis of precipitation and drought trends by a modified Mann–Kendall method: a case study of Lorestan province, Iran, Water Supply, 23 (4), 1557-1570, DOI: 10.2166/ws.2023.068.

Mann H.B., 1945, Nonparametric tests against trend, Econometrica, 13 (3), 245-259, DOI: 10.2307/1907187.

Marzouk O.A., 2021, Assessment of global warming in Al Buraimi, sultanate of Oman based on statistical analysis of NASA POWER data over 39 years, and testing the reliability of NASA POWER against meteorological measurements, Heliyon, 7 (3), DOI: 10.1016/j.heliyon.2021.e06625.

Mirabbasi R., Ahmadi F., Jhajharia D., 2020, Comparison of parametric and non-parametric methods for trend identification in groundwater levels in Sirjan plain aquifer, Iran, Hydrology Research, 51 (6), 1455-1477, DOI: 10.2166/nh.2020.041.

Muia V.K., Opere A.O., Ndunda E., Amwata D.A., 2024, Rainfall and temperature trend analysis using Mann-Kendall and Sen's slope estimator test in Makueni County, Kenya, Journal of Materials and Environmental Science, 15 (3), 349-367.

Musa M., Suleiman Y.M., Yahaya T.I., Tsado E.K., 2021, Statistical analysis of trend in extreme rainfall and temperature events in parts of north central states, Nigeria, Journal of Meteorology and Climate Science, 18 (2), 19-23.

Muthoni F.K., Odongo V.O., Ochieng J., Mugalavai E.M., Mourice S.K., Hoesche-Zeledon I., Mwila M., Bekunda M., 2019, Long-term spatial-temporal trends and variability of rainfall over Eastern and Southern Africa, Theoretical and Applied Climatology, 137, 1869-1882, DOI: 10.1007/s00704-018-2712-1.

Nisansala W.D.S., Abeysingha N.S., Islam A., Bandara A.M.K.R., 2020, Recent rainfall trend over Sri Lanka (1987-2017), International Journal of Climatology, 40 (7), 3417-3435, DOI: 10.1002/joc.6405.

Niyongendako M., Lawin A.E., Manirakiza C., Lamboni B., 2020, Trend and variability analysis of rainfall and extreme temperatures in Burundi, International Journal of Environment and Climate Change, 10 (6), 36-51, DOI: 10.9734/IJECC/2020/v10i630203.

Ogunrayi O.A., Akinseye F.M., Goldberg V., Bernhofer C., 2016, Descriptive analysis of rainfall and temperature trends over Akure, Nigeria, Journal of Geography and Regional Planning, 9 (11), 195-202, DOI: 10.5897/JGRP2016.0583.

Oloruntade A.J., Mohammad T.A., Ghazali A.H., Wayayok A., 2016, Spatial and temporal trends in mean, maximum and minimum temperature in the Niger-South Basin, Nigeria, Malaysian Journal of Civil Engineering, 28 (3), 365-381, DOI: 10.11113/mjce.v28.15981.

Oloyede A., Ozuomba S., Asuquo P., Olatomiwa L., Longe O.M., 2023, Data-driven techniques for temperature data prediction: big data analytics approach, Environmental Monitoring and Assessment, 195, DOI: 10.1007/s10661-023-10961-z.

Pandey B., Negi V., Anand S., Ranjan O., Yadav G., Srivastava S., 2023, Estimation of anomalies and temporal temperature and precipitation trends in the Cryospheric Himalayan Highland Region (CHHR), Uttarkashi, Uttarakhand, India, Mausam, 74 (1), 29-42, DOI: 10.54302/mausam.v74i1.875.

Posite V.R., Ahana B.S., Abdelbaki C., Zerga A., Guadie A., 2024, Analysis of temperature and rainfall trends in Beni City, Democratic Republic of Congo, Journal of Earth System Science, 133 (2), DO: 10.1007/s12040-024-02308-0.

Rahman M.A., Yunsheng L., Sultana N., 2017, Analysis and prediction of rainfall trends over Bangladesh using Mann-Kendall, Spearman's rho tests and ARIMA model, Meteorology and Atmospheric Physics, 129 (4), 409-424, DOI: 10.1007/s00703-016-0479-4.

Rahmani V., Hutchinson S.L., Harrington Jr J.A., Hutchinson J.M., Anandhi A., 2015, Analysis of temporal and spatial distribution and change-points for annual precipitation in Kansas, USA, International Journal of Climatology, 35 (13), 3879-3887, DOI: 10.1002/joc.4252.

Ringard J., Dieppois B., Rome S., Diedhiou A., Pellarin T., Konaré A., Diawara A., Konaté D., Dje B.K., Katiellou G.L., Seidou Sanda I., Hassane B., Vischel T., Garuma G.F., Mengistu G., Camara M., Diongoue A., Gaye A.T., Descroix L., 2016, The intensification of thermal extremes in west Africa, Global and Planetary Change, 139, 66-77, DOI: 10.1016/j.gloplacha.2015.12.009.

Rouamba S., 2017, Variabilité climatique et accès à l'eau dans les quartiers informels de Ouagadougou, thèse de doctorat unique en géographie, Université Ouaga I Pr Joseph KI-ZERBO, 445 pp.

Rouamba S., Yaméogo J., Sanou K., Zongo R., Yanogo I.P., 2023, Trends and variability of extreme climate indices in the Boucle du Mouhoun (Burkina Faso), GEOREVIEW: Scientific Annals of Stefan cel Mare University of Suceava. Geography Series, 33 (1), 70-84, DOI: 10.4316/GEOREVIEW.2023.01.07.

Sanogo A., Kabange R.S., Owusu P.A., Djire B.I., Donkoh R.F., Dia N., 2023, Investigation into recent temperature and rainfall trends in Mali using Mann-Kendall trend test: case study of Bamako, Journal of Geoscience and Environment Protection, 11 (3), 155-172, DOI: 10.4236/gep.2023.113011.

Sen P.K., 1968, Estimates of the regression coefficient based on Kendall's tau, Journal of the American Statistical Association, 63(324), 1379-1389, DOI: 10.1080/01621459.1968.10480934.

Talib S.A.A., Idris W.M.R., Neng L.J., Lihan T., Rasid M.Z.A., 2024, Irregularity and time series trend analysis of rainfall in Johor, Malaysia, Heliyon, 10 (9), DOI: 10.1016/j.heliyon.2024.e30324.

Toma M.B., Belete M.D., Ulsido M.D., 2023, Trends in climatic and hydrological parameters in the Ajora-Woybo watershed, Omo-Gibe River basin, Ethiopia, SN Applied Sciences, 5 (1), DOI: 10.1007/s42452-022-05270-y.

Trisos C., Adelekan I., Totin E., Ayanlade A., Efitre J., Gemeda A., Kalaba K., Lennard C., Masao C., Mgaya Y., Ngaruiya G., Olago D., Simpson N., Zakieldeen R., Jessica Thorn J., 2022, Africa, [in:' Climate Change 2022: Impacts, Adaptation and Vulnerability, Contribution of Working Group II to the Sixth Assessment Report of the Intergovernmental Panel on Climate.

Umeh S.C., Gil-Alana L.A., 2024, Trends in temperatures in Sub-Saharan Africa. Evidence of global warming, Journal of African Earth Sciences, 213, DOI: 10.1016/j.jafrearsci.2024.105228.

Wickramasinghe A., Muthukumarana S., Schaubroeck M., Wanasundara S.N., 2023, An anomaly detection method for identifying locations with abnormal behavior of temperature in school buildings, Scientific Reports, 13 (1), DOI: 10.1038/s41598-023-49903-7.

Wijngaard J.B., Klein Tank A.M.G., Können G.P., 2003, Homogeneity of 20$^{th}$ century European daily temperature and precipitation series, International Journal of Climatology, 23, 679-692, DOI: 10.1002/joc.906.

Worku M.A., Feyisa G.L., Beketie K.T., 2022, Climate trend analysis for a semi-arid Borana zone in southern Ethiopia during 1981-2018, Environmental Systems Research, 11 (1), DOI: 10.1186/s40068-022-00247-7.

Xu Z.X., Li J.Y., Liu C.M., 2007, Long-term trend analysis for major climate variables in the Yellow River basin, Hydrological Processes: An International Journal, 21 (14), 1935-1948, DOI: 10.1002/hyp.6405.

Yacoub E., Tayfur G., 2019, Trend analysis of temperature and precipitation in Trarza region of Mauritania, Journal of Water and Climate Change, 10 (3), 484-493, DOI: 10.2166/wcc.2018.007.

Yaméogo J., Rouamba S., 2023, Extreme temperature in Burkina Faso: decadal spatio-temporal changes between 1960 and 2019, European Journal of Theoretical and Applied Sciences, 1 (6), 441-450, DOI: 10.59324/ejtas.2023.1(6).43.

Yanogo I.P., Yaméogo J., 2023, Recent rainfall trends between 1990 and 2020: contrasting characteristics between two climate zones in Burkina Faso (West Africa), Glasnik Srpskog Geografskog Drustva, 103 (1), 87-106, DOI: 10.2298/GSGD2301087Y.

Yue S., Pilon P., Cavadias G., 2002, Power of the Mann–Kendall and Spearman's rho tests for detecting monotonic trends in hydrological series, Journal of Hydrology, 259 (1), 254-271, DOI: 10.1016/S0022-1694(01)00594-7.

Zakwan M., 2021, Trend analysis of groundwater level using innovative trend analysis, [in:] Groundwater Resources Development and Planning in the Semi-Arid Region, C.B. Pande, K.N. Moharir (eds.), Cham: Springer International Publishing, 389-405.

Zeitoun M., 2024, Analysis of temperature anomalies during the spring months in Jordan, International Journal of Geoinformatics, 20 (1), 88-98, DOI: 10.52939/ijg.v20i1.3029.

# Combined approach to the analysis of near-surface wind speed tendencies at the Vernadsky Station, West Antarctic Peninsula

Liudmyla Gorbachova, Borys Khrystiuk, Vitalii Shpyg

Ukrainian Hydrometeorological Institute

Denys Pishniak

National Antarctic Scientific Center of Ukraine

Abstract

In Antarctica, studying the near-surface wind regime is important because its dynamics directly affect the continent's ice shelves. The near-surface wind is also important for analyzing global and regional climate. Vernadsky Station has a fairly long observation series of near-surface wind speed. These data are widely used to research changes, variability, and trends in the near-surface wind regime on the Antarctic Peninsula. The observation series, however, has gaps and incorrect values associated with periodical updates of measurement devices. Thus, the observation data require careful evaluation of homogeneity and stationarity. The objective of this study was to investigate the homogeneity, stationarity, and tendencies of the near-surface wind speed in the area of the Vernadsky Station based on a combined approach using several statistical and graphical methods. The methods' diverse properties support more robust estimates. Consequently, five statistical tests (standard normal Alexandersson test, Buishand test, Pettitt test, von Neumann relation, and Mann-Kendall test) and three graphical methods (chronological graph, mass curve, and residual mass curve) were employed. Most of the observation series is homogeneous and stationary, except the mean annual and February mean monthly near-surface wind speeds, which display both decreasing and increasing phases in their long-term cyclical fluctuations, which are continuing. Violation of homogeneity and stationarity results from the comparison of different phases of cyclic fluctuations (decrease and increase), which have different statistical characteristics. We show that over the past 20 years at the station, the near-surface wind speed has tended to increase in all months of the year.

Keywords

Antarctica, graphic methods, homogeneity, stationarity, statistical tests.

Submitted 3 January 2025, revised 7 February 2025, accepted 12 March 2025

DOI: 10.26491/mhwm/202905

## 1. Introduction

In Antarctica, the near-surface wind (NSW) regime is no less important than changes in the air temperature; both of these characteristics are used to analyze the state of the global and regional climate (Parish, Cassano 2001; Ramesh, Soni 2018). NSW in the coastal zone and over continental Antarctica is partially related to atmospheric circulation and its intensity (Tymofeyev et al. 2017; de Brito Neto et al. 2022). Therefore, changes in the NSW regime reflect changes in the climate system over all of Antarctica. Spence et al. (2014), Hazel (2019), and Alkama et al. (2020) showed that changes in the NSW regime around Antarctica affect the continent's ice shelves. Thus, in the NSW regime, there is a decrease in the magnitude of easterly and southerly wind components and an increase in the magnitude of the westerly wind component. Because the westerly winds, generally of marine origin, are warmer, there is greater heat transfer to the floating glaciers of Antarctica and, accordingly, melting of the ice sheets. The latter effect contributes to global sea level rise. Some studies assess the potential of Antarctic flows to generate wind energy (Yu et al. 2020; Wang et al. 2023), and it has been shown that the strongest winds on Earth close to sea level are formed over Antarctica at coastal sites in Adélie Land (Parish 1988; Turner et al. 2009). However, the low air temperatures make working there difficult for man and machine alike (Yu et al. 2020).

Usually, in Antarctica, changes and trends in NSW are studied through observations from meteorological stations and through reanalysis (Tymofeyev et al. 2017; Dong et al. 2020). Although observations yield reliable information about the characteristics of the wind in specific places in Antarctica, the data contain gaps and incorrect values. The number of gaps, in relation to the total length of the data series, are, however, generally few. For example, at the Vernadsky Station, missing data are approximately 0.07% of the total (Tymofeyev et al. 2017). Gaps in the data record may be caused by interruptions in observations due to the replacement, repair, and adjustment of equipment. Incorrect values may be related to both human errors in recording and the difficulties of conducting instrumental observations in harsh weather conditions. In addition, research stations are predominately located near the Antarctic coasts, which results in fewer observational data records for studying the central part of the continent. Reanalysis of data makes it possible to obtain a spatial distribution of the NSW, however, mitigating certain limitations of the observational data. While this approach generalizes and simplifies the characteristics of the NSW, it does allow for obtaining its general tendencies (Turner et al. 2009).

At the Vernadsky Station, the NSW regime is shaped by regional features such as the local foehn winds, which are generated in the mountains of the Antarctic Peninsula (King, Turner 1997). Many researchers use the observational data from this station to investigate the changes, variability, and tendencies of the NSW regime (van Lipzig et al. 2004; Turner et al. 2009; Tymofeyev et al. 2017; Dong et al. 2020; Andres-Martin et al. 2024). For example, van Lipzig et al. (2004) modeled the NSW regime over the Antarctic Peninsula, including data from observations from the Vernadsky Station. Turner et al. (2009) reported that since the 1950s, one of the greatest statistically significant increases in the NSW speed has been in the area of the Vernadsky Station. Tymofeyev et al. (2017) reported that, according to the data from the Vernadsky Station, an increase in the NSW speed is seen under conditions of increased air temperature, which is a manifestation of climate change in the study region. This phenomenon reflects changes in atmospheric circulation, primarily the strengthening of the westerly wind and increase of cyclogenesis in the Antarctic. Statistical inhomogeneity in the wind speed series was revealed. Dong et al. (2020) reported that six recent global reanalysis products show positive trends in the annual and summer wind speeds for the 1980-2018 period, which are linked with positive polarity of the southern annular mode. It should be noted that observational data from the Vernadsky Station were also used as input to the reanalysis. Andres-Martin et al. (2024) reported that the observed annual trends in the NSW speed exhibit a generally positive trend, marked by a strong seasonal variability at the northern Antarctic Peninsula.

The Vernadsky Station NSW speed data require careful assessment of homogeneity and stationarity. Such analysis is also needed in view of climatic changes, which can cause violations of the homogeneity and stationarity of observational series. In previous studies (Tymofeyev et al. 2017; Andres-Martin et al. 2024), the NSW homogeneity, stationarity, and tendencies at the Vernadsky Station were analyzed exclusively by statistical tests. Kundzewicz and Robson (2000; 2004) recommended applying more graphical analysis to confirm the results of evaluating the tendencies of time series by standard statistical tests. Graphical analysis is especially important when statistical analyses do not have unambiguous interpretations or when only one statistical test (or several statistical tests with the same properties) is used (Robson 2002). So, for more reliable results, a complex approach using various tests and methods is recommended (Kundzewicz, Robson 2004; Gorbachova et al. 2022).

A significant amount of research is devoted to statistical analysis of time series. Much scientific interest was sparked by the monograph of Box and Jenkins (1970), in which the methodological foundations of time series analysis in various fields, such as economics, natural sciences, etc., were developed. The most widespread methods for assessing the homogeneity and stationarity of an observational series are various parametric and non-parametric statistical criteria (tests) described and recommended by WMO guidelines (WMO 1990; 2018). Criteria such as the Alexandersson, Terry, Buishand, Pettitt, Spearman, von Neumann, Wald-Wolfowitz, and Mann-Kendall tests are the most widely used.

Graphic analysis of the homogeneity and stationarity evaluation of observation series is based on various graphs, such as correlation (x/y plot), histogram, mass curve, double mass curve, residual mass curve, and chronological graph. Among these, mass curve analysis, double mass analysis, and residual mass curve are the most widely used. Klemeš (1987) and Gorbachova (2016) reported that at the end of the 19th and during the 20th century, these methods were developed by W. Rippl, A. Schoklitsch, J. Novotny, C. Merriam, M. Kohler, L. Weiss and W. Wilson, J. Searcy and C. Hardison, and K. Ehlert. The methods of the mass curve and residual mass curve were developed by Rippl (1883). Subsequently, Schoklitsch (1923) and Novotny (1925) proposed to calculate the residual mass curve of the mean flow value (Klemeš 1987). In 1937, Merriam invented a double mass curve for flow analysis, combining precipitation and river flow information. Kohler (1949) proposed using the slope coefficient of the double mass curve to correct violations of the homogeneity of a series of precipitation observations. Weiss and Wilson (1953) investigated the estimation of significance of change in the double mass curve slope. Searcy and Hardison (1960) developed a fundamental method for analysis of time series based on the use of a double mass curve and a residual mass curve for homogeneity analyses of observation series of precipitation, hydrologic flows, and sediment flow. Ehlert (1972) presented a modified version of the double residual mass curve in which the relative accumulation of deviations derives from the mean of two observation series, used to homogenize the precipitation observation series. In these investigations, methodological recommendations for applying each approach separately and for solving a separate task were developed. More recent approaches to assessing the homogeneity and stationarity of observation series using graphical methods have been developed by Gorbachova (2014; 2016), and applied to analyses of hydrometeorological observation series (Gorbachova et al. 2018; 2022; Romanova et al. 2019; Zabolotnia et al. 2019; 2022; Khrystiuk, Gorbachova 2023).

The objective of this paper is to investigate the homogeneity, stationarity, and tendencies of NSW speed at the Vernadsky Station based on a combined analytical approach, one consisting of the use of several statistical and graphical methods. These methods are described in Section 2, while in Section 3 they are applied in analyses of the data.

## 2. Study area, data, and methods

### 2.1. Study area

Until 1996, the Vernadsky Station was the British Faraday station. On February 6, 1996, the British flag was solemnly taken down, and the flag of Ukraine was raised. The Vernadsky Station is located off the western coast of the Antarctic Peninsula on Galindez Island, Argentine Islands Archipelago (Fig. 1), at coordinates 65.25°S, 64.27°W. The climate is marine subarctic, dominated by large-scale circumpolar circulation in the atmosphere and ocean (King, Turner 1997).


Fig. 1. Location of the Vernadsky Station (background graphic from Klok, Kornus 2021).

The mountains of the Antarctic Peninsula and the meridional orientation of its coastline are the chief influences on NSW and air temperature regimes in the area of the Vernadsky Station (Turner et al. 2009). As a result, these regimes are specific to the locality, a matter discussed in detail by Gorbachova et al. (2022), Khrystiuk et al. (2023), and Shpyg et al. (2024).

### 2.2. Data

In this study of the period 1955-2022 at the Vernadsky Station, the NSW speed data (10 m above ground) for eight measurements per day (0, 3, 6, 9, 12, 15, 18, 21 UTC) were provided by the state institution National Antarctic Scientific Center, Ukraine (NASC). Over the life of the Vernadsky Station, various instruments and complexes have been used to measure NSW speed. From 1955 to 1966 a Munro Mk. 1 indicator was used to measure wind speed, followed from 1967 to January 1976 by a Munro Mk. 1B indicator.

Since February 1976, a Munro Mk. 4A indicator has been installed at the station, and in March 1980 it was transferred to a new weather mast. During January 10-24, 1984, an automatic meteorological station SCAWS (Synoptic and Climatological Automatic Weather Station) was installed and tested, and on January 1, 1986, it began to be used in operational mode; that is, this date must be considered the date of the device update. In December 1990, the MAWS (Modular Automatic Weather Station) automatic weather station was installed and on April 1, 1992 began to be used in operational mode. Since February 20, 2011, a Ukrainian-made Mobile Meteorological Complex (MMC), "Troposphere" (Mobile AWS "Troposphere"), became the main measuring complex at Vernadsky Station. In February 2019, MAWS was dismantled, and a Vaisala AWS-310 automatic weather station was installed, which began working in test mode. Measurements from MMC "Troposphere" continue to be sent to the data exchange system of the World Meteorological Organization. On April 1, 2020, the official transition to the Vaisala AWS-310 automatic weather station was made, and it became the main source of meteorological data for the international exchange system (i.e., formation of WMO SYNOP and CLIMAT summaries). Currently, MMC "Troposphere" works as a reserve. So, the Vernadsky and record of NSW speed contains gaps incorrect values resulting from frequent replacement of equipment.

Therefore, the Vernadsky NSW speed data were checked for missing values and gross errors. This process involved two stages: a semantic check and a review of the data based on parameters of the meteorological values. The semantic check was done to identify cases when year, month, date, time, and values of NSW speed were missing using the British Antarctic Survey database; it included searching for missing measurement record identifiers (e.g., values of –99.9). Furthermore, a more detailed analysis of the series of observations revealed the presence of several types of errors, with examples as follows:

- Explicit errors in recording the meteorological value. These are revealed when a value goes beyond the data range obtained over the entire period of observation, or when a value is significantly greater than the nearest two measurements.
- Implicit (hidden) errors. These are identified when the value of the meteorological quantity seems correct by itself, but the value appears erroneous in the context of another additional meteorological quantity or quantities. For example, a wind speed value is zero, but a wind direction value is reported (i.e., has values from 1° to 360°).

## 2.3. Methodology

The homogeneity, stationarity, and trends of the NSW speed series at the Vernadsky Station were evaluated with a combined approach comprising five statistical and three graphical methods. Statistical homogeneity means that the statistical properties of any one part of an overall dataset are the same as any other part (WMO 1990). Homogeneity was tested by two parametric (standard normal Alexandersson, Buishand) and two non-parametric (Pettitt, von Neumann relation) methods. Stationarity of the observation series means that its statistical characteristics do not change over time. In stationary time series, there is no trend in the mean or variance over time (WMO 1990). In this study, establishing the trend equation for the time series and correlation coefficients between variables were determined by the Pearson method. The statistical significance of the trend was evaluated using the non-parametric Mann-Kendall test.

The series was processed using RStudio Software 1.4.1717 with the following functions (R Core Team 2017):

- pettitt.test – Pettitt test;
- br.test – Buishand test;

- snh.test – standard normal Alexandersson test;
- VonNeumannTest – von Neumann relation;
- MannKendall – Mann-Kendall test;
- gml – construction of a linear trend;
- cor.test – determination of the correlation coefficient by the Pearson method.

Graphical methods make it possible to trace trends over time and identify periods of change, if any, to analyze cyclic fluctuations and their characteristics (e.g., phases of increase and decrease, their duration, synchronicity, and phasing). Three graphical methods were used in this research: mass curve, residual mass curve, and chronological graph. A mass curve is a graph of cumulative values of hydrometeorological characteristics, which, under constant conditions, is a straight line with a slope, relative to the abscissa axis, that is constant over time. The deviation of the hydrometeorological characteristic from a straight line on the graph is an indicator of change that implies change in the controlling factors, e.g., a change in the climate regime (Gorbachova 2014; Gorbachova et al. 2022). Short- and long-term cyclical fluctuations can be investigated by the residual mass curve. The residual mass curve is a graph of successively accumulated deviations of a hydrometeorological value from its initial value, for example, an arithmetic mean, depending on time or dates (Gorbachova et al. 2022). The chronological graph allows one to trace the changes and fluctuations of a hydrometeorological characteristic over time.

## 3. Results

### 3.1 Primary analysis of observational data

For the period 1955-2022 at Vernadsky Station, the observational data for NSW speed contains 198,696 points, of which 27,377 (almost 14% of the total number) have gaps and incorrect values (Fig. 2). Gross mechanical errors and significant outliers in the observation series were removed.

Most of the data that were considered erroneous and excluded from the research series in the period of 2014-2019 related to incorrect operation of the software, which occurred at low wind speeds and when wind changed direction through the 360° mark. The annual average number of observations is 2966. The largest number of gaps and incorrect values in the observations (1064) occurred in 1955, and the smallest number occurred in 2006 (2) (Fig. 2). There was also a significant number of gaps and incorrect values in the observations in 2019 (1108).

Based on eight measurements per day (viz., measurements every three hours), daily averages and mean monthly and mean annual values of the NSW speed were calculated. Mean monthly values of the NSW speed were not calculated for those months in which the number of missing records in the observations was 33% or more of the total number of records, where there were no observations for three consecutive days or more, or where there were 10 or more missing records in the observations at a given observation time (i.e., 0, 3, 6, 9, 12, 5, 18, or 21 UTC). Mean annual values of the NSW speed were not calculated for those years in which mean monthly values were not determined for four months of the year or if mean monthly values were not determined for two or more consecutive months in the year.

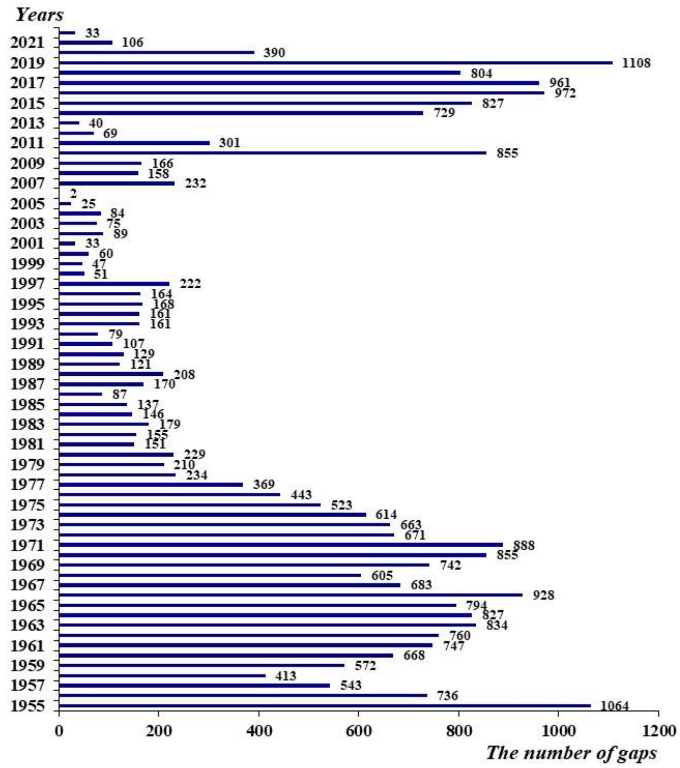


Fig. 2. The number of gaps and incorrect values (missing records) of observation series of the near-surface wind speed in the area of the Vernadsky Station in 1955-2022.

After data quality control, it turned out that even though the total duration of observation was 68 years, the mean duration of all of the records was only 49 years. The longest record of NSW speed has observations for 58 years (September), and the shortest record for 39 years (mean annual NSW speed) (Fig. 3).

During the observation period, the mean annual values of NSW speed ranged from 3.5 to 6.1 m/s. The multi-annual NSW speed is 4.8 m/s. The highest multi-annual mean monthly NSW speed was observed in September (6.0 m/s), and the lowest in January (3.6 m/s). The lowest mean monthly value of NSW speed was observed in June 1997 (1.7 m/s), and the highest in October 1955 (9.3 m/s).


Fig. 3. Observation periods and durations for near-surface wind speed in the area of the Vernadsky Station for the period 1955-2022.

### 3.2. Statistical analysis

Applying the four statistical tests at the 1% level of significance to assess the homogeneity of mean annual values of NSW speed in the area of the Vernadsky Station showed that all of the annual values indicated a violation of homogeneity in 1998, when the values of their statistics exceeded the critical values (Table 1). Therefore, the series of mean annual values of NSW speed in the area of the Vernadsky Station is inhomogeneous. Along with this, however, the tests indicate homogeneity of mean monthly values, which did not exceed critical values of the statistics of two or more tests for any month of year (Table 2). Thus, the series of mean monthly values is homogeneous, but the series of mean annual values is inhomogeneous. This is a contradictory result.

In addition, the tests show years in which trends in the mean monthly NSW speeds possibly change. However, for most months, the years of change, according to various tests, do not coincide, a finding that also fails to illuminate the multi-year NSW speed trends. For example, in February, the year of change is 2001, according to the Buishand test, and 1998 according to the Pettitt test. It can be assumed that such ambiguous results depend on the properties, features, and characteristics of the statistical tests themselves and result from the different durations of observation series with their many missing records (Figs. 2, 3).

Table 1. Results of tests of homogeneity of mean annual near-surface wind speed in the area of the Vernadsky Station according to statistical tests at the 1% level of significance.

| Test | The value of statistic | Critical value | Year of disturbance of homogeneity | *p*-value |
|---|---|---|---|---|
| Alexandersson | **14.9** | 11.2 | 1998 | 0.0009 |
| Buishand | **2.01** | 1.76 | 1998 | 0.0003 |
| Pettitt | **271** | 251 | 1998 | 0.0008 |
| von Neumann | **1.30** | 1.33->2.00 | - | 0.0000 |

Table 2. Results of testing homogeneity of mean monthly near-surface wind speed in the area of the Vernadsky Station according to statistical tests at the 1% level of significance

| Test | Alexandersson test | Buishand test | Pettitt test | von Neumann relation |
|---|---|---|---|---|
| January | | | | |
| Year of homogeneity disturbance | 1990 | 1990 | 1990 | - |
| The value of statistics | 6.79 | 1.33 | 172 | 2.12 |
| *p*-value | 0.1202 | 0.1650 | 0.1081 | 0.5287 |
| February | | | | |
| Year of homogeneity disturbance | 2010 | 2001 | 1998 | - |
| The value of statistics | 9.79 | **1.75** | **222** | 1.33 |
| *p*-value | 0.0226 | 0.0103 | 0.0303 | <0.0001 |
| March | | | | |
| Year of homogeneity disturbance | 1957 | 2003 | 2003 | - |
| The value of statistics | 6.66 | 1.54 | 217 | 1.80 |
| *p*-value | 0.1341 | 0.0580 | 0.2181 | 0.0024 |
| April | | | | |
| Year of homogeneity disturbance | 2005 | 1997 | 1997 | - |
| The value of statistics | 8.07 | 1.63 | 294 | 1,85 |
| *p*-value | 0.0674 | 0.0335 | 0.0788 | 0.0106 |

| Test | Alexandersson test | Buishand test | Pettitt test | von Neumann relation |
|---|---|---|---|---|
| May | | | | |
| Year of homogeneity disturbance | 2005 | 1998 | 1998 | - |
| The value of statistics | 6.35 | 1.37 | 258 | 1.93 |
| *p*-value | 0.1638 | 0.1481 | 0.0582 | 0.1839 |
| June | | | | |
| Year of homogeneity disturbance | 1956 | 2007 | 2007 | - |
| The value of statistics | 6.12 | 1.60 | 189 | 1.67 |
| *p*-value | 0.1792 | 0.0369 | 0.3724 | <0.0001 |
| July | | | | |
| Year of homogeneity disturbance | 1974 | 1974 | 1974 | - |
| The value of statistics | 5.62 | 1.23 | 191 | 1.81 |
| *p*-value | 0.2264 | 0.2848 | 0.3230 | 0.0053 |
| August | | | | |
| Year of homogeneity disturbance | 1989 | 1989 | 2000 | - |
| The value of statistics | 1.89 | 0.89 | 106 | 1.99 |
| *p*-value | 0.8984 | 0.7773 | 0.8733 | 0.5336 |
| September | | | | |
| Year of homogeneity disturbance | 2012 | 2005 | 2005 | - |
| The value of statistics | 6.13 | 1.63 | 208 | 1.72 |
| *p*-value | 0.1888 | 0.0342 | 0.5408 | <0.0001 |
| October | | | | |
| Year of homogeneity disturbance | 1964 | 1976 | 1976 | - |
| The value of statistics | 9.78 | 1.69 | 236 | 1.61 |
| *p*-value | 0.0303 | 0.0218 | 0.2782 | <0.0001 |
| November | | | | |
| Year of homogeneity disturbance | 2009 | 2009 | 2009 | - |
| The value of statistics | 10.7 | **1.79** | 249 | 1.61 |
| *p*-value | 0.0136 | 0.0089 | 0.1722 | <0.0001 |
| December | | | | |
| Year of homogeneity disturbance | 2004 | 2004 | 2004 | - |
| The value of statistics | 6.70 | 1.53 | 173 | 1.60 |
| *p*-value | 0.1221 | 0.0534 | 0.1572 | <0.0001 |

Note: Statistical values that exceed critical values are in bold.

The Mann-Kendall test was one of the tests used to assess the stationarity of the NSW speed series at the Vernadsky Station. The analysis of results shows that significant trends at the 1% level are found for only two series, namely, mean monthly values for February and mean annual values (Table 3). The mean annual values series is non-stationary, while the mean monthly values series from which this series is calculated is stationary. This result is also illogical and contradictory, like the previous finding obtained from the assessment of homogeneity of the series of NSW speed observations.

In general, when evaluating record homogeneity and stationarity, difficulties arise with the interpretation of results, since it is impossible to unambiguously establish the long-term tendencies and changes. That is why homogeneity and stationarity were further assessed by graphic methods.

Table 3. Results of tests of stationarity of the near-surface wind speed series according to the Mann-Kendall test at a significance level of 1%, the Vernadsky Station.

| Near-surface wind speed | Trend equation | $\tau$ | $p$-value | Statistical significance of trend |
|---|---|---|---|---|
| Mean annual | y = 0.03·x – 53.2 | 0.491 | <0.0001 | yes |
| January | y = 0.02·x – 34.8 | 0.192 | 0.0918 | no |
| February | y = 0.03·x – 64.6 | 0.289 | 0.0950 | yes |
| March | y = 0.004·x – 2.80 | 0.089 | 0.3441 | no |
| April | y = 0.01·x – 19.1 | 0.114 | 0.2322 | no |
| May | y = 0.02·x – 45.5 | 0.204 | 0.0435 | no |
| June | y = -0.003·x + 10.0 | –0.040 | 0.9666 | no |
| July | y = -0.01·x + 16.3 | –0.024 | 0.8156 | no |
| August | y = 0.01·x – 12.7 | 0.072 | 0.5088 | no |
| September | y = 0.003·x – 0.07 | 0.002 | 0.9893 | no |
| October | y = -0.01·x + 22.1 | –0.040 | 0.6787 | no |
| November | y = 0.01·x – 9.90 | 0.066 | 0.4945 | no |
| December | y = 0.02·x – 28.1 | 0.144 | 0.1955 | no |

Note: $\tau$ is a statistic used to measure the ordinal association between near-surface wind value and time.

### 3.3. Graphical analysis

The chronological graph of the mean annual NSW speed shows a turning point in 1998, which confirms the inhomogeneity and non-stationarity of this series according to statistical tests (Fig. 4, Tables 1, 3). At the same time, the mass curve shows that the cumulative values do not deviate from a straight line, which indicates homogeneity of mean annual NSW speed (Fig. 5).

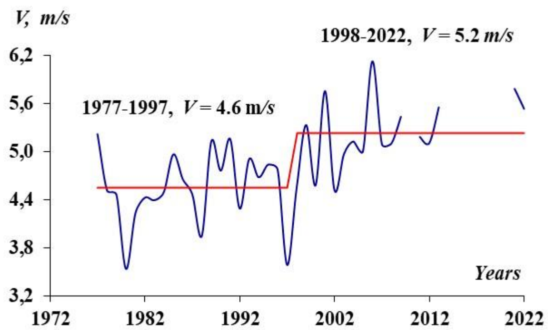


Fig. 4. Chronological graph of the mean annual near-surface wind speed in the area of the Vernadsky Station.

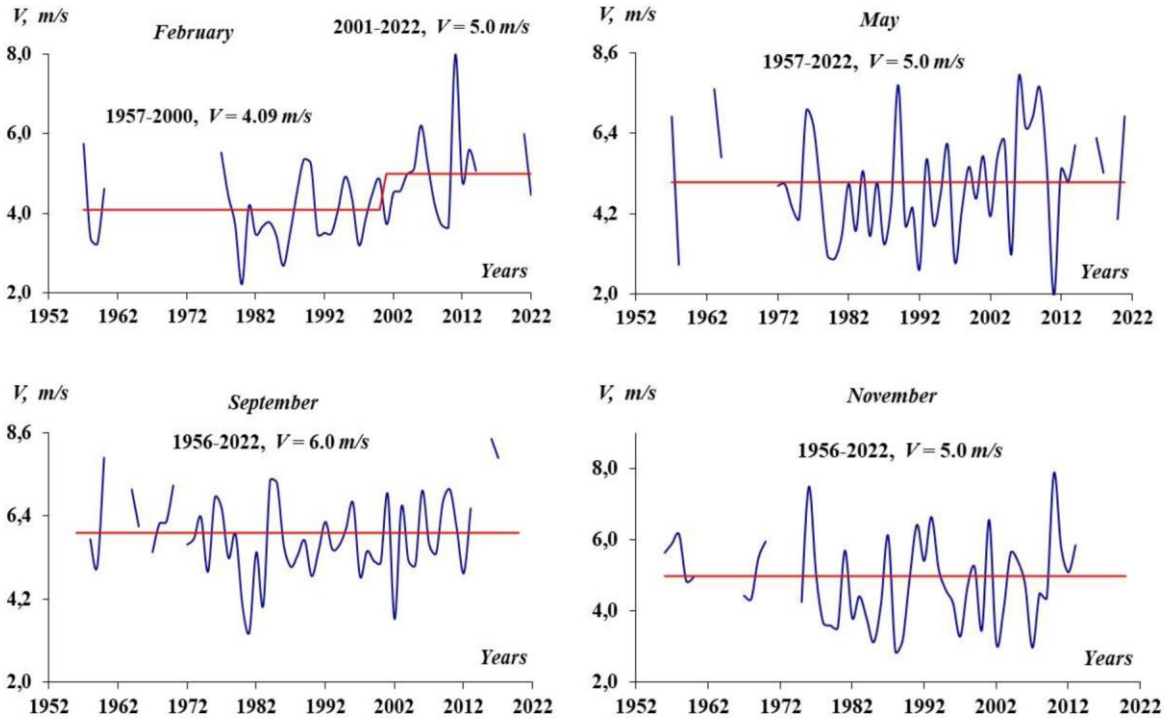


Fig. 5. Chronological graphs of the mean monthly values near-surface wind speed for individual months in the area of the Vernadsky Station.

Analysis of the residual mass curve of mean annual NSW speed showed that in 1998, there was a transition from a decrease to an increase (Fig. 5). At the same time, the beginning of the decreasing phase cannot be clearly determined by the residual mass curve of the mean annual NSW speed, since there are many missing records. Similarly, it is impossible to determine the end of the increasing phase, which continues to the present.

According to the graphical analysis, the mean monthly series are mostly homogeneous and stationary. The chronological graphs of the mean monthly NSW speed thus show no changes in the observation series, except for the month of February (Fig. 5).

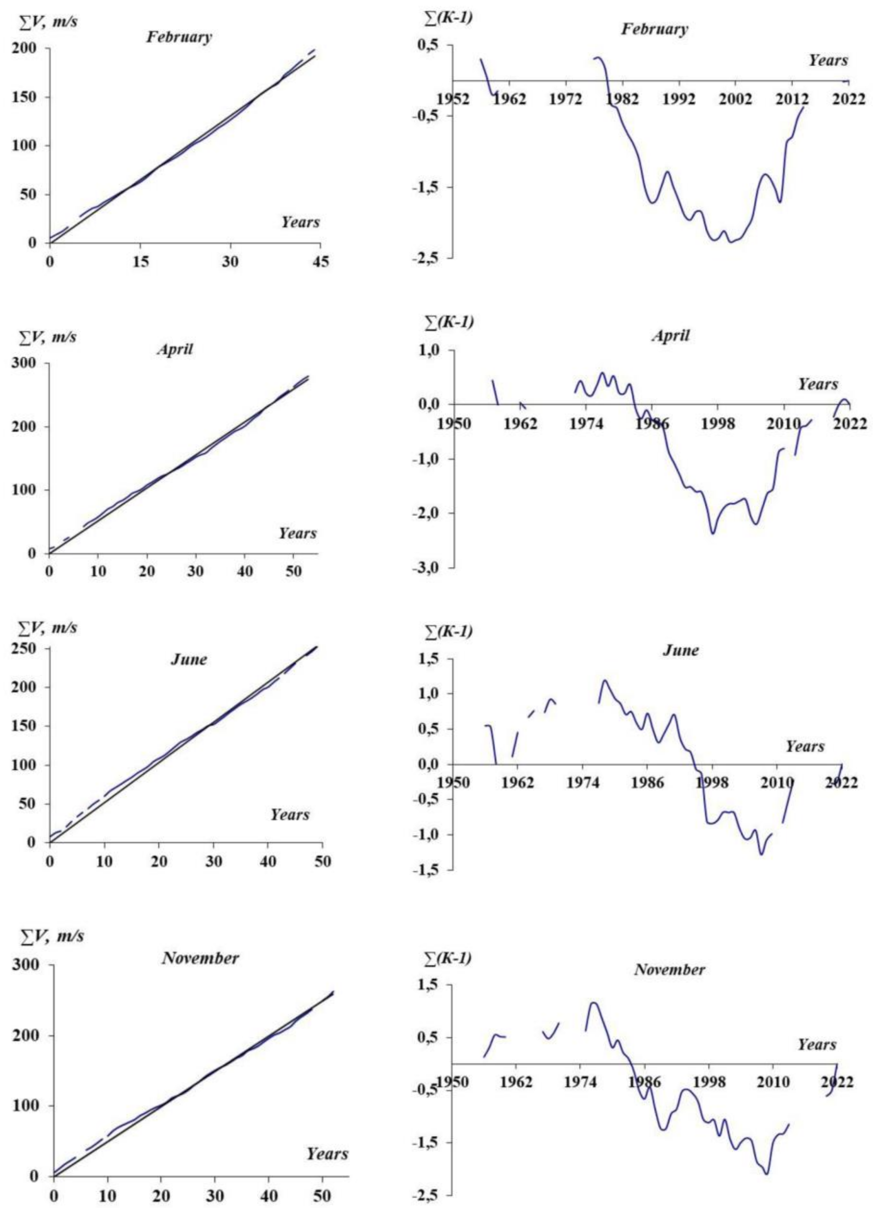


Fig. 6. Mass curves (left) and residual mass curves (right) of mean monthly near-surface wind speed for individual months in the area of the Vernadsky Station.

This result coincides with the results obtained by statistical tests (Tables 1, 2). At the same time, the mass curves of monthly NSW speed do not show deviations from a straight line, which indicates the homogeneity of these series of observations (Fig. 6 – left). The residual mass curves of mean monthly NSW speed indicate short- and long-term cyclical fluctuations (Fig. 6 – right). Non-stationarity of the mean monthly series for February, which is the same as for the mean annual observation series (per the Mann-Kendall statistical test, Table 3), is only due to the decreasing and increasing phases of long-term cyclic fluctuations (Fig. 6). Therefore, the February series is quasi-stationary. The observation series for other months are stationary because they contain both decreasing and increasing phases, as well as the final or initial phases of adjacent cycles. In all months of the year, there has been a tendency of an increasing near-surface wind speed at the Vernadsky Station during the past 20 years.

## 4. Discussion

Even at the end of the 19th century, the German scientist Eduard Brückner studied the cyclical fluctuations of the climate and proposed the 35-year-long Brückner cycle of cold, damp weather alternating with warm, dry weather in northwestern Europe (Stehr, Storch 2000). Throughout the 20th century, research into hydrometeorological quantities' fluctuations and changes over time was conducted using various approaches and methods. Many investigations have shown that short- and long-term cycles of different durations are observed in time series of atmospheric precipitation, air temperature, and river flow throughout the world (Gorton 1931; Karl 1988; Pekárová et al. 2003; Nidzgorska-Lencewicz, Czarnecka 2019; dos Santos et al. 2023).

Our study shows that NSW speeds, both mean annual and mean monthly, in the area of the Vernadsky Station have short- and long-term cyclical fluctuations. Pekárová et al. (2003) reported that in the different phases of cyclic fluctuations of hydrometeorological characteristics, there are observed tendencies that have different signs. So, the decreasing phase has values of hydrometeorological parameters significantly lower than the values observed in the increasing phase. This pattern results in differences in the mean values for these phases of cyclic fluctuations. Therefore, an observation series that has only decreasing and increasing phases of long-term cyclical fluctuations is classified as non-homogeneous and non-stationary by the statistical tests. This is exactly the result obtained by the statistical tests for the observation series of the mean annual and February mean monthly NSW speeds in the area of the Vernadsky Station. At the same time, this result is influenced by a short series of observations, since the series of observations in other months are longer and partially cover the adjacent cycles of long-term cyclical fluctuations. The observation series of the mean annual and February mean monthly NSW speeds have both decreasing and increasing phases, although these series are unfinished (i.e., they continue). So, such series must be classified as quasi-stationary. That is why, for such series, it is important to periodically repeat the analyses. A combined application of statistical and graphic methods, as we have applied here, will support more reliable estimates of homogeneity, stationarity, and tendencies of observation series.

## 5. Conclusions

At the Vernadsky Station, measurements of NSW speed were checked for missing records (e.g., those resulting from mechanical problems). The analysis showed that a significant part of the data contains errors, and these may be especially relevant for some years. Subsequently, incorrect data were removed from the study. Thus, new series of statistically reliable data for mean annual and mean monthly NSW speeds for the period 1955-2022 were generated. As a result of this data editing, the series obtained for individual months were of different durations. For example, the resulting series for September had the longest duration (58 years), and the series of annual mean NSW speed had the shortest duration (39 years).

The series of mean annual and February mean monthly NSW speeds are quasi-homogeneous and quasi-stationary since they only have the phases of decrease and increase for long-term cyclic fluctuations. The other series of NWS speed observations are homogeneous and stationary. Where the Vernadsky NWS speed series lack homogeneity and stationarity, according to statistical tests, it is caused by comparing the different phases of cyclic fluctuations (i.e., decreasing and increasing phases), which have different statistical characteristics.

During the past 20 years at the Vernadsky Station, according to the residual mass curves, NSW has an increasing tendency in all months of the year. Similar results were obtained in several previous papers (Turner et al. 2009; Dong et al. 2020; Andres-Martin et al. 2024). The multi-annual NSW speed is 4.8 m/s. The highest multi-annual mean monthly NSW speed was observed for September (6.0 m/s), and the lowest was observed for January (3.6 m/s).

We emphasize that using a combination of statistical approaches as applied in this analysis allows more robust results and could be applied to other hydrometeorological variables or characteristics.

## Acknowledgment

This research was conducted within project No. H/13-2023 from 18.08.2023, "Features of the spatio-temporal distribution of wind speed and atmospheric humidity near the Earth surface and their impact on the state of the snow cover in the area of the Vernadsky Station" that funded by the State Institution "National Antarctic Scientific Center" of the Ministry of Education and Science of Ukraine.

## References

Alkama R., Koffi E.N., Vavrus S.J., Diehl T., Francis J.A., Stroeve J., Forzieri G., Vihma T., Cescatti A., 2020, Wind amplifies the polar sea ice retreat, Environmental Research Letters, 15, 124022, DOI: 10.1088/1748-9326/abc379.

Andres-Martin M., Azorin-Molina C., Serrano E., González-Herrero S., Guijarro J.A., Bedoya-Valestt S., Utrabo-Carazo E., Vicente Serrano S.M., 2024, Near-surface wind speed trends and variability over the northern Antarctic Peninsula, 1979-2022, Atmospheric Research, 309, 107568, DOI: 10.1016/j.atmosres.2024.107568.

Box G.E.P., Jenkins G.M., 1970, Time Series Analysis: Forecasting and Control, Holden-Day, San Francisco, 553 pp.

de Brito Neto F.A., Mendes D., Spyrides M.H.C., 2022, Analysis of extreme wind events in the Weddell Sea region (Antarctica) at Belgrano II Station, Journal of South American Earth Sciences, 116, 103804, DOI: 10.1016/j.jsames.2022.103804.

Dong X., Wang Y., Hou S., Ding M., Yin B., Zhang Y., 2020, Robustness of the recent global atmospheric reanalyses for Antarctic near-surface wind speed climatology, Journal of Climate, 33 (10), 4027-4043, DOI: 10.1175/JCLI-D-19-0648.1.

Ehlert K.W., 1972, Homogeni tets kontroll av hydrologiska tidsserier, (in Swedish), Nordisk Hydrologisk Konferanse, Sandefjord, 47-59, available online (data access 19.03.2025).

Gorbachova L.O., 2014, Methodical approaches the assessment of the homogeneity and stationarity of hydrological observation series, (in Ukrainian), Hydrology, Hydrochemistry and Hydroecology, 1 (32), 22-31.

Gorbachova L.O., 2016, Place and role of hydro-genetic analysis among modern research methods runoff, (in Ukrainian), Proceedings of Ukrainian Hydrometeorological Institute, 268, 73-81.

Gorbachova L., Khrystiuk B., Shpyg V., Pishniak D., 2022, Estimation of tendencies, homogeneity and stationarity of air temperature at the Ukrainian Antarctic Akademik Vernadsky station during 1951-2020, Geofizicheskiy Zhurnal, 44 (4), 183-194, DOI: 10.24028/gj.v44i4.264848.

Gorbachova L., Zabolotnia T., Khrystyuk B., 2018, Homogeneity and stationarity analysis of the snow-rain floods in the Danube basin within Ukraine, Acta Hydrologica Slovaca, 19 (1), 35-41.

Gorton A.F., 1931, Cyclical variations in precipitation, runoff, and lake-levels and their relation to long-range forecasting, Eos, Transactions American Geophysical Union, 12 (1), 88-90, DOI: 10.1029/tr012i001p00088.

Hazel J.E., 2019, Exploring the Wind-Driven Near-Antarctic Circulation, Doctoral dissertation, University of California, Los Angeles, available online https://escholarship.org/uc/item/1gs7z5zm (data access 19.03.2025).

Karl T.R., 1988, Multi-year fluctuations of temperature and precipitation: The gray area of climate change, Climatic Change, 12, 179-197, DOI: 10.1007/BF00138938.

Khrystiuk B., Gorbachova L., 2023, Spatial-temporal tendencies of the ice regime of the Dnipro Cascade reservoirs, (in Ukrainian), Visnyk of V.N. Karazin Kharkiv National University, Series "Geology. Geography. Ecology", 59, 249-259, DOI: 10.26565/2410-7360-2023-59-18.

Khrystiuk B., Gorbachova L., Shpyg V., Pishniak D., 2023, Changes in extreme temperature indices at the Ukrainian Antarctic Akademik Vernadsky station, 1951-2020, Meteorology Hydrology and Water Management, 10 (1), 95-106, DOI: 10.26491/mhwm/150883.

King J.C., Turner J., 1997, Antarctic Meteorology and Climatology, Cambridge University Press, 409 pp.

Klemeš V., 1987, One hundred years of applied storage reservoir theory, Water Resources Management, 1, 159-175, DOI: 10.1007/BF00429941.

Klok S.V., Kornus A.O., 2021, Intra-annual and long-periodic components in the changes of precipitation over the Antarctic Peninsula and their possible causes, Journal of Geology, Geography and Geoecology, 30 (3), 490-490, DOI: 10.15421/112144.

Kohler M.A., 1949, On the use of double-mass analysis for testing the consistency of meteorological records and for making required adjustments, Bulletin of the American Meteorological Society, 30, 188-195, DOI: 10.1175/1520-0477-30.5.188.

Kundzewicz Z.W., Robson A.J., (eds.), 2000, Detecting Trend and Other Changes in Hydrological Data, World Climate Programme Data and Monitoring, WCDMP-45, WMO/TD-No. 1013, World Meteorological Organization, Geneva.

Kundzewicz Z.W., Robson A.J., 2004, Change detection in hydrological records – a review of the methodology, Hydrological Sciences Journal, 49 (1), 7-19, DOI: 10.1623/hysj.49.1.7.53993.

van Lipzig N.P.M., King J.C., Lachlan-Cope T.A., van den Broeke M.R., 2004, Precipitation, sublimation, and snow drift in the Antarctic Peninsula region from a regional atmospheric model, Journal of Geophysical Research: Atmospheres, 109 (D24), DOI: 10.1029/2004JD004701.

Merriam C.F., 1937, A comprehensive study of the rainfall on the Susquehanna Valley, Transactions American Geophysical Union, 18 (2), 471-476, DOI: 10.1029/TR018i002p00471.

Nidzgorska-Lencewicz J., Czarnecka M., 2019, Cyclical variability of seasonal precipitation in Poland, Quarterly Journal of the Hungarian Meteorological Service, 123 (4), 455-468, DOI: 10.28974/idojaras.2019.4.3.

Novotný J., 1925, Hydrology, (in Czech), Ceská matice technická, Prague.

Parish T.R., 1988, Surface winds over the Antarctic continent: A review, Reviews of Geophysics, 26 (1), 169-180, DOI: 10.1029/RG026i001p00169.

Parish T.R., Cassano J.J., 2001, Forcing of the wintertime Antarctic boundary layer winds from the NCEP–NCAR Global Reanalysis, Journal of Applied Meteorology and Climatology, 40 (4), 810-821, DOI: 10.1175/1520-0450(2001)040<0810:FOTWAB>2.0.CO;2.

Pekárová P., Miklánek P., Pekár J., 2003, Spatial and temporal runoff oscillation analysis of the main rivers of the world during the 19$^{th}$-20$^{th}$ centuries, Journal of Hydrology, 274 (1-4), 62-79, DOI: 10.1016/S0022-1694(02)00397-9.

R Core Team, 2017, R: A language and environment for statistical computing, R Foundation for Statistical Computing, Vienna, Austria, available online at https://www.r-project.org/ (data access 02.04.2025).

Ramesh K.J., Soni V.K., 2018, Perspectives of Antarctic weather monitoring and research efforts, Polar Science, 18, 183-188, DOI: 10.1016/j.polar.2018.04.005.

Rippl W., 1883, The capacity of storage reservoirs for water supply, Minutes of the Proceedings of the Institute of Civil Engineers, 71 (1883), 270-278, DOI: 10.1680/imotp.1883.21797.

Robson A.J., 2002, Evidence for trends in UK flooding, Philosophical Transactions of the Royal Society A, 360 (1796), 1327-1343, DOI: 10.1098/rsta.2002.1003.

Romanova Y., Shakirzanova Z., Ovcharuk V., Todorova O., Medvedieva I., Ivanchenko A., 2019, Temporal variation of water discharges in the lower course of the Danube River across the area from Reni to Izmail under the influence of natural and anthropogenic factors, Energetika, 65 (2-3), 144-160, DOI: 10.6001/energetika.v65i2-3.4108.

dos Santos L.O.F., Machado N.G., Biudes M.S., Geli H.M.E., Querino C.A.S., Ruhoff A.L., Ivo I.O., Lotufo Neto N., 2023, Trends in precipitation and air temperature extremes and their relationship with sea surface temperature in the Brazilian midwest, Atmosphere, 14 (3), 426, DOI: 10.3390/atmos14030426.

Searcy J.K., Hardison C.H., 1960, Double-Mass Curves. Manual of Hydrology: Part 1. General Surface-Water Techniques, Geological Survey Water-Supply Paper 1541-B, Washington, United States Government Printing Office.

Schoklitsch A., 1923, Graphical Hydraulics, (in German), B.G. Teubner, Leipzig.

Shpyg V., Shchehlov O., Pishniak D., 2024, Snow cover at the Akademik Vernadsky station: response on wind, temperature and precipitation variations, Ukrainian Antarctic Journal, 22 (1), 6-23, DOI: 10.33275/1727-7485.1.2024.724.

Spence P., Griffies S.M., England M.H., Hogg A.McC., Saenko O.A., Jourdain N.C., 2014, Rapid subsurface warming and circulation changes of Antarctic coastal waters by poleward shifting winds, Geophysical Research Letters, 41 (13), 4601-4610,

Stehr N., Storch H., (eds.), 2000, Eduard Brückner - The Sources and Consequences of Climate Change and Climate Variability in Historical Times, Kluwer Academic Publishers.

Turner J., Chenoli S.N., Samah A., Marshall G., Phillips T., Orr A., 2009, Strong wind events in the Antarctic, Journal of Geophysical Research: Atmospheres, 114 (D18), D18103, DOI: 10.1029/2008JD011642.

Tymofeyev V.E., Beznoshchenko B.O., Shcheglov O.A., 2017, On the near-surface atmospheric circulation in the region of the Antarctic Peninsula, (in Russian), Ukrainian Antarctic Journal, 16, 66-80, DOI: 10.1016/S0045-8732(97)83155-5.

Wang K.-S., Wu D., Zhang T., Wu K., Zheng C.-W., Yi C.-T., Yu Y., 2023, Climatic trend of wind energy resource in the Antarctic, Journal of Marine Science and Engineering, 11 (5), 1088, DOI: 10.3390/jmse11051088.

Weiss L.L., Wilson W.T., 1953, Evaluation of significance of slope changes in double mass curves, Transactions American Geophysical Union, 34 (6), 893-896, DOI: 10.1029/TR034i006p00893.

WMO, 1990, On the Statistical Analysis of Series of Observations, Technical Note No. 143, WMO-No. 415, World Meteorological Organization, Geneva.

WMO, 2018, Guide to Climatological Practices, WMO-No. 100, World Meteorological Organization, Geneva.

Yu L., Zhong Sh., Sun B., 2020, The climatology and trend of surface wind speed over Antarctica and the Southern Ocean and the implication to wind energy application, Atmosphere, 11 (1), DOI: 10.3390/atmos11010108.

Zabolotnia T., Gorbachova L., Khrystyuk B., 2019, Estimation of the long-term cyclical fluctuations of snow-rain floods in the Danube basin within Ukraine, Meteorology Hydrology and Water Management, 7 (2), 3-11, DOI: 10.26491/mhwm/99752.

Zabolotnia T., Parajka J., Gorbachova L., Széles B., Blöschl G., Aksiuk O., Tong R., Komma J., 2022, Fluctuations of Winter Floods in Small Austrian and Ukrainian Catchments, Hydrology, 9 (2), 38, DOI: 10.3390/hydrology9020038.

# Using extreme frequency analysis to explain the impact of hurricanes Pauline (1997) and Otis (2023) on Acapulco, Mexico

Alfonso Gutierrez-López, Martin Muñoz Mandujano, Mauricio Arturo Ibarra-Corona, Jose Alejandro Vargas-Diaz

Universidad Autonoma de Queretaro, Mexico

Abstract

The severity of hurricanes and cyclones in Mexico increases each year. A key area of research represents the development of a mathematical model to predict their tracks and points of impact. The IBTrACS database contains data on hurricanes and tropical cyclone tracking; it is the most comprehensive global collection of tropical cyclones. This database was developed in collaboration with all Regional Specialized Meteorological Centers of the World Meteorological Organization (WMO). Using the track, wind speed, and atmospheric pressure data for each of the hurricane and cyclone occurrences from 1851 to 2022, probabilistic type I extreme value models were applied to extreme winds and atmospheric pressure. With the help of a simple Bayesian model the probabilities were computed of a hurricane or cyclone with wind of a certain magnitude occurring at a given latitude and longitude; an event occurs when specified atmospheric pressure conditions are met. The data collected correspond to the area between west longitudes 115.5° and 85° and north latitudes 10° and 32°. This database can be managed, in the future, for the forecast of hurricane and cyclone tracks.

Keywords

Hurricane; cyclone; hurricane track; wind speed; atmospheric pressure; Gumbel distribution; probabilistic analysis; Hurricane Otis; Hurricane Paulina.

Submitted 31 December 2024, revised 27 February 2025, accepted 30 May 2025

DOI: 10.26491/mhwm/205741

## 1. Introduction

The impact of hurricanes in coastal regions is a significant threat to human life, urban infrastructure, and economic stability, particularly in vulnerable areas with high population density. In recent decades, hurricanes Pauline [1997], John [1978], and more recently, Otis [2023] have caused significant destruction to the port of Acapulco, Mexico, resulting in substantial human casualties, forced displacement, and economic devastation. The intensity of these events is not solely attributable to the strength of the winds or the amount of precipitation, but also to structural factors such as unplanned urban expansion, the fragility of the electrical system, and the lack of institutional preparedness (Hallegatte et al. 2018; Simpson et al. 2023). Recent studies on hurricanes with similar impacts, such as Sandy [2012] in the United States and Dorian [2019] in the Bahamas, have allowed more accurate modeling of the relationship between storm size, wind speed, and resulting economic losses. For instance, Collins et al. (2021) demonstrated that economic damages are influenced by factors beyond maximum sustained wind, including tropical storm wind radius, sea level, and territorial exposure. These quantitative approaches have been validated using Bayesian methods and machine learning models. This validation process has revealed the complexity of damage attribution (Chavas et al. 2016; Geiger et al. 2018). Additionally, compound events, such as "hurricane-blackout-heat wave," are emerging as new forms of systemic risk in urban and coastal areas.

Research on vulnerable electrical systems in Gulf of Mexico and Southeast Asian regions has elucidated this phenomenon, demonstrating but I'm that the loss of electrical power exponentially increases the risk to public health during and after tropical cyclones (Feng et al. 2025; Lewis 2022). This phenomenon was evident after Otis passed through Acapulco, where communication and medical care systems collapsed for more than 72 hours. From a socioeconomic perspective, disasters such as Pauline and Otis should be understood as "socially constructed disasters," where poverty, urban planning, and institutional weakness amplify the damage caused by natural phenomena. The work of Koks et al. (2019) demonstrates that indirect effects, such as job losses, school disruptions, and forced migration can exceed the direct losses estimated by insurers and governments. Due to the increased frequency and intensity of extreme weather events exacerbated by climate change, there is an urgent need to develop a comprehensive risk management strategy that incorporates climate monitoring, resilient land use planning, and improved rapid response systems. More robust approaches to hurricane risk management are being proposed, including integrated predictive models, multi-hazard analysis, and data science-based strategies (Zscheischler et al. 2018; Gran Castro, Ramos De Robles 2019). Floods can be extreme events in most countries in Latin America and the Caribbean (LAC) (Molina-Aguilar, Gutierrez-Lopez 2020). In general, these floods result from torrential rains produced by convective systems (Khurana et al. 2017). Many of these extreme storms are also caused by hurricane-cyclones that affect the Pacific Ocean coast, the Gulf of Mexico, and the Caribbean region (Hallegatte et al. 2013). Although hurricane rains can sometimes benefit cultivated areas and fill reservoirs (Breña-Naranjo et al. 2015), in most cases, they cause disasters (Jaimes et al. 2014). However, in developing countries, such as most LAC countries, there is often a lack of effort in following the development and tracking of these extreme phenomena (Leroux et al. 2018). Due to the limited number of radars, meteorological satellites, and ground-based warning systems, predicting the impact site of hurricane-cyclones in LAC remains a challenging task (Heming et al. 2019; Magnusson et al. 2019). Recent studies have mapped the East Coast of the United States, using colors to indicate the probability of a hurricane occurrence at each site (Gori et al. 2022). Monitoring extreme phenomena like hurricanes and the rain-fields they produce is critical for mitigating the risks of flooding, particularly in coastal areas. For example, Hurricane Otis in October 2023 and Hurricane Pauline in October 1997 devastated the city of Acapulco on the Pacific-coast of Mexico. Forecasting of storm tracks is typically carried out using data from sensors installed on specialized aircraft (Aberson, Franklin 1999). Forecasting can also employ global models (Chen et al. 2013; Nishimura, Yamaguchi 2015; Hon 2020), high-definition satellite imagery (Weng et al. 2007; Cui et al. 2013), or even fuzzy clustering techniques (Nath et al. 2015). Currently, few studies use wind speed and pressure data to predict hurricane tracks based on probabilistic estimates of simultaneous occurrence. This paper utilizes statistical data to analyze the climatology and track of hurricane-cyclones that have impacted the coasts of Mexico from 1851 to 2022. The aim is to map the zones of joint probability of occurrence of wind speed and pressure data using a Bayesian formulation.

## 2. Materials and methods

This work is based on the premise that a mathematical model for track forecasting, which accounts for the physiographic and meteorological conditions of a hurricane, can accurately represent and predict the behavior of hurricane rainfall in space and time. The variability of the rainfall fields produced by hurricanes is directly proportional to the joint probability calculated with the wind and atmospheric pressure data.

## 2.1. Parameters for data collection

Data selection was based on research needs and recommendations from previous studies. Specifically, Knapp et al. (2010) used the International Best Track Archive for Climate Stewardship (IBTrACS). Tropical hurricanes and tropical storms track data were carefully collected from the International Best Track Archive for Climate Stewardship (IBTrACS). It is the most complete global collection of tropical cyclones available. It merges recent and historical tropical cyclone data from multiple agencies to create a unified, publicly available, best-track dataset that improves inter-agency comparisons. IBTrACS was developed collaboratively through all the World Meteorological Organization (WMO) Regional Specialized Meteorological Centers, as well as other organizations and individuals from around the world (available at: https://www.ncei.noaa.gov/data/international-best-track-archive-for-climate-stewardship-ibtracs/v04r00/access/csv/). The data were built as a time-series database in Excel (CSV). Probabilistic models for extreme values and a Bayesian analysis were performed using a Visual Basic program. The data collected are for the area between longitudes 116° and 85° west and latitudes 12° and 30° north.

## 2.2 Description of data collection

Historical data for hurricanes and tropical storms are available from 1851 to 2022. The original database is composed of storm identifier, year, basin, sub-basin, data-name provided by the agency, time in Universal Time Coordinates (UTC), nature of event (disturbance, tropical, extratropical, or subtropical), latitude, longitude, maximum sustained wind speed from the WMO agency for the current location, and atmospheric pressure at the ocean surface in hectopascals. After processing the original data, the resulting files contain in addition the following results: frequency in years of wind speed occurrence, probability of wind speed occurrence, reduced Gumbel variable for wind speed, and estimated value of wind speed based on the extreme event model. Other variables include: frequency in years of pressure occurrence, probability of pressure occurrence, reduced Gumbel variable for pressure, and estimated value of pressure based on the extreme event model. From the Bayesian analysis, we derived the probability that a hurricane or tropical storm with a certain wind magnitude will happen at a specific latitude and longitude, given that a specific pressure event occurs. The general scheme of all available data is shown in Figure 1. In summary, there are 19,246 records with a total of 288,690 data points.

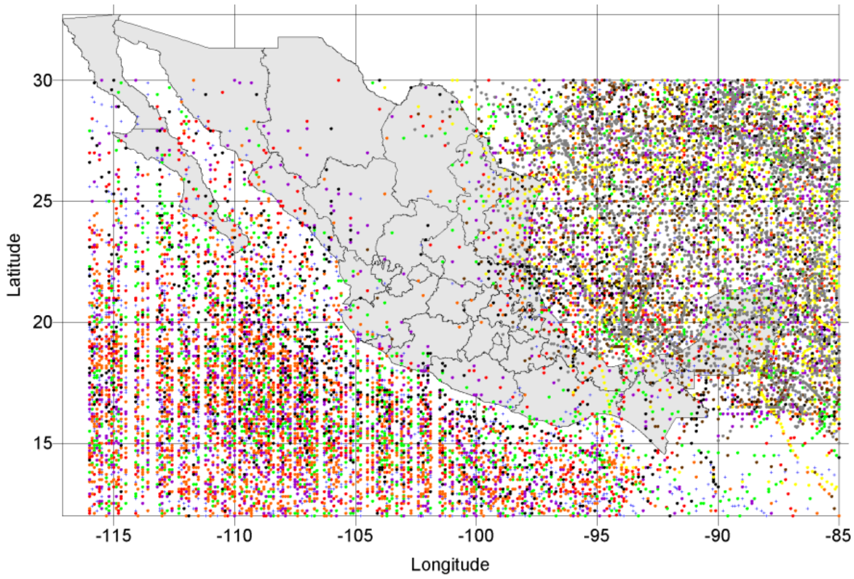

Fig. 1. Sites with information available on the Atlantic and Pacific coasts of Mexico.

## 3. Results

### 3.1 Generalized Extreme-Value Distribution (GEV)

All available data were transformed into a time series. Frequency analysis was applied as described in Gutierrez-Lopez (2022). The Generalized Extreme Value distribution (GEV) was used to model extreme wind speed and atmospheric pressure for all events at all sites. Figures 2 and 3 show the result of this fit to the characteristic climatological variable data. The theory of extreme values is concerned with events at the tails of probability distributions. Gumbel proposed the characteristic function of these extremes, which allows for their adjustment based on the sample size of the maximum events of a time series (Molina-Aguilar et al. 2019).

$$F\left(q_i\right) = \Pr\left(Q \le q_i\right) = e^{\left(-\left[1+\frac{q_i-\varepsilon}{\lambda}k\right]^{-\frac{1}{k}}\right)}; \quad where\ q_i, \varepsilon, \lambda, k \in R \tag{1}$$

Equation (1) represents the (GEV and establishes three types of distribution, which graphically generate asymptotic behaviors according to the values adopted from the parameters of location ($\varepsilon$), scale ($\lambda$) and shape ($k$). $F$ represents the probability of non-exceedance for the probability distribution function; $q_i$ is the order assigned to the maximum annual expenditure in the time series. In the case where $k$ tends to 0 and

$-\infty < q_i < \infty$ is defined as Type I (EV1) called the Gumbel function. If $k < 0$ and $\varepsilon + \lambda/k < q_i < \infty$ is defined as Type II, known as the Frechet function. Finally, if $k > 0$ and $-\infty < q_i < \varepsilon + \lambda/k$, a Type III or Weibull function is generated. Its probability density function (*fdp*), is obtained from the ratio of change ($q_i$) with respect to the independent variable $Q$, with the form:

$$\frac{dF(q_i)}{dq} = f(q_i) = \frac{1}{\lambda} e^{\left(-\left[1-\frac{q_i-\varepsilon}{\lambda}k\right]^{\frac{1}{k}}\right)} \left[1-\frac{q_i-\varepsilon}{\lambda}k\right]^{\frac{1}{k}-1} \tag{2}$$

The Gumbel distribution (EV1) is one of the three distributions generated from the GEV, in which the random variable presents bias to the right.

$$F(q_i) = e^{-e^{\left(-\frac{q_i-\varepsilon}{\lambda}\right)}} \tag{3}$$

*fdp* for EV1 is:

$$f(q_i) = \frac{1}{\lambda} e^{-e^{\left(-\frac{q_i-\varepsilon}{\lambda}\right)}} e^{\left(-\frac{q_i-\varepsilon}{\lambda}\right)} \tag{4}$$

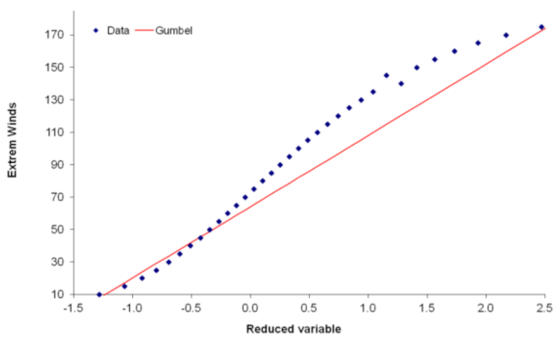

Fig. 2. Fit of the EV1 distribution to wind speed values.

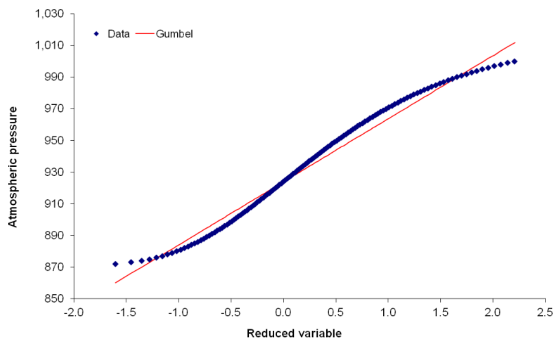

Fig. 3. Fit of the EV1 distribution to atmospheric pressure values.

### 3.2. Bayesian model

For a given value of $q$, $X$ follows a binomial law B(n;$q$). The set of possible values of q can be characterized probabilistically according to a Bayesian model (Saporta 2011). The model is based on previous events which allow establishing the frequency of occurrence of $q$. Everything comes down to the fact that $q$ is a variable between (0,1) that has a prior probability distribution $f(q)$. Thus, we obtain a model that attempts to deduce $q$ from $X$. Then it aims to find the posterior probability distribution of $q$; that is:

$$f(q/X) = \frac{P(X/q)f(q)}{P(X)} = \frac{q^X(1-q)f(q)}{\int_0^1 q^X(1-q)f(q)dq} \tag{5}$$

In this sense, $q$ can be estimated by choosing either the mean posterior probable value or the extreme posterior value. Figures 4, 5, and 6 show some examples of the results of this procedure for different time lags.

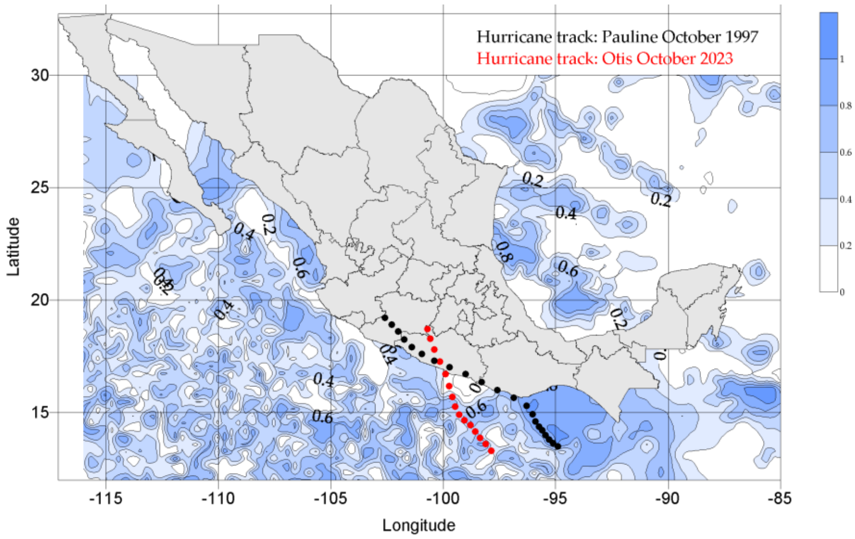


Fig. 4. Probability that a hurricane or tropical storm with a specific wind magnitude will happen at (latitude, longitude) given that a specific atmospheric pressure occurs (1980-1995).

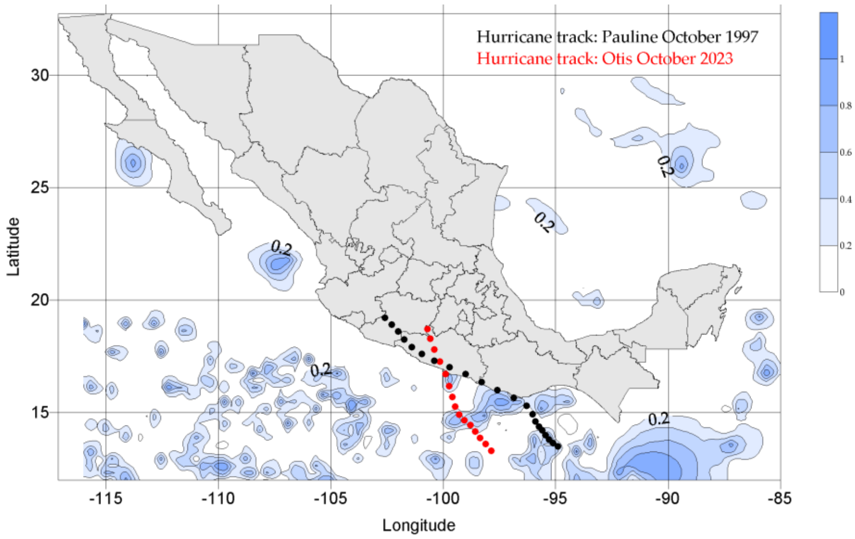


Fig. 5. Probability that a hurricane or tropical storm with specific wind magnitude will happen at (latitude, longitude) given that a specific atmospheric pressure occurs (2006-2013).

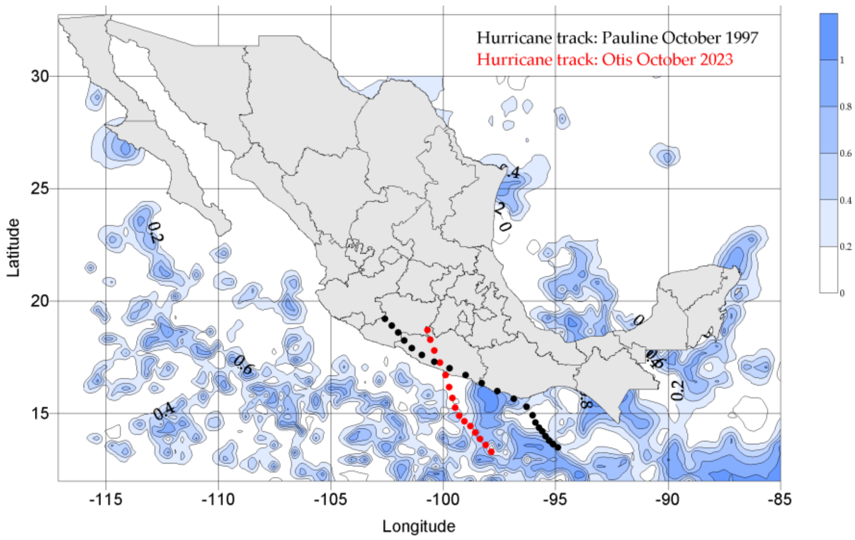

Fig. 6. Probability that a hurricane or tropical storm with specific wind magnitude will happen at (latitude, longitude) given that a specific atmospheric pressure occurs (2014-2022).

## 4. Damage assessment: Hurricanes Pauline [1997] and Otis [2023] in Acapulco

### 4.1. Hurricane Pauline [1997]

On October 8, 1997, Hurricane Pauline hit Acapulco as a Category 4 storm. It caused extreme rainfall (up to 411 mm in less than 24 hours), which led to flash floods, debris flows, and landslides. The most affected areas were hillsides and marginal urban areas. Homes built in highly vulnerable conditions collapsed in these areas. There were approximately 160 deaths and more than 260 missing persons, in addition to hundreds of injured and displaced individuals. The urban infrastructure was severely damaged. Streets were destroyed, bridges collapsed, and the water and drainage networks were rendered useless. Homes were swept away by floodwaters. The direct economic losses resulting from the disaster were estimated at $450 million, primarily affecting the housing, commercial, and tourism sectors. Hydrological studies of the La Sabana River basin demonstrate how geomorphology and land use influenced the torrential response, exacerbating the effects of the rainfall associated with Pauline (Rodríguez Esteves 2017).

### Hurricane Otis [2023]

On October 25, 2023, Hurricane Otis made landfall as a Category 5 cyclone, with sustained winds of 270 km/h and gusts up to 330 km/h. It became the strongest hurricane ever recorded on the Mexican Pacific coast. Its rapid intensification was unusual: it went from a tropical storm to a Category 5 hurricane in less than 12 hours, leaving little time for preparation or evacuation. The damage ranged from severe coastal erosion (up to 76 meters on some beaches) and collapsed storm drains to the complete disruption of communication, electricity, and drinking water networks. The estimated cost of the damage ranges from $9.9 billion to $14.8 billion. This has had a severe impact on the region's tourism economy, as well as on thousands of homes, hotels, schools, and hospitals. Post-event satellite images reveal geographical alterations along the coastline and the presence of new landslides, confirming the multi-threat nature of Otis's impact (Ramírez-Herrera et al. 2025). However, a study by the University of California indicates that the historical loss of mangroves in Acapulco since the 1980s has contributed significantly to the area's current vulnerability. Adequate mangrove coverage is estimated to have dampened up to 25% of the storm's energy in low-lying coastal areas (Hook 2025).

## 5. Discussion

Mexico is the most affected country in the world by hurricanes and tropical storms, which can strike its two coasts simultaneously. Because of its location and atmospheric conditions, in 2013, hurricanes Ingrid and Manuel hit Mexico's coasts at the same time. It is extremely urgent to provide a database with all the hurricanes and tropical storms that have occurred in this area (Molina-Aguilar, Gutiérrez-López 2020). The original database presents hurricane or tropical storm name, location, wind speed, and atmospheric pressure information for all events from 1851 to 2022. This information is not directly available anywhere in Mexico. Therefore, this database and its computational tool for look-up are of significant importance. The processed extreme wind and pressure data are fitted to a probability distribution of extreme value type I; the database shows the estimated values for the wind and atmospheric pressure for each of the 539 hurricanes and tropical storms analyzed. After processing the primary data, the files contain the following results: date, name, latitude, longitude, frequency in years of winds and atmospheric pressure occurrence (Leroux et al. 2018; Bieli et al. 2019), probability and frequency of extreme winds and pressure, estimated value of extreme winds and atmospheric pressure based on the extreme event model, and the probability that a hurricane or tropical storm with some wind magnitude will happen at a location where a specific pressure event occurs. The calculation of the conditional probability over the whole study area is the initial step to estimate hurricane and tropical storm tracks (Khurana et al. 2017; Heming et al. 2019).

## 6. Conclusions

The maps shown in Figures 4-6 provide information on the probability of a hurricane occurring with a specific wind speed and atmospheric pressure. The use of Bayesian analysis allows for the observation of vulnerable coastal zones as well as areas at sea susceptible to the occurrence of a hurricane with this combination of wind speed and atmospheric pressure. The frequency of cyclones is greater in the Mexican Pacific (1.8/year) than in the Gulf of Mexico (0.4/year). During the August-September period, when the incidence is at its highest, rainfall increases up to three to four times the normal average. The tracks of Hurricanes Otis and Pauline correspond to the maximum probability zones for these areas. To prevent damage caused by hurricanes of extraordinary intensity, it is important to explore general concepts. This work uses only two variables, but it should be complemented with data on high tide, storm-waves, precipitation, and other relevant factors. The analysis of frequencies using extreme distributions is appropriate and allows for the calculation of probabilities of occurrence.

### 6.1. Expected use of results

The first step in estimating cyclone tracks (Nath et al. 2015; Magnusson et al. 2019; Hon 2020) is to calculate the conditional probability over the entire study area, followed by a geostatistical analysis (variogram) of the predominant directions. With the estimated probability, it is possible to determine future tracks with a significant degree of accuracy (Nishimura, Yamaguchi 2015; Tang et al. 2021; Trošelj, Lee 2021).

## References


Aberson S.D., Franklin J.L., 1999, Impact on hurricane track and intensity forecasts of GPS dropwindsonde observations from the first-season flights of the NOAA Gulfstream-IV Jet Aircraft, Bulletin of the American Meteorological Society, 80 (3), 421-427., DOI: 10.1175/1520-0477(1999)080<0421:IOHTAI>2.0.CO;2.

Bieli M., Sobel A.H., Camargo S.J., Tippett M.K., 2019, A statistical model to predict the extratropical transition of tropical cyclones. Weather and Forecasting, 35 (2), 451-466, DOI: 10.1175/WAF-D-19-0045.1.

Breña-Naranjo A., Pedrozo-Acuña A., Pozos-Estrada O., Jiménez-López S.A., López-López M.R., 2015, The contribution of tropical cyclones to rainfall in Mexico, Physics and Chemistry of the Earth, Parts A/B/C, 83-84, 111-122, DOI: 10.1016/j.pce.2015.05.011.

Chavas D.R., Lin N., Dong W., Lin Y., 2016, Observed tropical cyclone size revisited, Journal of Climate, 29 (8), 2923-2939, DOI: 10.1175/JCLI-D-15-0731.1.

Chen G., Yu H., Cao Q., Zeng Z., 2013, The performance of global models in TC track forecasting over the Western North Pacific from 2010 to 2012, Tropical Cyclone Research and Review, 2 (3), 149-158, DOI: 10.6057/2013TCRR03.02.

Collins J., Polen A., McSweeney K., Colón-Burgos D., Jernigan I., 2021, Hurricane risk perceptions and evacuation decision-making in the age of COVID-19, Bulletin of the American Meteorological Society, 102 (4), E836-E848, DOI: 10.1175/BAMS-D-20-0229.1.

Cui L., Shi L., Yin Q., Yu W., Lu X., Liu J., 2013, Application of satellite cloud imagery in track analysis of tropical cyclones, Tropical Cyclone Research and Review, 2 (4), 222-232, DOI: 10.6057/2013TCRR04.04.

Feng K., Lin N., Gori A., Xi D., Ouyang M., Oppenheimer M., 2025, Hurricane Ida's blackout-heatwave compound risk in a changing climate, Nature Communications, 16 (1), DOI: 10.1038/s41467-025-59737-8.

Geiger T., Frieler K., Bresch D.N., 2018, A global historical data set of tropical cyclone exposure (TCE-DAT), Earth System Science Data, 10 (1), 185-194, DOI: 10.5194/essd-10-185-2018.

Gori A., Lin N., Xi D., Emanuel K., 2022, Tropical cyclone climatology change greatly exacerbates US extreme rainfall-surge hazard, Nature Climate Change, 12 (2), 171-178, DOI: 10.1038/s41558-021-01272-7.

Gran Castro J.A., Ramos De Robles S.L., 2019, Climate change and flood risk: vulnerability assessment in an urban poor community in Mexico, Environment and Urbanization, 31 (1), 75-92, DOI: 10.1177/0956247819827850.

Gutierrez-Lopez A., 2022, Methodological guide to forensic hydrology, Water, 14 (23), DOI: 10.3390/w14233863.

Hallegatte S., Green C., Nicholls R.J., Corfee-Morlot J., 2013, Future flood losses in major coastal cities, Nature Climate Change, 3 (9), 802-806, DOI: 10.1038/nclimate1979.

Hallegatte S., Maruyama R., Jun E., Walsh B., 2018, Building back better: achieving resilience through stronger, faster, and more inclusive post-disaster reconstruction, World Bank Group, Washington, D.C., available online at https://documents.worldbank.org/en/publication/documents-reports/documentdetail/420321528985115831 (data access 30.05.2025)

Heming J.T., Prates F., Bender M.A., Bowyer R., Cangialosi J., Caroff P., Coleman T., Doyle J.D., Dube A., Faure G., Fraser J., Howell B.C., Igarashi Y., McTaggart-Cowan R., Mohapatra M., Moskaitis J.R., Murtha J., Rivett R., Sharma M., Short C.J., 2019, Review of recent progress in tropical cyclone track forecasting and expression of uncertainties, Tropical Cyclone Research and Review, 8 (4), 181-218, DOI: 10.1016/j.tcrr.2020.01.001.

Hon K.-K., 2020, Tropical cyclone track prediction using a large-area WRF model at the Hong Kong Observatory, Tropical Cyclone Research and Review, 9 (1), 67-74, DOI: 10.1016/j.tcrr.2020.03.002.

Hook B., 2025, Mangrove Loss in Acapulco Likely Worsened the Devastation of Hurricane Otis, Scripps Institution of Oceanography, available online at https://scripps.ucsd.edu/news/mangrove-loss-acapulco-likely-worsened-devastation-hurricane-otis (data access 30.05.2025).

Jaimes M.A., Niño M., Huerta B., 2014, Hurricane event-based method to create regional hazard maps for heavy rainfall-induced translational landslides, Natural Hazards, 76 (2), 1143-1161, DOI: 10.1007/s11069-014-1539-z.

Khurana T., Bhattacharya S.K., Kotal S.D., 2017, Some special characteristics of track and intensity of typhoons over the Western North Pacific, Tropical Cyclone Research and Review, 6 (3-4), 82-93, DOI: 10.6057/2017TCRRh3.03.

Knapp K.R., Kruk M.C., Levinson D.H., Diamond H.J., Neumann C.J., 2010, The International Best Track Archive for Climate Stewardship (IBTrACS): Unifying tropical cyclone best track data, Bulletin of the American Meteorological Society, 91, 363-376, DOI: 10.1175/2009BAMS2755.1.

Koks E.E., Rozenberg J., Zorn C., Tariverdi M., Vousdoukas M., Fraser S., Hallegatte S., 2019, A global multi-hazard risk analysis of road and railway infrastructure assets, Nature Communications, 10, 2677, DOI: 10.1038/s41467-019-10442-3.

Leroux M.-D., Wood K., Elsberry R.L., Cayanan E.O., Hendricks E., Kucas M., Otto P., Rogers R., Sampson B., Yu Z., 2018, Recent advances in research and forecasting of tropical cyclone track, intensity, and structure at landfall, Tropical Cyclone Research and Review, 7 (2), 85-105, DOI: 10.6057/2018TCRR02.02.

Lewis C.T., 2022, Climate change and the Caribbean: challenges and vulnerabilities in building resilience to tropical cyclones, Climate, 10 (11), DOI: 10.3390/cli10110178.

Magnusson L., Doyle J.D., Komaromi W.A., Torn R.D., Tang C.K., Chan J.C.L., Yamaguchi M., Zhang F., 2019, Advances in understanding difficult cases of tropical cyclone track forecasts, Tropical Cyclone Research and Review, 8 (3), 109-122, DOI: 10.1016/j.tcrr.2019.10.001.

Molina-Aguilar J.P., Gutiérrez-López A., 2020, Daños económicos y sociales por huracanes e inundaciones en México: periodo de 2010 a 2015, Aqua-LAC, 12 (2), 67-77, DOI: 10.29104/phi-aqualac/2020-v12-2-06.

Molina-Aguilar J.P., Gutierrez-Lopez A., Raynal-Villaseñor J.A., Garcia-Valenzuela L.G., 2019, Optimization of parameters in the generalized extreme-value distribution type 1 for three populations using harmonic search, Atmosphere, 10 (5), DOI: 10.3390/atmos10050257.

Nath S., Kotal S.D., Kundu P.K., 2015, Application of fuzzy clustering technique for analysis of North Indian Ocean tropical cyclone tracks, Tropical Cyclone Research and Review, 4 (3), 110-123, DOI: 10.6057/2015TCRRh3.02.

Nishimura M., Yamaguchi M., 2015, Selective ensemble mean technique for tropical cyclone track forecasts using multi-model ensembles, Tropical Cyclone Research and Review, 4 (2), 71-78, DOI: 10.6057/2015TCRR02.03.

Ramírez-Herrera M.T., Coca O., Gaidzik K., Vargas Espinosa V.H., 2025, Hurricane Otis: category 5 storm effects and cascading hazards in Acapulco Bay, Mexico, Global and Earth Surface Processes Change, 3, DOI: 10.1016/j.gespch.2025.100004.

Rodríguez Esteves J.M., 2017, Los desastres recurrentes en México: el huracán Pauline y la tormenta Manuel en Acapulco, Guerrero, Disertaciones Anuario Electrónico Estudios de Comunicación Social, 10 (2), DOI: 10.12804/revistas.urosario.edu.co/disertaciones/a.4778.

Saporta G., 2011, Probabilités analyse et des données et statistique, TECHNIP, Paris, France, 493 pp.

Simpson N.P., Williams P.A., Mach K.J., Berrang-Ford L., Biesbroek R., Haasnoot M., Segnon A.C., Campbell D., Musah-Surugu J.I., Joe E.T., Nunbogu A.M., Sabour S., Meyer A.L.S., Andrews T.M., Singh C., Siders A.R., Lawrence J., van Aalst M., Trisos C.H., 2023, Adaptation to compound climate risks: a systematic global stocktake, IScience, 26 (2), DO: 10.1016/j.isci.2023.105926.

Tang C.K., Chan J.C.L., Yamaguchi M., 2021, Large tropical cyclone track forecast errors of global numerical weather prediction models in western North Pacific basin, Tropical Cyclone Research and Review, 10 (3), 151-169, DOI: 10.1016/j.tcrr.2021.07.001.

Trošelj J., Lee H.S., 2021, Modelling typhoon-induced extreme river discharges: a case study of Typhoon Hagibis in Japan, Journal of Hydrology: Regional Studies, 34, DOI: 10.1016/j.ejrh.2021.100776.

Weng F., Zhu T., Yan B., 2007, Satellite data assimilation in numerical weather prediction models. Part II: Uses of rain-affected radiances from microwave observations for hurricane vortex analysis, Journal of the Atmospheric Sciences, 64 (11), 3910-3925, DOI: 10.1175/2006JAS2051.1.

Zscheischler J., Westra S., van den Hurk B.J.J.M., Seneviratne S.I., Ward P.J., Pitman A., AghaKouchak A., Bresch D.N., Leonard M., Wahl T., Zhang X., 2018, Future climate risk from compound events, Nature Climate Change, 8 (6), 469-477, DOI: 10.1038/s41558-018-0156-3.

**Reviewers cooperating with Editorial Board of Meteorology Hydrology and Water Management Magazine in 2024**

Bibek Acharya
A.D. Ampitiyawatta
Nejc Bezak
Maciej Bełcik
Bogdan Bochenek
Witold Bochenek
Wiesław Gądek
Liudmyla Gorbachova
Wojciech Jakubowski
Jakub Jurasz
Jānis Kaminskis
Michał Kasina
Egidijus Kasiulis
Valeriy Khokhlov
Arash Malekian
Zoya Mateeva
Bogdan Ozga-Zieliński
Lucian Sfîcă
Zbynek Sokol
K Sreelash
Gabriel Stachura
Ewa Szalinska van Overdijk
Vazha Trapaidze
Yevheniia Vasylenko
Tomasz Walczykiewicz
Katarzyna Wartalska
Marcin Wdowikowski
Joanna Wibig

**THANK YOU**

METEOROLOGY HYDROLOGY AND WATER MANAGEMENT

IMGW-PIB Science Journal since 2013